

**A COMPOSITE TRACER ANALYSIS APPROACH TO RESERVOIR  
CHARACTERIZATION**

A Thesis

by

ADEDAYO STEPHEN OYERINDE

Submitted to the Office of Graduate Studies of  
Texas A&M University  
in partial fulfillment of the requirements for the degree of

MASTER OF SCIENCE

August 2004

Major Subject: Petroleum Engineering

**A COMPOSITE TRACER ANALYSIS APPROACH TO RESERVOIR  
CHARACTERIZATION**

A Thesis

by

ADEDAYO STEPHEN OYERINDE

Submitted to Texas A&M University  
in partial fulfillment of the requirements  
for the degree of

MASTER OF SCIENCE

Approved as to style and content by:

---

Akhil Datta-Gupta  
(Chair of Committee)

---

Robert A. Wattenbarger  
(Member)

---

Yalchin R. Efendiev  
(Member)

---

Stephen A. Holditch  
(Head of Department)

August 2004

Major Subject: Petroleum Engineering

## ABSTRACT

A Composite Tracer Analysis Approach to Reservoir Characterization.

(August 2004)

Adedayo Stephen Oyerinde, B.S., University of Ibadan, Ibadan, Nigeria;

Chair of Advisory Committee: Dr. Akhil Datta-Gupta

In the quest for production optimization from established resources, there is a continual interest in secondary and tertiary recovery methods. The success of these enhanced recovery methods, however, rely to a large extent on a sound understanding of fluid dynamics and migration paths in the reservoir. To this end, several approaches to reservoir characterization have been put to test with varying degrees of success.

The unique ability of tracers to provide direct information on preferential fluid flow paths in the reservoir, and the sensitivity of partitioning tracers to fluid saturation distribution has highlighted the prospects of a detailed reservoir characterization through interwell tracer tests.

In a broad sense, analysis of interwell tracer tests fall into two categories, analytical and inverse modeling. While most of the analytical methods are laden with limiting assumptions, the method of moments boasts rigorous formulation and accurate estimates of swept volume and average saturation of bypassed oil. The inverse modeling infers permeability and saturation distribution by matching the tracer response. An extremely effective approach to the inverse modeling methods computes sensitivities based on streamlines.

The accurate modeling of tracer flow requires accounting for complex phenomena such as transverse dispersion. Also, it is sometimes desired to model pertinent tracer components through compositional simulation. This necessitates the inclusion of a physical dispersion tensor and, hence, the well established finite difference formulation.

In this work, we have coupled the finite difference and streamline simulation techniques for the inversion-based reservoir characterization to take advantage of the robustness of the finite difference formulation and computational efficiency of streamline simulation. We have also extended the formalism of the inversion technique for fluid distribution estimation to scenarios with mobile oil saturations and have attempted integrating the analytical and inverse-modeling techniques to facilitate detailed reservoir characterization. We have demonstrated the feasibility of our approach on both synthetic and field cases.

## **DEDICATION**

I dedicate this work to my family, teachers, and friends.

## ACKNOWLEDGMENTS

I would like to express my deep gratitude to my graduate advisor Dr. Akhil Datta-Gupta for his invaluable advice, and unparalleled academic guidance.

My sincere appreciation goes to the members of my graduate committee, Dr. Robert Wattenbarger, and Dr. Yalchin Efendiev, for their scrutiny of, and contributions to this research.

I acknowledge the management of Esso exploration and production, and Schlumberger Oilfield Services Nigeria for affording me the chance to achieve one of my ambitions.

I couldn't possibly or adequately express my gratitude to Hao Cheng and Ahmed Daoud for their constructive discussions, time, and effort during the course of this research.

To all my friends, I say a big thank you for making my stay at Texas A&M University worthwhile and memorable. You always were heralds of light in the midst of darkness.

## TABLE OF CONTENTS

CHAPTER	Page
I INTRODUCTION .....	1
1.1 Background .....	1
1.2 Literature review .....	4
1.3 Objectives of the study .....	7
1.4 Thesis outline .....	7
II ANALYTICAL TRACER INTERPRETATION TECHNIQUES .....	8
2.1 Theory of method of moments .....	8
2.1.1 Allocating injection volume to producers .....	10
2.1.2 Mass balance in waterflood tracers and swept volume calculations .....	11
2.1.3 Applying MOM to partitioning tracers .....	12
III MOMENT ANALYSIS ON RANGER FIELD .....	16
3.1 Description of data set .....	16
3.1.1 Well production and injection rates .....	18
3.2 Swept pore volume computation using MOM .....	20
3.2.1 Net swept volume computation using tritium .....	22
3.3 Estimating average oil saturation using MOM .....	23
3.3.1 Estimating average oil saturation using tritium and TBA .....	24
3.4 Results of MOM on Ranger field .....	28
3.5 Discussion of MOM results .....	29
IV FUNDAMENTALS OF STREAMLINE BASED INVERSION APPROACH TO RESERVOIR CHARACTERIZATION USING PITT .....	31
4.1 Two-step inversion of partitioning interwell tracer tests (PITT) .....	31
4.2 Summary of streamline-based inversion method .....	32
4.2.1 Analytic computation of sensitivity .....	32
4.2.2 Generalized travel-time inversion .....	32
4.2.3 Model assessment .....	34
4.3 Construction of inversion model .....	35
4.4 Fundamentals of streamline simulation for obtaining analytical sensitivities .....	37
4.4.1 Streamline simulation fundamentals .....	37
4.4.2 Convective tracer transport .....	38
4.4.3 Computation of sensitivity of tracer response to reservoir parameters .....	40
4.4.4 Accounting for mobile oil saturations .....	43
4.5 Inversion algorithm .....	44
V SYNTHETIC CASES ON SATURATION AND PERMEABILITY INVERSION .....	46

CHAPTER	Page
5.1 Description of data set .....	46
5.2 Saturation inversion .....	47
5.3 Permeability inversion .....	49
5.4 Sequential inversion .....	52
5.5 Conclusion .....	55
 VI RANGER FIELD : INVERSION APPROACH TO RESERVOIR CHARACTERIZATION .....	  56
6.1 Description of data set .....	56
6.1.1 Reservoir model .....	58
6.1.1 Well production and injection rates .....	63
6.1.2 Observed tracer data .....	63
6.1.3 Manual history match with finite difference approach .....	67
6.1.4 Result of permeability inversion .....	73
6.1.5 Comparison of results with manual history matching approach .....	76
6.1.6 Result of saturation inversion .....	78
 VII INTEGRATING ANALYTICAL AND INVERSION RESULTS .....	 80
7.1 Consistency between analytical and inversion results .....	80
7.1.1 “Low” permeability trend in the north-west direction .....	80
7.1.2 Highest permeability and low NTG in the south-east direction .....	81
7.1.3 High permeability and high NTG in the region south of the injector .....	82
7.1.4 High oil saturation south of the injector .....	82
 VIII CONCLUSIONS AND RECOMMENDATIONS .....	 83
8.1 Consistency between analytical and inversion results .....	83
8.2 Recommendations .....	84
 NOMENCLATURE .....	 85
 REFERENCES .....	 87
 APPENDIX A. MOM SWEPT VOLUME CALCULATIONS USING AVERAGE RATES ...	 91
 APPENDIX B. MOM SWEPT VOLUME CALCULATIONS WITH VARIABLE RATES ...	 101
 APPENDIX C. COMPUTING SENSITIVITIES WITH RESPECT TO SHIFT -TIME .....	 116
 VITA .....	 119

## LIST OF TABLES

	Page
Table 3.1 Tracer injection summary.....	17
Table 3.2 Average production and injection rates.....	19
Table 3.3 Actual well production and injection rates.....	20
Table 3.4 Summary of normalization calculations.....	21
Table 3.5 Swept pore volume calculation (Well 19) using tritium.....	23
Table 3.6 First temporal moment calculation (Well 37) using tritium.....	25
Table 3.7 First temporal moment calculation (Well 37) using TBA.....	27
Table 3.8 Results of MOM calculations on Ranger.....	29
Table 6.1 Amount and injection location of tracer.....	57
Table 6.2 Initial reservoir model (Illiasov et al.).....	59
Table 6.3 Relative permeability parameters.....	62
Table 6.4 Actual well production and injection rates.....	64
Table 6.5 Summary of Allison et al. <sup>9</sup> key model properties.....	68
Table A.1 Swept pore volume calculation (Well 37) using tritium.....	93
Table A.2 MOM parameter estimates (Well 37) using tritium.....	94
Table A.3 Swept pore volume calculation (Well 39) using tritium.....	96
Table A.4 MOM parameter estimates (Well 39) using tritium.....	97
Table A.5 Swept pore volume calculation (Well 40) using tritium.....	99
Table A.6 MOM parameter estimates (Well 40) using tritium.....	100
Table B.1 Cumulative injected volume versus concentration (Well 39) using NaSCN.....	103
Table B.2 Cumulative produced volume versus concentration (Well 39) using NaSCN.....	106



Table B.3	MOM parameter estimates (Well 39) using NaSCN.....	108
Table B.4	Cumulative injected volume versus concentration (Well 40) using NaSCN. ....	111
Table B.5	Cumulative produced volume versus concentration (Well 40) using NaSCN. ....	113
Table B.6	MOM parameter estimates (Well 39) using NaSCN.....	115

## LIST OF FIGURES

		Page
Fig. 3.1	Tracer injection pattern.....	18
Fig. 3.2	Semi-log plot of observed tritium concentration versus time for Well 19. ....	22
Fig. 3.3	Semi-log plot of observed tritium concentration versus time for Well 37. ....	25
Fig. 3.4	Semi-log plot of observed TBA concentration versus time for Well 37. ....	27
Fig. 4.1	A schematic of typical PITT responses (Illiasov et al. <sup>2</sup> ). ....	32
Fig. 4.2	Concept of generalized travel time. Data shift (top), optimal cross-correlation (bottom).....	33
Fig. 4.3	Flowchart for history matching finite-difference models using streamline derived sensitivities. ....	45
Fig. 5.1	Reference saturation distribution.....	46
Fig. 5.2	Saturation distribution after inversion. ....	48
Fig. 5.3	Saturation distribution after inversion based on the formulation of Illiasov et al. ....	48
Fig. 5.4	Initial (right) partitioning tracer elution observed and calculated from the eight producers versus final match (left) on saturation inversion. ....	49
Fig. 5.5	Reference permeability distribution. ....	50
Fig. 5.6	Permeability distribution obtained on generalized travel-time inversion. ....	51
Fig. 5.7	Initial (right) conservative tracer elution observed and calculated from the eight producers versus final match (left) on permeability inversion. ....	52
Fig. 5.8	Refining of permeability and saturation distributions during sequential inversion. ....	53
Fig. 5.9	RMS error on travel time and amplitude during sequential inversion (saturation). ....	54
Fig. 5.10	RMS error on travel time and amplitude during sequential inversion (permeability).....	55

	Page
Fig. 6.1	Tracer injection pattern (Illiasov <sup>2</sup> )..... 58
Fig. 6.2	Net-gross ratio distribution – layered view (Illiasov <sup>2</sup> ). ..... 60
Fig. 6.3	Net-gross ratio distribution – 3D cut-away view (Illiasov <sup>2</sup> )..... 60
Fig. 6.4	Initial permeability distribution – layered view (Illiasov <sup>2</sup> )..... 61
Fig. 6.5	Initial permeability distribution - 3D cut-away view (Illiasov <sup>2</sup> ). ..... 62
Fig. 6.6	Observed normalized tracer concentrations at production wells (Illiasov et al. <sup>2</sup> ). ..... 65
Fig. 6.7	Observed normalized tritium and TBA tracer concentrations at production wells. (Illiasov et al. <sup>2</sup> )..... 66
Fig. 6.8	Observed normalized NaSCN and TBA tracer concentrations at production wells. (Illiasov et al. <sup>2</sup> )..... 67
Fig. 6.9	Permeability fields for layers 1, 2, and 3 of the finite-difference model (Allison et al. <sup>9</sup> ) ..... 69
Fig. 6.10	Saturation distribution for layers 1,2, and 3 of the finite-difference model (Allison et al. <sup>9</sup> ). ..... 69
Fig. 6.11	Tritium match for the finite-difference model (Allison et al. <sup>9</sup> ). ..... 70
Fig. 6.12	NaSCN match for the finite-difference model (Allison et al. <sup>9</sup> )..... 71
Fig. 6.13	TBA match for the finite-difference model (Allison et al. <sup>9</sup> ). ..... 72
Fig. 6.14	Comparison of calculated and observed normalized concentration using initial permeability distribution. .... 73
Fig. 6.15	Comparison of calculated and observed normalized concentration after match. .... 74
Fig. 6.16	Rapid fall in RMS of amplitude and Travel-Time misfit. .... 75
Fig. 6.17	Layer permeability after match (left) and permeability adjustments to initial model (right). .... 76
Fig. 6.18	Major permeability changes in layer one for manual history match ..... 77
Fig. 6.19	Permeability changes in each layer necessary to obtain match. .... 77

	Page
Fig. 6.20	Observed and calculated partitioning tracer response before (right) and after (left) saturation inversion ..... 78
Fig. 6.21	Layer saturation distribution before (left) and after (right) inversion. .... 79
Fig. 7.1	Contour map of permeability distribution after inversion. .... 81
Fig. A.1	Semi-log plot of observed tritium concentration versus time for Well 37 ..... 92
Fig. A.2	Semi-log plot of observed tritium concentration versus time for Well 39 ..... 95
Fig. A.3	Semi-log plot of observed tritium concentration versus time for Well 40 ..... 98
Fig. B.1	Semi-log plot of NaSCN concentration versus injected volume for Well 39 ..... 102
Fig. B.2	Semi-log plot of NaSCN concentration versus produced volume for Well 39 ..... 102
Fig. B.3	Semi-log plot of NaSCN concentration versus injected volume for Well 40 ..... 109
Fig. B.4	Semi-log plot of NaSCN concentration versus produced volume for Well 40 ..... 110

# CHAPTER I

## INTRODUCTION

### 1.1 Background

On primary recovery, a significant amount of the original oil in place is left unrecovered. The fate of a business venture is often determined by enhanced oil recovery methods aimed at economically recovering the bypassed oil. The success of these methods requires a sound understanding of fluid dynamics and migration paths in the reservoir. Although seismic, geologic and depositional environment studies, as well as reservoir simulation, can provide very valuable insight into the feasibility of secondary or tertiary projects, significant information about the actual distribution of the fluid transmissibility of a reservoir are contained in pressure transient testing and interwell tracer tests. The global nature of the probing ability of pressure transient tests and inherent lack of resolution in terms of “small scale” features undermines their suitability for detailed reservoir characterization.

Over the years, a succession of advancements in design and implementation of tracer tests have drawn attention to them as a reliable means of delineating fluid migration paths in the reservoir. Novel applications such as construction of fractional flow curves, residual oil and connate water saturation have further accentuated the potential of tracer tests as adequate tools for reservoir description and characterization.

Broadly, there are two classifications of tracers; these are radioactive and chemical tracers. Radioactive tracers are chemical compounds which contain radioactive isotopes that disintegrate to a stable state and may emit beta or gamma radiation, depending on the isotope. Chemical tracers for water can be categorized into dyes, ionic, and organic tracers. The choice of tracer for an application is driven by environmental concerns, anticipated exposure to rock material, transit time, and reservoir property sought amongst others. In terms of application, tracers are categorized into conservative and partitioning tracers. This classification is based on the relative interaction of the tracers with the water and other phases present in the reservoir.

---

This thesis follows the style and format of *SPE Journal*.

The conservative, also called 'non-partitioning' or 'aqueous' tracers move with the velocity of the water phase in the reservoir without interaction with other phases as they move through the reservoir. These tracers have found successful applications in characterizing fluid flow between wells. Partitioning tracers are soluble in the water phase as well as the oil or gas phases present in the reservoir. The solubility of partitioning tracers in the immobile oil or gas in a reservoir results in the frontal advance rate being less than the injection fluid velocity. Driven by the tracer concentration gradient, tracer molecules will diffuse from the tracer slug into the stationary oil or gas. After the slug passage, a reversal in concentration gradient occurs, initiating the diffusion of tracer molecules from the stationary phases back into injection water. It is this chromatographic delay that serves as the basis for residual oil saturation determination and fluid distribution estimation.

Partitioning tracers have gained application in two different types of tracer tests. The first is the Single Well Partitioning Tracer Tests (SWPTT), and the second, Partitioning Interwell Tracer Tests (PITT)

A single well partitioning tracer test is an in-situ method for measuring fluid saturations in reservoir. The measurement can be for residual oil saturation or for connate water saturation. In either case, the saturation measurement is carried out where one phase is effectively stationary in the pore space and the other phase can flow to the wellbore. These tests are used primarily to measure target oil saturations before initiating enhanced oil recovery (EOR) operations, measure the effectiveness of EOR agents in a single well pilot, or assess a field for bypassed oil targets. The test for residual oil saturation is carried out by the injection and back production of water-carrying chemical tracers in a single well. The injected volume is divided into two parts, one of water carrying a small concentration of an alkyl ester into the formation and the second a push volume that pushes the ester away from the well bore. A material balance tracer, normally an alcohol, is added to the entire injection volume to differentiate it from the formation water being displaced. After the ester and push injections are completed, the well is shut in for a period of time depending on the reactivity of the ester and the reservoir temperature. The shut in period allows a portion of the ester to react with water in the reservoir forming a new tracer in-situ. Since Alkyl esters are made by the reaction of an alcohol with an organic acid, hydrolysis at reservoir temperature breaks it down to the starting products. The acid formed during the reaction is consumed by the natural base components of the reservoir and is not observed. It is the alcohol tracer formed that is a partitioning tracer making for the separation of the elution

profiles of the produced tracers in back production, and in essence, possible estimation of bypassed oil saturation. Partitioning interwell tracer tests also rely on the concept of retardation of tracers in estimating residual oil saturations but as the name suggests, on a larger scale than the SWPTT.

During a PITT, both conservative and partitioning tracers are injected into the reservoir through injection wells. The observed separation between the conservative and the partitioning tracers, which depend on the amount and distribution of oil contacted by the partitioning tracers as well as the partitioning coefficient of the tracer, can be used to infer in-situ oil distribution in the tracer swept area of the reservoir. The combination of both conservative and partitioning tracers in a single test affords the opportunity of obtaining direct information on reservoir heterogeneity and fluid migration patterns, as well as saturation distribution in the reservoir. The ability of PITTs to probe and characterize interwell regions increases their value over SWPTTs.

The trend in the past had been an analytical approach to interpretation of tracer tests. These analytical methods varied in application from determining number of layers<sup>1</sup> to producing estimations of average swept volumes and oil saturations in the reservoir with techniques also varying from mere inspection of elution profile to non-linear regression.

Improved computational capabilities as achieved by the advent of super-processors have brought into lime light an approach based on inverse modeling once considered prohibitive. However, the processing feat still offers little room for practical application of computationally intensive approaches to solving the inverse problem such as numerical perturbation, adjoint method, and gradient based methods. The distinction of the methods derives from the manner in which the sensitivities are calculated.

In the recent past, a novel approach to solving the inverse problem for field applications based on streamline simulation was proposed<sup>2</sup>.

In this research, the requirement for accurate modeling of tracer flow accounting for complex phenomena such as transverse dispersion as well as the desire to model pertinent tracer components through compositional simulation is considered and the inadequacy of streamline models to cater for these concerns has led to the coupling of a commercial finite difference reservoir simulator, which serves as the forward model, to streamline-based inversion algorithm. This method borrows from the idea of sensitivity computation along streamlines and takes advantage of the robustness of finite difference formulation and the computational efficiency of streamline simulation.

This research also extends the present formulation to fluid saturation distribution estimation in the presence of mobile oil and attempts to integrate analytical approaches to tracer analysis with inverse-based methods.

We have applied our work with success to synthetic and filed cases.

## 1.2 Literature review

Tracer tests have been conducted in both petroleum and groundwater fields with remarkable success. This has led to simultaneous development in interpretation techniques in both fields. While in the petroleum field, the development in interpretative capabilities has been driven by production optimization, in the groundwater field, the design and implementation of aquifer remediation schemes for removal of the contaminant from the soil remains the principal drive.

Methods of analysis of tracer tests in both petroleum and groundwater applications can be divided into three categories.

- analytical methods,
- stochastic methods via cokrigging, and
- direct profile match with simulation.

Analytical methods also vary in application. Some are aimed at characterizing reservoir heterogeneity and dynamics of fluid flow, while others applied in determination of average oil or Non-Aqueous Phase Liquids (NAPL) in the reservoir and aquifer respectively.

In the petroleum industry, Cooke<sup>3</sup> initiated an approach for determining reservoir oil saturation using PITT data. In his approach, the breakthrough times of the two types of tracers are used in computing the average saturation in the swept region.

As a result of poor quantitative definition of the breakthrough time, an improvement over Cooke's method was proposed by Tang<sup>4</sup>. Tang's proposition laid emphasis on using any common 'landmarks' such as peaks and valley on the elution curves rather than a breakthrough time, which often required estimation through a polynomial fit in determining oil saturation. Tang further proposed that reservoir oil saturation can be evaluated over the whole production curve by comparing the production times of the partitioning and non-partitioning tracers at a given landmark defined as equal normalized concentrations, recovery or normalized recovery. This improved method yields several values of average in-situ oil for different landmarks being indicative of variability in oil saturation encountered by the tracers in migrating from injectors to



producers. An arithmetic average of the estimated values of oil saturation can then be used to represent the average oil saturation. A similar analytical method in the groundwater field applies a method called ‘Method of Moments’ in determining average saturation of NAPL saturations in the Aquifer. This method relies on computation of first temporal moments of the tracer responses over the entire production curve and then using this moment to evaluate an average NAPL saturation in the tracer-swept region. This method has been extended to the petroleum industry and in this research; we have applied this to a field case.

Dean presented a technique for fractional-flow modeling using chemical tracers.<sup>5</sup> His approach is based on combining the theory of tracer movement and that of Buckley-Leverette for two-phase flow in establishing the fact that chemical tracers flowing with oil and brine in a reservoir follow characteristic oil saturation.

By modeling tracer elution profiles using stream functions and hyper elliptic integrals and imposing several limiting assumptions such as specific flood pattern or Mobility ratio and homogenous reservoir layers, several authors have attempted determining the number and properties of layers of a reservoir by matching observed peaks in the elution profile.

Abbaszadeh, drawing from previous works by Bingham, proposed a non-linear regression technique of matching the tracer elution profile, thereby determining the optimal number of layers and corresponding estimates of conductivity and porosity-thickness products.

James et al. introduced a stochastic approach for estimating spatial distribution of NAPL. The method utilizes a cokrigging algorithm to simultaneously evaluate spatial variation of NAPL and hydraulic conductivity. This method treats NAPL distribution and conductivity as spatially correlated random fields. The method, through a non-linear Gauss-Newton search technique identifies spatial distribution of NAPL that minimizes in a least-square sense, the temporal moment predictions from the observed values measured at extraction wells. The James et al. method is a solution to an inverse problem aimed at obtaining permeability and saturation distribution by matching first temporal moment of tracer profiles. Complications of this method arise from the requirement of existence of prior and cross-covariance models that might be difficult to determine in the field.

Even though the analytic methods for analyzing tracer data are simple and easy to apply, they rely on averaging the difference in tracer responses and provide only average estimates. Potentially, every observed data point on a tracer profile carries important information about

reservoir properties. Thus, the direct profile match is desirable but difficult because it involves the solution of computationally intensive inverse problems.

The direct profile match methods essentially adjust reservoir parameters and saturations in order to obtain a fit on the observed response. Early attempts involved a manual adjustment of these parameters until a “match” is obtained. The ad-hoc nature of parameter adjustment and the time spent in obtaining a match deemed acceptable makes this method quite impractical for large cases.

Attempts to improve on the profile match resulted in efforts dedicated to solving an inverse problem which in some cases proved computationally prohibitive. Most of these attempts tried to solve the inverse problem by automated history matching with finite-difference simulators. The inherent computational intensity makes them hardly feasible for fine-scale field models. Gradient-based inversion methods, which are directly compatible with commercial finite-difference simulators, rely on calculation of sensitivity coefficients in order to employ efficient gradient based technique for optimization. Computation of sensitivities often becomes more expensive than solving fluid flow problem and is often responsible for excessive computational time associated with finite-difference automated history matching. Although gradient-free optimization methods such as simulated annealing and genetic algorithm have been utilized for data integration, the slow convergence based on random perturbation prevents them from being extensively used.

Vasco et al.<sup>6</sup> presented a computationally efficient approach to solving the inverse problem using streamline simulation. The computational efficiency results from the possibility of deriving analytical equations for sensitivities along streamlines. Yoon<sup>7</sup> et al. proved the utility of the streamline-based inversion method for estimation of NAPL saturation from PITT data using a synthetic case and applied the method to a field test at Hill Air force Base Operating unit 1. Illiasov et al.<sup>5</sup> applied this to a multi-well field-scale PITT test at Ranger field to determine spatial distribution of in-situ oil.

The shortcomings of streamline simulation have been the motivation behind the approach utilized in this research. Results obtained from application to synthetic cases as well as the Ranger case gives us confidence on the applicability of the approach.

### **1.3 Objectives of the study**

The objectives of this study are split into three principal parts. The first part involves the modification of the streamline-based inverse approach of reservoir characterization using tracer data by incorporating finite difference simulation to take advantage of the robustness and complexity of the finite difference formulation, and the computational efficiency of streamline simulation.

The second part of the research is an extension of the saturation inversion during PITT to mobile oil saturations, and the third part is an integration of established analytical interpretation methods with the inversion-based numerical approaches.

### **1.4 Thesis outline**

We first discuss the basics of the Method of Moments (MOM) as an analytic approach to tracer interpretation in terms of estimating average swept volumes and saturation of bypassed oil. In the next section, we apply the MOM to the Ranger field case and discuss the result.

Next, we introduce the fundamentals of streamline-based inversion approach to reservoir characterization. In this section, we detail how sensitivities are obtained from streamlines and show how we have coupled finite difference and streamline simulation techniques to obtain a robust and computationally efficient inversion algorithm. Our extension of the saturation inversion to cases with mobile oil saturations and thus, modified expressions for the sensitivity calculations are then presented.

Finally, we apply our approach to a nine-spot, two-dimensional synthetic case and then to the field case study mentioned above. We then compare our results to previous works done on the field case for the purpose of validation.

## CHAPTER II

### ANALYTICAL TRACER INTERPRETATION TECHNIQUES

#### 2.1 Theory of method of moments

The method of moments has its roots in the chemical process industry where it is used to analyze non-ideal flow in chemical reactors. In this application, a stimulus is applied by injecting a tracer at the inlet of the system either in the form of a narrow pulse (delta function) or as a continuous injection (step function), and the tracer response as a function of cumulative time is monitored at the output. The tracer distribution curve generated at the outlet is used to analyze flow through the reactor.

Analysis of the tracer distribution curve is done by relating the moments of the distribution curve to possible flow models in the reactor. The first moment of the tracer distribution curve is the mean residence time. The second moment (the variance) can be related to the Peclet number, a dimensionless number giving the ratio of convective to dispersive forces. From these moments alone, flow conditions varying from plug flow to fully mixed flow can be described in a reactor.

In the petroleum industry, it is the analysis of tracer flow through a porous medium that is of interest. If the injected water in a water flood traverses a volume only once in passing through the reservoir, then moment analysis can be used to define that volume.

The mean of any distribution is given by its first moment. For the produced tracer distribution (produced tracer concentration vs. cumulative volume injected) at each well, the first moment of the distribution, is given by:

$$\bar{V} = \frac{\int_0^{\infty} C(V)VdV}{\int_0^{\infty} C(V)dV} \quad (2.1)$$

Considering the discrete nature of production data, the integrals in Eq.2.1 can be approximated by the summation. Hence, the first moment of the distribution, representing the average injected volume is given by:

$$\bar{V} = \frac{\sum_0^{\infty} C(V)V\Delta V}{\sum_0^{\infty} C(V)\Delta V} \quad (2.2)$$

The limit of the summation in Eq. 2.2 above is shown to go to infinity. This would require carrying out the summation across the entire tracer profile. However, due to limitations in the detection capability and the need for profile interpretation before the arrival of entire tracer profile at the observation well, there often is a need to complete the distribution curves by extrapolation of collected data.

To extrapolate data from a distribution curve, it is necessary to predict the path of the curve and be able to calculate the expected values to the end of the curve. This has two requirements: first to find a function that can reasonably be expected to describe the data path; second, that the function be bounded, i.e. the value to infinity is fixed and calculable. Both the error function and exponential functions have been seen to satisfy these requirements but the exponential function has been successful for this purpose. Experience shows that most field data, given enough time, will show an exponential decline. The moments of the response curve can then be obtained by dividing the data into two parts, one representing the data from zero to point  $V_e$  where it can be treated as exponential, and the second covering the extrapolation of the exponential part from  $V_e$  to infinity. Eq. 2.1 can then be re-written as:

$$\bar{V} = \frac{\int_0^{V_e} C(V)VdV + \int_{V_3}^{\infty} C(V)VdV}{\int_0^{V_e} C(V)dV + \int_{V_e}^{\infty} C(V)dV} \quad (2.3)$$

Approximating the fit to the tail of the tracer curve by an exponential decline as proposed by Dean, with the exponential equation below;

$$C = C_e e^{-\left(\frac{V-V_e}{a}\right)} \quad (2.4)$$

where the reciprocal of  $a$  is the slope of the line and  $C_e$  is the measured tracer concentration at the value of  $V_e$  for which the exponential fit starts.

Substituting Eq.2.4 in the rightmost terms of both the numerator and denominator of Eq. 2.3 and evaluating the integral gives Eqs. 2.5 and 2.6 respectively.

$$\int_{V_e}^{\infty} C_e e^{-\left(\frac{V-V_e}{a}\right)} dV = aC_e \quad (2.5)$$

$$C_e \int_{V_e}^{\infty} V e^{-\left(\frac{V-V_e}{a}\right)} dV = aC_e (a + V_e) \quad (2.6)$$

Substituting Eqs. 2.5 and 2.6 into 2.3, the expression for the first moment is given below.

$$\bar{V} = \frac{\int_0^{V_e} C(V)VdV + aC_e(a + V_e)}{\int_0^{V_e} C(V)dV + aC_e} \quad (2.7)$$

Representing this in a discrete form, Eq. 2.7 can be written as:

$$\bar{V} = \frac{\sum_0^{V_e} C(V)V\Delta V + aC_e(a + V_e)}{\sum_0^{V_e} C(V)\Delta V + aC_e} \quad (2.8)$$

Eq. 2.8 is used in estimating of the average swept pore volume.

### 2.1.1 Allocating injection volume to producers

During tracer-tagged water injection into a reservoir, depending on the fluid migration pattern, wells draining the flood pattern produce different quantities of the injected tracer. The relative amount of produced water from these wells relates to the relative tracer production from the wells. The total amount of tracer,  $m_{ip}$ , produced at any given well,  $p$ , from injector I is given by the integral of the produced tracer concentration as a function of the produced water,  $\int C(V)_{ip} dV$ . Since the distribution of tracer is equivalent to the distribution of the injected water, the fraction of injected water,  $f$ , can be expressed as:

$$f = \frac{m_{ip}}{M} \quad (2.9)$$

where,  $M$  represents the total amount of injected tracer.

### 2.1.2 Mass balance in waterflood tracers and swept volume calculations

A major problem with waterflood tracers lies in the fact that not all injected tracer is recovered. This happens because not all the water injected will be confined within the planned flood pattern. Also, when there is excessive dilution of the tracers as they travel over long distances between the injection and production wells, the tracer concentrations at the producers are lower than the detection limit. Hence, though tracer is produced, no measurement is made and that quantity of tracer goes unaccounted for.

Comparing the amount of recovered tracer to the total amount injected gives an indication of how much of the injected water escapes the flood pattern.

The pore volume swept is given by Eq. 2.8 above. Since water moves in the reservoir in accordance with the gradients arising from the producing wells (pressure sinks) and injection wells (pressure sources) distributed through the reservoir, the volume swept by the injected water is a response to these forces. The fraction of this swept volume that can be attributed to a given production well is reduced by the fraction of the total injected water that arrives there (Eq. 2.9). The Equation for the net swept volume for well  $i$  is therefore given by:

$$\bar{V}_{si} = f\bar{V}_s = \frac{m_i}{M_i}\bar{V}_s \quad (2.10)$$

Combining Eqs 2.8, 2.9, and 2.10, the net volume swept by well  $i$  is can be written as:

$$\bar{V}_{si} = \left( \frac{\sum_0^{V_e} C(V)\Delta V + aC_e}{M_i} \right)_{pro} \left( \frac{\sum_0^{V_e} C(V)V\Delta V + aC_e(a+V_e)}{\sum_0^{V_e} C(V)\Delta V + aC_e} \right)_{inj} \quad (2.11)$$

The subscripts *pro* and *inj* indicate that the terms in parenthesis are to be estimated from plots of concentration versus cumulative produced water and cumulative injected water respectively.

The derivations above assume that the pattern obtained by connecting the nearest producers surrounding each injector with lines will define the flow between injectors and producers. This is often not the case; the actual flow may bypass some wells in the pattern as mentioned above. Swept volume estimates using Eq. 2.11 is still valid even if the pattern turns out to be different from expectations.

### 2.1.3 Applying MOM to partitioning tracers

Himmelblau and Bischoff showed that for a single-phase non-reactive flow in a packed bed, the pore volume is given by the dimensionless mean residence time calculated from the tracer response curve resulting from the imposition of an idealized instantaneous tracer pulse (the Dirac delta function) into the vessel entrance stream. The dimensionless mean residence time is given by:

$$\bar{t}_D = \frac{\int_0^{\infty} t_D C_D(t_D) dt_D}{\int_0^{\infty} C_D(t_D) dt_D} \quad (2.12)$$

where,  $\bar{t}_D = \frac{\int_0^t q dt}{V_p}$  and  $C_D = \frac{C - C_{initial}}{C_{injected} - C_{initial}}$  with q representing volumetric flow rate and  $V_p$ , pore volume.

The dimensionless mean residence time in Eq. 2.12 above represents the first moment of a concentration versus dimensionless time plot.

A corrected mean residence time  $\bar{t}_D^*$  was defined assuming a constant input tracer concentration with a dimensionless duration time of  $\bar{t}_{DS}$ . The corrected mean residence time is then expressed as:

$$\bar{t}_D^* = \bar{t}_D - \frac{t_{DS}}{2} \quad (2.13)$$

Considering a permeable medium flowing  $N_p$  phases, the overall flux  $F_i$  and total fluid phase concentration  $C_i$  of component i are

$$F_i = \sum_{j=1}^{N_p} f_j C_{ij} \quad (2.14)$$

$$C_i = \sum_{j=1}^{N_p} S_j C_{ij} \quad (2.15)$$



where  $C_{ij}$  is the concentration of component  $i$  in phase  $j$ ,  $f_j$ , the fractional flow of phase  $j$ , and  $S_j$  the saturation of phase  $j$ . Lake<sup>8</sup> defined the residence time for component  $i$ , as the inverse of the specific concentration velocity for component  $i$ . This is expressed as

$$\overline{t_{Di}^*} = \frac{C_i}{F_i} = \frac{S_j + S_k K_{kj}^i}{f_j + f_k K_{kj}^i} \quad (2.16)$$

where  $K_{kj}^i$  is the partitioning coefficient of tracer  $i$  defined as the ratio of the concentration of tracer  $i$  in phase  $k$  to that in phase  $j$ . Eq. 2.16 is the basis for the estimation of saturation for two phases using partitioning tracers.

Consider a three-dimensional permeable medium containing oil or non-aqueous phase liquid at an average residual saturation  $S_N$ , and through which water is flowing at a constant rate  $q$ . At time zero, a second water stream containing two nonabsorbent tracers are introduced at the injection well or wells with a duration time of  $t_s$ . Tracers 1 and 2 have partitioning coefficients of  $K_{N,W}^1$  and  $K_{N,W}^2$ , respectively.

Applying Eq. 2.16 to Tracers 1 and 2 gives

$$\overline{t_{D1}^*} = S_w + S_N K_{N,W}^1 \quad (2.17)$$

$$\overline{t_{D2}^*} = S_w + S_N K_{N,W}^2 \quad (2.18)$$

Including the saturation constraint

$$S_w + S_N = 1 \quad (2.19)$$

The tracer swept pore volume is implicitly included in  $\overline{t_D^*}$ .

$$V_p = \frac{\overline{qt_1}}{\overline{t_{D1}^*}} = \frac{\overline{qt_2}}{\overline{t_{D2}^*}} \quad (2.20)$$

where

$$\overline{t_1} = \frac{\int_0^{t_f} t C_{D1}(t) dt}{\int_0^{t_f} C_{D1}(t) dt} - \frac{t_s}{2} \quad (2.21)$$

$$\bar{t}_2 = \frac{\int_0^{t_f} t C_{D2}(t) dt}{\int_0^{t_f} C_{D2}(t) dt} - \frac{t_s}{2} \quad (2.22)$$

where  $t_f$  is the tracer test cutoff time.

Solving Eq. 2.17 through 2.22, the average oil saturation is given as

$$S_N = \frac{\bar{t}_2 - \bar{t}_1}{(K_{N,W}^2 - 1)\bar{t}_1 - (K_{N,W}^1 - 1)\bar{t}_2} \quad (2.23)$$

The swept pore volume can then be obtained as

$$V_P = \frac{q\bar{t}_1}{1 - S_N(1 - K_{N,W}^1)} = \frac{q\bar{t}_2}{1 - S_N(1 - K_{N,W}^2)} \quad (2.24)$$

And the volume of oil detected is

$$V_N = S_N V_P = \frac{q(\bar{t}_2 - \bar{t}_1)}{(K_{N,W}^2 - K_{N,W}^1)} \quad (2.25)$$

In an interwell partitioning tracer test, both a conservative (zero partitioning coefficients) and a partitioning tracer are injected at the injection well. Hence, Eqs. 2.23 and 2.25 can be simplified to

$$S_N = \frac{\bar{t}_p - \bar{t}_n}{(K_{N,W} - 1)\bar{t}_n + \bar{t}_p} \quad (2.26)$$

and

$$V_N = \frac{q(\bar{t}_p - \bar{t}_n)}{K_{N,W}} \quad (2.27)$$

where  $K_{N,W}$  is the partitioning coefficient of the partitioning tracer, and  $\bar{t}_n$  and  $\bar{t}_p$ , the first temporal moments of the conservative and partitioning tracers respectively.

If the analysis is made in terms of a plot of concentration versus cumulative volume of produced fluid, the equivalents of Eq.2.26 and 2.27 are

$$S_N = \frac{\bar{V}_p - \bar{V}_n}{(K_{N,W} - 1)\bar{V}_n + \bar{V}_p} \quad (2.28)$$

$$V_N = \frac{\overline{V}_p - \overline{V}_n}{K_{N,W}} \quad (2.29)$$

where  $\overline{V}_p$ , and  $\overline{V}_n$ , are obtained as the first moments of a plot of concentration versus cumulative produced volume for the partitioning and conservative tracers respectively.

## CHAPTER III

### MOMENT ANALYSIS ON RANGER FIELD

#### 3.1 Description of data set

A multi-well multi-tracer interwell tracer injection study was carried out in McCleskey sandstone of the Ranger field, Texas. The first description of this data set was offered by Lichtenberger.<sup>11</sup> The dataset was also described later by Allison et al.<sup>9</sup> in the paper based on Allison's work that can also be found in his M.S thesis.<sup>10</sup> We used these references as the main sources of data in our work

The 320-acre area of interest includes 13 producing and 4 injection wells, injecting 7 different tracers. The seven tracers injected included 5 conservative tracers consisting of four decaying (tritium, Cobalt-57, Cobalt-58, Cobalt-60) and one chemical tracer (sodium thiocyanate, NaSCN) and two partitioning tracers (tertiary butyl alcohol, TBA, and Isopropyl alcohol IPA).

All tracers were injected in small slugs on the same day except for TBA, which was injected in a small slug twenty days later than the others. Tracer sampling continued for 826 days after injection of the first set of tracers. Tracer injection pattern is shown in Fig. 3.1 below. Injection locations and the amounts of each tracer injected are given in Table 3.1. The partitioning coefficients defined as the ratio of tracer concentration in oil phase to that in water phase, of TBA and IPA are 0.2 and 0.04 respectively.

**Table 3.1 – Tracer injection summary.**

<b>Tracer</b>	<b>Well</b>	<b>Amount</b>	<b>Half-life</b>
tritium	38	10 Ci	4475 days
NaSCN	38	5655 lbs	-
IPA	38	880 gals	-
TBA	38	880 gals	-
Co-57	41	30 mCi	270 days
Co-58	45	100 mCi	71 days
Co-60	42	30 mCi	1920 days

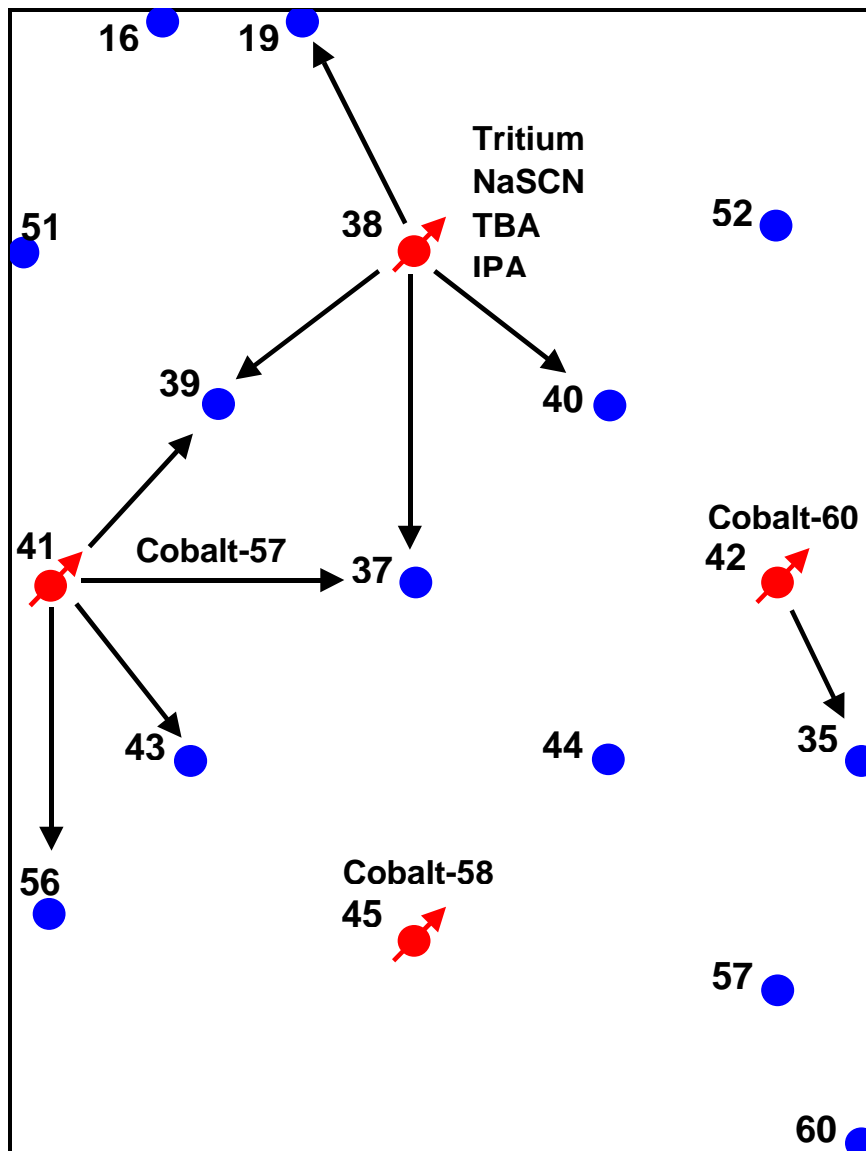


**Fig. 3.1 – Tracer injection pattern.**

### 3.1.1 Well production and injection rates

We averaged well production and injection rates over the life of the project for our MOM analysis. These average rates were calculated on the basis of the well data presented by Lichtenberger<sup>11</sup>, Allison et al.<sup>9</sup>, and Allison.<sup>13</sup> The average production and injection rates for all wells are summarized in Table 3.2. The actual well data on which we based our averages are presented in Table 3.3. Locations of production and injection wells are shown in Fig. 3.1.

**Table 3.2 – Average production and injection rates.**

<b>Production Wells</b>	<b>Production Rate (bbl/day)</b>
16	17
19	16
35	17
37	403
39	424
40	25
43	454
44	142
51	36
52	10
56	77
<b>Production Wells</b>	<b>Production Rate (bbl/day)</b>
57	42
60	20
<b>Injection wells</b>	<b>Injection Rate (bbl/day)</b>
38	839
41	587
42	168
45	84

**Table 3.3 – Actual well production and injection rates.**

Wells	Time, days							
	0-100	101-200	201-300	301-400	401-500	501-600	601-700	701-826
<b>Production wells</b>	<b>Production rate, bbl/day</b>							
16	7	7	20	20	20	20	20	20
19	4	4	14	14	16	56	24	0
35	0	0	0	35	28	40	35	0
37	156	210	236	310	410	448	560	792
39	305	300	350	318	343	423	540	735
40	4	8	60	56	80	0	0	0
43	195	226	211	251	340	426	844	1002
44	89	89	139	139	139	178	178	178
51	14	14	43	43	43	43	43	43
52	10	10	10	10	10	10	10	10
56	31	36	49	66	75	79	95	164
57	42	42	42	42	42	42	42	42
60	20	20	20	20	20	20	20	20
<b>Injection wells</b>	<b>Injection rate, bbl/day</b>							
38	439	483	597	662	783	893	1176	1503
41	307	338	418	463	548	625	823	1052
42	88	97	119	132	157	179	235	301
45	44	48	60	66	78	89	118	150

### 3.2 Swept pore volume computation using MOM

In making estimates of the net swept volumes and saturations, the tracers used were tritium, sodium thiocyanate (NaSCN), and tertiary butyl alcohol (TBA). Due to low recovery of Cobalt and Isopropyl alcohol (IPA), we deemed it unreliable to base any analysis on them. Tritium and NaSCN are both conservative tracers and as such are used for swept volume calculations. TBA is a partitioning tracer that allows for saturation estimates.

Working with average production and injection rates as shown in Table 3.3, Eq. 2.11 can be further reduced to a more compact form in which only the plot of concentration versus time is



used to obtain the first temporal moment. Multiplying the first temporal moment by the injection or production rate then yields average injected or produced volume respectively. The net swept volume is obtained by taking into account the relative distribution of injected water as discussed in Chapter II.

$$\bar{V}_s = A \frac{q_p q_{inj}}{M} \left\{ \sum_0^{tb} (C(t)t\Delta t) + a(a + tb)Cb \right\} \quad (3.1)$$

where  $A$  is a conversion factor obtained on normalization calculations,  $q_p$ , and  $q_{inj}$  represent average production and injection rates respectively.

The normalization calculations are shown in Table 3.4.

**Table 3.4 – Summary of normalization calculations.**

Parameter	tritium	NaSCN	TBA
Slug Size	20 days		
Slug Size	10 Ci	5655 lbs	880 gals
Injection Rate	840 bbl/day		
Observed Units	pC/mL	ppm	ppm
Normalization Concentration	3744 pC/mL	960 ppm	960 ppm

$$Tritium\_Conc = \frac{10(Ci)1e12 \left( \frac{pC}{Ci} \right)}{20(days)840 \left( \frac{bbl}{day} \right) 159 \left( \frac{L}{bbl} \right) 1000 \left( \frac{mL}{L} \right)} = 3744 \left( \frac{pC}{mL} \right) \quad (3.2)$$

$$TBA\_Conc = \frac{880(gal)1e6 \left( \frac{ppm}{gal} \right)}{20(days)840 \left( \frac{bbl}{day} \right) 42 \left( \frac{gal}{bbl} \right)} = 1247(ppm) \quad (3.3)$$

$$NaSCN\_Conc = \frac{5655(lb)1e6 \left( \frac{ppm}{lb} \right)}{20(days)840 \left( \frac{bbl}{day} \right) 5.615 \left( \frac{ft^3}{bbl} \right) 62.43 \left( \frac{lb}{ft^3} \right)} = 960(ppm) \quad (3.4)$$

### 3.2.1 Net swept volume computation using tritium

To estimate the first temporal moment, a semi-log plot of concentration versus time (Fig. 3.2 and Table 3.5) is made in order to model the exponential decline described in Chapter II as a straight line. This facilitates the evaluation of the constant  $a$  in the derivation above.

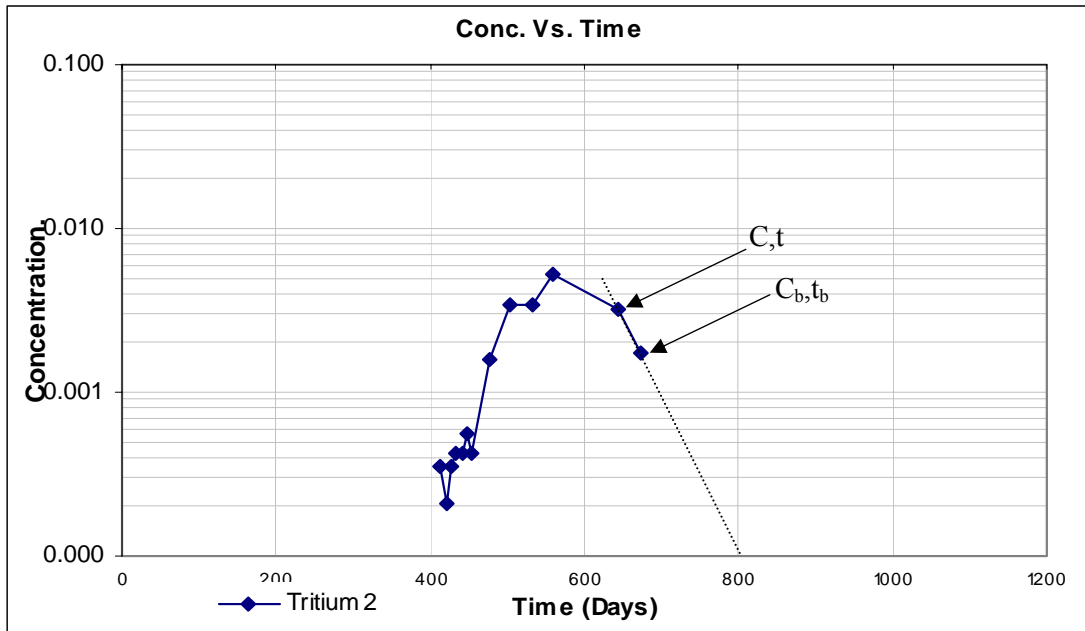


**Fig. 3.2 – Semi-log plot of observed tritium concentration versus time for Well 19.**

Constant  $a$  is evaluated at the point of data extrapolation from the equation

$$1/a = \frac{\ln(C_b / C)}{(t - t_b)} \quad (3.5)$$

The first temporal moment is then estimated as

$$\bar{t} = \frac{\sum_0^{tb} C(t)t\Delta t + a(a + tb)Cb}{\sum_0^{tb} C(t)\Delta t} = 567.1 \text{ days} \quad (3.6)$$

To estimate the amount of tritium produced at Well 19, we use

$$m = q_p (\text{bbl} / \text{day}) \cdot \left\{ \sum_0^{tb} C(t)\Delta t + aCb \right\} (\text{day}) * K (\text{pc} / \text{ml}) * (158987 \text{ ml} / \text{bbl}) \quad (3.7)$$

where  $K$ , is given in the normalization table (Table 3.4). The fraction of tritium produced in Well 19 is obtained by dividing produced tritium by the total amount injected (10Ci). Hence,

$$f = \frac{m}{M} = 0.000891672$$

The net swept volume is then given by

$$\bar{V}_s = f * \bar{q}_{inj} (bbl / day) * \bar{t} (days) = 425bbl$$

**Table 3.5 – Swept pore volume calculation (Well 19) using tritium.**

Time (days)	Concentration (ppm)	C*Time (ppm-day)	Delt, Δt (days)	C*Time* Δt (ppm-day <sup>2</sup> )	C*Delt(Δt) (ppm-day)
308	0	0	308	0	0
342	0	0	34	0	0
370	0	0	28	0	0
413	0.00035	0.144426	413	59.64798	0.144426
420	0.00021	0.088116	7	0.616812	0.001469
426	0.00035	0.148972	6	0.893833	0.002098
434	0.00042	0.182106	8	1.456851	0.003357
441	0.00042	0.185044	7	1.295305	0.002937
448	0.000559	0.250611	7	1.754278	0.003916
454	0.00042	0.190498	6	1.14299	0.002518
476	0.001608	0.765408	22	16.83898	0.035376
504	0.003427	1.727208	28	48.36182	0.095956
532	0.003427	1.823164	28	51.04859	0.095956
560	0.005315	2.9764	28	83.3392	0.14882
644=t	0.003217=C	2.071748	84	174.0268	0.270228
672=t <sub>b</sub>	0.001748=C <sub>b</sub>	1.174656	28	32.89037	0.048944
700	0			473.3138	0.856

### 3.3 Estimating average oil saturation using MOM

The estimation of oil saturation using tracers relies on the retardation of partitioning tracers on contacting oil in their migration path. This results in a time shift between the elution profiles of the conservative and partitioning tracers. As discussed in Chapter II, it is the difference in the

first temporal moments of the conservative and the partitioning tracers that facilitates saturation estimation.

As shown in Chapter II, to estimate saturation, we use the equations below:

$$S_o = \frac{1}{1 + k / \Delta t_r} \quad (3.8)$$

where,

$$\Delta t_r = \frac{\bar{t}_p - \bar{t}_n}{\bar{t}_n} \quad (3.9)$$

The subscripts  $p$ , and  $n$  represent partitioning and non-partitioning tracers respectively.

### 3.3.1 Estimating average oil saturation using tritium and TBA

The estimate of average oil saturation requires only knowledge of the first temporal moments of the elution profiles of both the conservative and partitioning tracers as well as the partitioning coefficient of the partitioning tracers. The observation data for the partitioning and conservative tracers are given in tables 3.6 and 3.7 respectively, while the elution profiles are shown in Figs. 3.3 and 3.4.

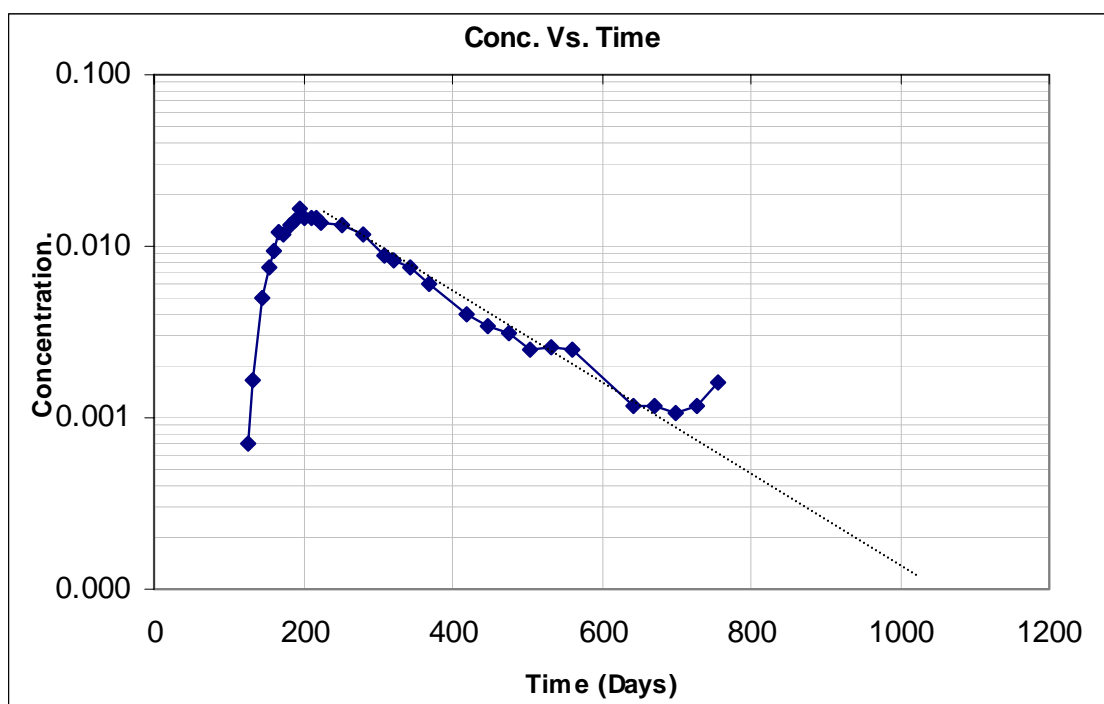


Fig. 3.3 – Semi-log plot of observed tritium concentration versus time for Well 37.

Table 3.6 – First temporal moment calculation (Well 37) using tritium.

Time	Conc	C*t	Delt.	C.t.Delt	C*Delt
120	0	0	120	0	0
126	0.0006993	0.088111804	126	11.10208728	0.088111804
133	0.001678	0.223174	7	1.562218	0.011746
146	0.004965	0.724889985	13	9.42356981	0.064544999
154	0.007552	1.163008031	8	9.304064246	0.060416002
161	0.009301	1.497461048	7	10.48222734	0.065107002
168	0.01196	2.00928	7	14.06496	0.08372
174	0.01154	2.00796	6	12.04776	0.06924
182	0.01329	2.41878	8	19.35024	0.10632
189	0.01427	2.69703	7	18.87921	0.09989
196	0.01643	3.22028	7	22.54196	0.11501
202	0.01441	2.91082	6	17.46492	0.08646
210	0.01455	3.0555	8	24.444	0.1164

**Table 3.6 continued**

Time	Conc	C*t	Delt.	C.t.Delt	C*Delt
217	0.01455	3.15735	7	22.10145	0.10185
224	0.01392	3.11808	7	21.82656	0.09744
252	0.01322	3.33144	28	93.28032	0.37016
280	0.01154	3.2312	28	90.4736	0.32312
308	0.008951	2.756907969	28	77.19342314	0.250627997
322	0.008322	2.679683871	14	37.5155742	0.116507994
342	0.007483	2.559185966	20	51.18371932	0.149659998
370	0.005944	2.199280037	28	61.57984104	0.166432003
420	0.004056	1.703520084	50	85.1760042	0.20280001
448	0.003427	1.535296	28	42.988288	0.095956
476	0.003147	1.497972	28	41.943216	0.088116
504	0.002517	1.26856805	28	35.51990541	0.070476003
532	0.002587	1.376283947	28	38.53595051	0.072435997
560	0.002517	1.409520056	28	39.46656157	0.070476003
644	0.001189	0.765716	84	64.320144	0.099876
				973.771774	3.242899811

$$\bar{t}_n = \frac{\left( \sum_0^{tb} C(t)t\Delta t \right) + a(a+t_b)C_b}{\left( \sum_0^{tb} C(t)t\Delta t \right) + aC_b} \approx 334.2days \quad (3.10)$$

where  $a$  is evaluated as shown previously from the exponential approximation.

Similar calculation for TBA elution profile in the same well (Fig. 3.4) gives

$$\bar{t}_p = \frac{\left( \sum_0^{tb} C(t)t\Delta t \right) + a(a+t_b)C_b}{\left( \sum_0^{tb} C(t)t\Delta t \right) + aC_b} \approx 380.061days \quad (3.11)$$

Hence, with a TBA partitioning coefficient of 0.2, substitution into Eq. 3.8 gives

$$S_o = \frac{1}{1 + \frac{0.2}{\left(\frac{329.114 - 334.2}{334.2}\right)}} = 0.436$$

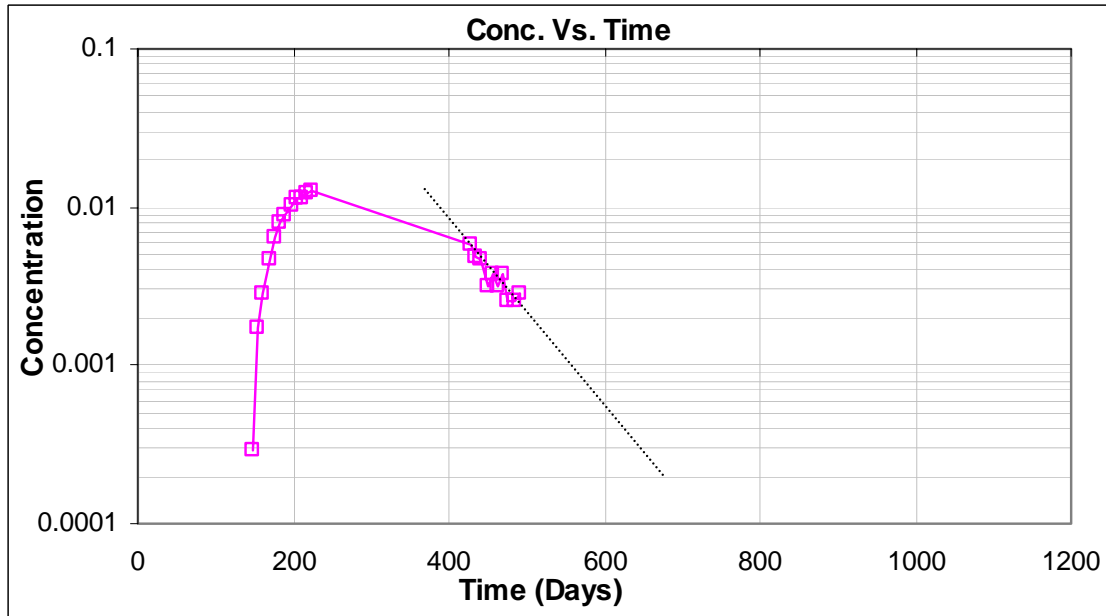


Fig. 3.4 – Semi-log plot of observed TBA concentration versus time for Well 37.

Table 3.7 – First temporal moment calculation (Well 37) using TBA.

Time	Conc	C*t	Delt.	C.t.Delt	C*Delt
126	0	0			
134	0	0			
141	0	0			
148	0.000288311	0.042670086	148	6.315172662	0.042670086
154	0.001729871	0.266400075	6	1.598400453	0.010379224
162	0.002883117	0.467065007	8	3.73652006	0.023064939
169	0.004612987	0.779594776	7	5.457163432	0.032290908
176	0.006342858	1.116342932	7	7.814400527	0.044400003
182	0.008072727	1.469236288	6	8.81541773	0.048436361
190	0.008937662	1.698155577	8	13.58524616	0.071501296

**Table 3.7 Continued**

Time	Conc	C*t	Delt.	C.t.Delt	C*Delt
197	0.010090909	1.987909027	7	13.91536319	0.070636361
204	0.011244156	2.293807763	7	16.05665434	0.07870909
210	0.011532467	2.421818091	6	14.53090855	0.069194803
218	0.012397402	2.702633725	8	21.6210698	0.099179219
225	0.012685714	2.854285607	7	19.97999925	0.088799997
428	0.005766234	2.467948007	203	500.9934454	1.170545433
434	0.004901298	2.12716334	6	12.76298004	0.029407788
442	0.004612987	2.038940183	8	16.31152147	0.036903895
449	0.003171429	1.42397155	7	9.967800847	0.022200002
456	0.003748051	1.709111447	7	11.96378013	0.02623636
462	0.003171429	1.465200125	6	8.791200747	0.019028573
470	0.003748051	1.761584167	8	14.09267334	0.029984411
477	0.002594805	1.237721899	7	8.664053294	0.018163634
484	0.002594805	1.255885533	7	8.79119873	0.018163634
490	0.002883117	1.412727492	6	8.47636495	0.017298704
				734.2413351	2.067194719

### 3.4 Results of MOM on Ranger field

The average swept pore volume, and saturation calculations were performed on four wells (19, 37, 39, and 40) in the area of interest using tritium, NaSCN, and TBA. These are detailed in the appendices A and B. The summary of the method of moments on these wells are shown in Table 3.8.



**Table 3.8 – Results of MOM calculations on Ranger.**

<b>tritium</b>	<b>Well 19</b>	<b>Well 37</b>	<b>Well 39</b>	<b>Well 40</b>
$f$ (Fraction of tracer produced)	0.0009	0.08	0.43	0.007
Net Swept Volume (bbls)	424	22800	120322	1130
Break Through* (days)	380	100	100	85
<b>sodium thiocyanate(NaSCN)</b>	<b>Well 19</b>	<b>Well 37</b>	<b>Well 39</b>	<b>Well 40</b>
$f$ (Fraction of tracer produced)	0.006	0.41	0.18	0.04
Net Swept Volume (bbls)	3058	109700	55903	7258
Break Through* (days)	420	95	150	65
<b>TBA and tritium</b>				
Average Oil Saturation	-	0.436	0.541	-
<b>TBA and NaSCN</b>				
Average Oil Saturation	-	0.491	0.388	-

\* Extrapolated estimates.

### 3.5 Discussion of MOM results

The chromatography delay in the tritium elution due to tritium exchange with immobile hydrogen as suggested by Lichtenberger<sup>11</sup> undermines the reliability of interpretations based on tritium data. Hence, in this research, whenever there is an inconsistency in the interpretation as given by tritium (HTO) data as compared with sodium thiocyanite (NaSCN), we have chosen to rather base analyses on NaSCN data.

Starting with the analyses of the conservative tracers, Table 3.8 shows a consistency in the fraction of tracers produced from Well-19 for both NaSCN and HTO. Also, both tracers indicate that the estimated breakthrough for Well-19 is the longest. Considering the spacing of wells (Fig. 3.1), this is evident of a non-preferential fluid migration in the north-west direction. This presumption is further buttressed by the estimated net swept volume being consistently the smallest for both HTO and NaSCN in Well-19.

The table also shows an agreement between HTO and NaSCN in analysis of tracer production at Well 40. This well records the shortest tracer breakthrough time of all the wells. However, it is worth noting that next to Well-19, the average net swept volume estimates from

tracer data in Well-40 is the smallest. Mindful of the spacing between the injector (Well-38) and producers (Well-40, and Well-39), an early tracer breakthrough with little swept volume is suggestive of high permeability streaks and small pore volume between the injector and Well-40 with a uniform porosity distribution across the field, the small pore-volume could be attributed to low Net-to-gross ratio (NTG) in this region.

A qualitative analysis of the region between the injector and Wells 39, and 37 poses a challenge as the HTO data for the wells are inconsistent with the NaSCN data. Since the reliability of HTO data is questionable, we base our analyses on NaSCN.

Results from the analyses on NaSCN indicate that Well-37 produced the largest amount of the tracer. Also, data shows that an earlier breakthrough occurs in Well-37 than Well-39. It would appear that there is a higher permeability trend in the region between the injector and Well-37 than that between the injector and Well-39 considering the larger spacing of Well-37 from the injector. The relatively quick breakthrough in Well-39 and associated large net swept volume estimate in this direction implies that not only a large permeability trend in this region but also, with a uniform porosity distribution across the reservoir, a high NTG ratio is expected in this region.

Average saturation estimates obtained by combining partitioning and conservative tracers are also given in Table 3.8. The higher partitioning coefficient of TBA over IPA and hence, greater sensitivity to saturation is the reason for its use in saturation estimation.

The table indicates that higher average oil saturation exists in the fluid migration path from the injector to Well-37 than the path from the injector to Well-39. The value of this information cannot be over stated as this presents us with the area of interest in an enhanced oil recovery project.

In summary, from the MOM calculations and ensuing analyses, we can qualitatively assess the area within the flood pattern. Assuming uniform porosity distribution, the deductions listed below can be made:

- Low permeability trend in the North –West direction
- Highest permeability trend and low NTG in the South-East direction
- High permeability and high NTG in the region south of the injector
- High oil saturations south of the injector.

**CHAPTER IV**  
**FUNDAMENTALS OF STREAMLINE BASED INVERSION**  
**APPROACH TO RESERVOIR CHARACTERIZATION USING PITT**

**4.1 Two-step inversion of partitioning interwell tracer tests (PITT)**

A schematic of a typical PITT response data is shown in Fig. 4.1. The approach to determining in-situ oil saturation from PITT data follows a two-step procedure. First inversion is done on the conservative tracer response to infer spatial distribution of permeability in the subsurface. Next, using this permeability distribution, the partitioning tracer response is inverted to determine the spatial distribution of remaining oil. With this saturation distribution, a check is made on the match of the conservative tracer, and if the match is unsatisfactory, a permeability inversion is again performed and this iterative procedure is followed until a satisfactory match on both tracers is obtained. In most cases, the first iteration will give sufficiently good results that can be improved upon only slightly with additional iterations. The streamline-based approach facilitates the two-step procedure because sensitivities of tracer response with respect to both permeability and saturation can be computed in a single simulation run.

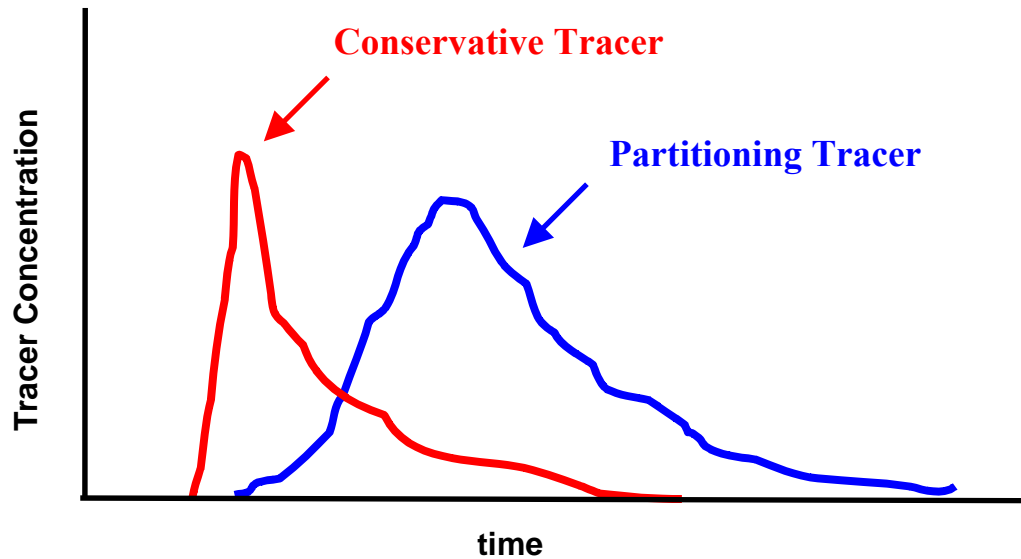


Fig. 4.1 – A schematic of typical PITT responses (Illiasov et al.<sup>2</sup>).

## 4.2 Summary of streamline-based inversion method

The streamline-based approach to production data integration, PITT data in particular, using streamline models follows the procedure outlined by Vasco et al.<sup>6</sup>, Yoon et al.<sup>7</sup> and most recently by Yoon.<sup>12</sup> Briefly, it involves the following major steps.

### 4.2.1 Analytic computation of sensitivity

Illasov et al.<sup>2</sup> derived an expression for sensitivity of time of flight to reservoir properties including permeability, porosity, and water saturation. The time of flight sensitivities can then be easily translated to tracer concentration sensitivities. The sensitivity computation involves simply evaluating one-dimensional integrals along streamlines and requires a single forward model run.

### 4.2.2 Generalized travel-time inversion

The approach to production data integration follows the concept of seismic travel time tomography and involves iterative linearization of the time of flight expression about a known initial model based on static data. Integration of production data involves a minimization of a least squares functional representing the difference between the observed data and the calculated response from a simulator. Production data misfit is represented by a generalized travel-time at each producing well. The generalized travel-time is computed by systematically shifting the

computed production response towards the observed data until the cross-correlation between the two is maximized. This concept is shown graphically in Fig. 4.2.

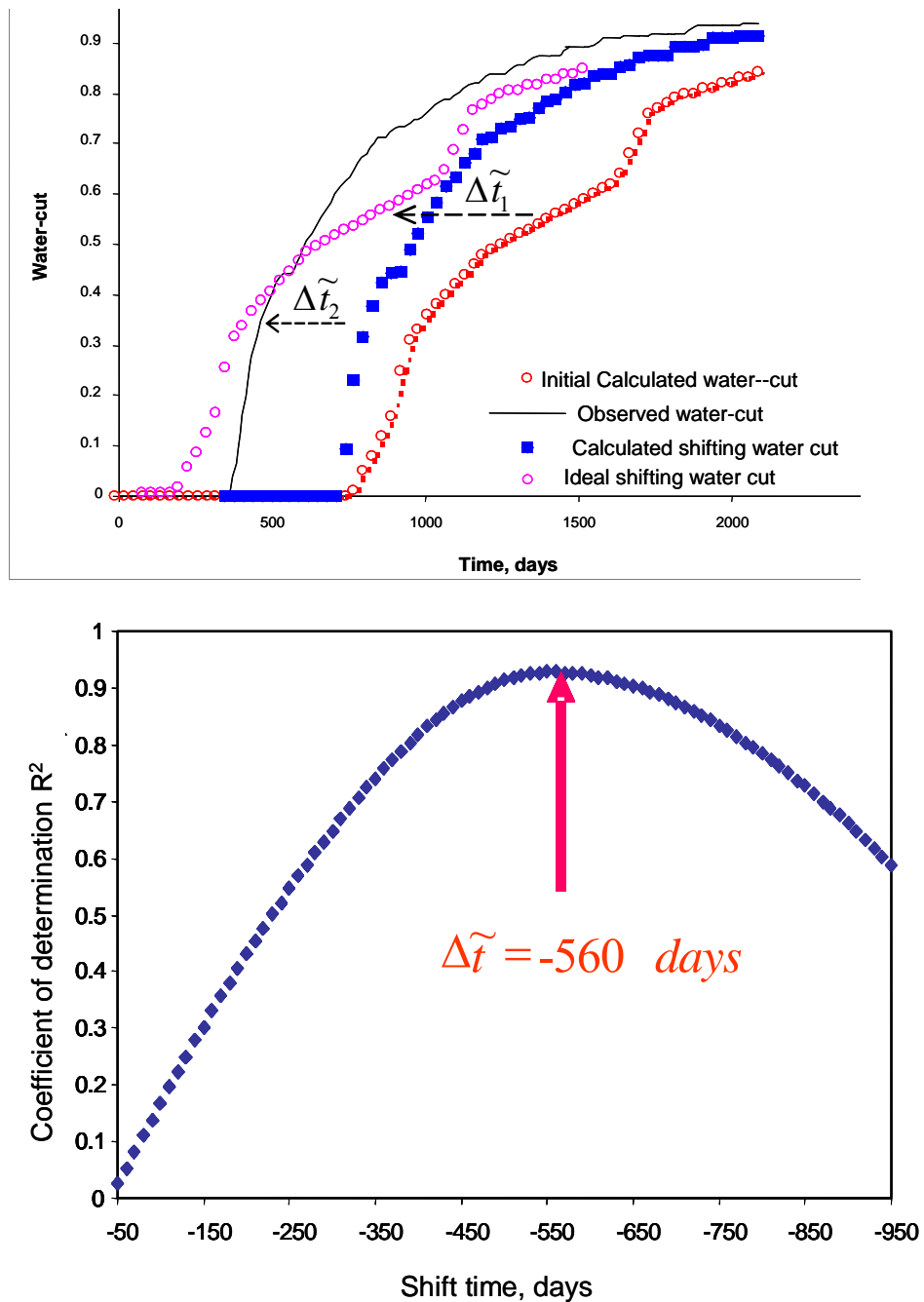


Fig.4.2 – Concept of generalized travel time. Data shift (top), optimal cross-correlation (bottom).

Production data misfit is most commonly represented as follows

$$J_p = \sum_{j=1}^{N_w} \sum_{i=1}^{N_{dj}} w_{ij} (y_j^{cal}(t_i) - y_j^{obs}(t_i))^2 \quad (4.1)$$

for  $i = 1, \dots, N_{dj}$ ,  $j = 1, \dots, N_w$ .

In Eq. 4.1,  $y_j(t_i)$  denotes the production data for well  $j$  at time  $t_i$ ,  $N_w$  and  $N_{dj}$  stand for the number of production wells and the number of observed data at each well, respectively and  $w_{ij}$  represents the data weights.

By defining a generalized travel-time, a match of the profile amplitudes is effectively achieved while most of the benefits of a ‘travel-time’ inversion are preserved. The approach entails determining, for each well, an optimal time-shift that minimizes the production data misfit at that well. The calculated response is systematically shifted in small time increments towards the observed response, and the data misfit is computed for each time increment. For a well  $j$ , the optimal shift will be given by the  $\Delta t_j$  that minimizes the misfit function Eq. (4.2),

$$J_p = \sum_{i=1}^{N_{dj}} [y_j^{obs}(t_i + \Delta t_j) - y_j^{cal}(t_i)]^2 = f(\Delta t_j) \quad (4.2)$$

or, alternatively maximizes the coefficient of determination given by

$$R^2(\Delta t_j) = 1 - \frac{\sum_{i=1}^{N_{dj}} [y_j^{obs}(t_i + \Delta t_j) - y_j^{cal}(t_i)]^2}{\sum_{i=1}^{N_{dj}} [y_j^{obs}(t_i) - \overline{y_j^{obs}(t_i)}]^2} \quad (4.3)$$

A detailed derivation of the sensitivity of the time-shift with respect to reservoir parameters is shown in Appendix C.

#### 4.2.3 Model assessment

Using techniques from geophysical inverse theory, we can quantify resolution and uncertainty associated with the permeability and saturation estimates obtained through inversion of the PITT data. This quantification requires computing model parameter resolution and covariance matrix as discussed by Datta-Gupta et al.<sup>36</sup>

### 4.3 Construction of inversion model

The primary objective of the inverse modeling is to find properties of the reservoir system that would minimize the differences between observed responses and the model's predictions. Mathematically, this can be expressed as

$$\min_{\mathbf{m}} \|\mathbf{d} - \mathbf{g}[\mathbf{m}]\|^2 \quad (4.4)$$

where  $\mathbf{d}$  is the data vector with  $N$  observations (observed tracer responses),  $\mathbf{g}$  is the forward model (simulated tracer responses),  $\mathbf{m}$  is the vector of  $M$  parameters (permeability and saturation for each gridblock in the model). Because of the nonlinearity between data and model parameters, we resort to an iterative minimization procedure. For example, at the  $k$ -th iteration step we obtain the following using a first order Taylor series expansion of  $\mathbf{g}[\mathbf{m}]$  around  $\mathbf{m}^k$ ,

$$\mathbf{g}[\mathbf{m}] = \mathbf{g}[\mathbf{m}^k] + \mathbf{G}\delta\mathbf{m} \quad (4.5)$$

where  $\delta\mathbf{m}$  is the parameter perturbation at  $k$ -th step and  $\mathbf{G}$  is the sensitivity matrix with sensitivity coefficient entries defined by

$$\mathbf{G} = \left. \frac{\partial \mathbf{g}[\mathbf{m}]}{\partial \mathbf{m}} \right|_{\mathbf{m}^k} \quad (4.6)$$

The residual (data misfit) vector  $\boldsymbol{\varepsilon}$  at the  $k$ -th iteration step will be given by

$$\boldsymbol{\varepsilon} = \mathbf{d} - \mathbf{g}[\mathbf{m}^k] \quad (4.7)$$

We can solve this linear system for  $\delta\mathbf{m}$  at each step by minimizing the linear least squares

$$J = \|\boldsymbol{\varepsilon} - \mathbf{G}\delta\mathbf{m}\|^2 = \sum_{i=1}^N \left( \varepsilon_i - \sum_{j=1}^M G_{ij} \delta m_j \right)^2 \quad (4.8)$$

and update our parameter vector with

$$\mathbf{m} = \mathbf{m}^k + \delta\mathbf{m} \quad (4.9)$$

In field situations, very often we have a large number of unknown parameters and limited measurements. Thus, the inverse problem tends to be ill-posed.<sup>14</sup> Solutions of such ill-posed problems suffer from non-uniqueness and instability. To circumvent the problem, we augment

the linear system of Eq. 4.4 by incorporating additional penalty terms, called the regularization. Two common approaches are to include model norm and model roughness constraints.

The regularized inverse problem entails solution of the following augmented objective function minimization.

$$J = \|\boldsymbol{\varepsilon} - \mathbf{G}\boldsymbol{\delta\mathbf{m}}\|^2 + \gamma_1^2 \|\boldsymbol{\delta\mathbf{m}}\|^2 + \gamma_2^2 \|\mathbf{L}\boldsymbol{\delta\mathbf{m}}\|^2 \quad (4.10)$$

where the respective terms are the data misfit, model norm constraint, and model roughness constraint and  $\gamma$ 's are the weighting factors for the model norm and roughness terms. The minimization of Eq. 4.10 is equivalent to solving the following augmented linear system in a least square sense,

$$\min_{\boldsymbol{\delta\mathbf{m}}} \left\| \begin{bmatrix} \mathbf{G} \\ \gamma_1 \mathbf{I} \\ \gamma_2 \mathbf{L} \end{bmatrix} \boldsymbol{\delta\mathbf{m}} - \begin{bmatrix} \boldsymbol{\varepsilon} \\ \mathbf{0} \\ \mathbf{0} \end{bmatrix} \right\|^2 \quad (4.11)$$

where,  $I$  is the identity matrix and  $L$ , a spatial difference operator of the form;

$$L = \begin{bmatrix} 1 & -1 & 0 & 0 \\ 0 & 1 & -1 & 0 \\ 0 & 0 & 1 & -1 \\ 0 & 0 & 0 & 1 \end{bmatrix}$$

for example the second spatial derivative of parameters measuring the model roughness. An iterative sparse matrix solver, LSQR<sup>15</sup> is used for solving this augmented linear system efficiently.

The norm constraint regulates how much the post-inversion model may differ from the initial model. By assigning a higher weighting factor to the norm constraint, we force the inversion to find the best match possible with a model that is not significantly different from the original model. We would do this if we were confident in the initial model and did not want the inversion to change it significantly. If, on the contrary, we think that the initial model is not very good and we can change it considerably, we relax the norm constraint by applying a lower weighting factor. This would allow the model to make larger departures from the initial model to better match the observed data.



The roughness constraint limits spatial roughness of the post-inversion parameter field or, in other words, limits by how much the neighboring parameter values differ from each other. Physically, this constraint accounts for the fact that production data is an integrated response and is best suited to resolve large-scale trends rather than small-scale fluctuations. Thus, by varying the weighting factor associated with the roughness constraint, we control to what degree we allow the inversion to make small-scale changes to the parameter field.

Overall, selection of the weighting factors is largely a trade-off between how well we want to match the observed data and by how much we allow the model to depart from the initial parameter field. If we already have a good initial model, we would start with relatively large weighting factors. However, with these weights, we may not be able to achieve a satisfactory match of the observed data. We then can either accept the match for the given deviation from the initial model or can continuously relax the constraints to allow the inversion to make larger and smaller-scale changes to the initial model. In most cases, achieving the best match of the observed data with the minimum changes to the initial model is our goal. Thus, usually, we would want to have the highest weights associated with each of the constraints that would still result in an acceptable match of the observed data.

#### **4.4 Fundamentals of streamline simulation for obtaining analytical sensitivities**

In this research, we used a finite difference simulator as the forward model and obtained sensitivities computed analytically along streamlines for the inversion phase for computational efficiency. The basis of computation of sensitivities along streamlines is highlighted below.

##### **4.4.1 Streamline simulation fundamentals**

The governing equation for fluid flow in porous media is based on the fundamental laws of physics. Conventional reservoir simulators solve the differential governing equation that is based on the following three equations: 1) Continuity Equation (Conservation of Mass), 2) Darcy Equation: empirical solution of Equation of Motion (Conservation of Momentum), and 3) Equation of State. Streamline simulators share the same basis. However, for incompressible flow movement, as often assumed in conventional streamline simulators, the EOS does not play any role. Although we can easily generalize our mathematical expressions into three-phase compressible fluid flow and gravity dominated flow, we will keep our interests in the case of

two-phase incompressible flow with no gravity effect for simplicity. There are four major steps in streamline simulation.

Step 1: Solving for pressure

Given petrophysical properties and boundary conditions, assuming steady state, pressure field is computed on physical grid like the way the FDM simulator does.

Step 2: Streamline tracing and time of flight computation

Based on the pressure field, velocity field is generated and streamline is traced. Then particle traveltime along streamline is computed. Using calculated travel time, we perform a coordinate transformation from 3D spatial coordinate into 1D traveltime coordinate along streamline, also referred to as ‘time of flight’ coordinate.

Step 3: Saturation advancing along streamlines

Taking advantage of the properties of the 1D traveltime coordinate system, fluid saturation is advanced along the streamlines by solving the 1D saturation equation analytically or numerically. Finally the saturation along streamlines are mapped back into the 3D spatial coordinate system onto the underlying grid.

Step 4: Pressure updating

Occasional pressure updating is necessary to take into account of total mobility changes due to saturation changes over times or well condition changes. For this updated pressure field, the streamlines are retraced and saturation is computed again.

These steps represent the streamline approach to simulation. For the robustness and generality, we have substituted the forward modeling aspect with conventional Finite Difference simulation. Hence, the approach in this research as detailed in chapter 5 eliminates steps 1 and 3.

#### 4.4.2 Convective tracer transport

Because tracers are often injected as a finite slug in small quantities, avoiding numerical dispersion in tracer transport modeling is a major concern. Utilizing streamline method in solute transport modeling is particularly useful because of its dispersion free simulation characteristic. For a solute transport, the convection-diffusion equation is given as

$$\phi \frac{\partial C(\mathbf{x}, t)}{\partial t} = \nabla \cdot [\mathbf{D}(\mathbf{x}) \cdot \nabla C(\mathbf{x}, t)] - \mathbf{v} \cdot \nabla C(\mathbf{x}, t) \quad (4.12)$$

where  $C$  is the tracer concentration and  $\mathbf{D}$  is the dispersion coefficient. If we assume convective transport only due to heterogeneous flow geometry, the neutral tracer transport equation becomes

$$\phi \frac{\partial C(\mathbf{x}, t)}{\partial t} + \mathbf{v} \cdot \nabla C(\mathbf{x}, t) = 0 \quad (4.13)$$

Neglecting dispersion effects is a tolerable assumption for the field-scale solute transports, because the macroscopic mixing is mainly attributed to the convective velocity variations from the subsurface heterogeneity. Applying coordinate transformation to time of flight, equation describing the transport of a neutral tracer in a heterogeneous permeable medium, Eq. 4.13, can be written in the time of flight coordinates as follows

$$\frac{\partial C(\tau, t)}{\partial t} + \frac{\partial C(\tau, t)}{\partial \tau} = 0 \quad (4.14)$$

For a unit impulse concentration source at  $(\tau, t) = (0, 0)$ , the solution to the above equation or the impulse response is given by

$$C(\mathbf{x}, t) = \delta(t - \tau(\mathbf{x})) \quad (4.15)$$

where  $\delta$  is the Dirac delta function. For an input with temporal variation  $C_0(t)$  at injection well, the observed concentration at producer can be obtained by convolution of the input and the impulse response as

$$C(t) = C_0(t - \tau) \quad (4.16)$$

The overall concentration response at the producer will be given by summing over the responses from all the streamlines reaching the producing well. The tracer response at a producer is obtained by integrating the contributions of individual streamlines

$$C(t) = \int_{all \psi} C_0(t - \tau) d\psi \quad (4.17)$$

Crane and Blunt<sup>16</sup> provides recent review of the convective as well as reactive solute transport modeling using streamline models.

#### 4.4.3 Computation of sensitivity of tracer response to reservoir parameters

Sensitivity calculations constitute a critical aspect of inverse modeling. By sensitivity, we mean the partial derivative of the production response with respect to model parameters such as permeability, porosity and saturation. Although several methods are available for computing sensitivities, for example, numerical perturbation method, direct method, or adjoint state method, these are limited by their computational costs and complex implementations. The streamline-based analytic sensitivity computation approach is extremely efficient and requires only a single simulation run.

For incompressible waterflooding in nondeformable media and given constant well conditions, change of pressure profile (and consequently of streamline trajectory) is mainly due to total mobility change via saturation change. However, the total mobility stays more or less constant for most of the moderate to unfavorable mobility ratio waterflooding, making stationary streamline assumption quite tolerable. Yoon<sup>12</sup> presented a synthetic waterflooding example for the end point mobility ratio of 1.43 that verified the assumption above. He demonstrated that a saturation solution with one pressure solving was nearly identical to the saturation from the numerical solution with 10 pressure solving. No significant difference among the saturation profiles indicates that single pressure update at the beginning of simulation and stationary streamlines thereafter would be a valid assumption.

It is possible to analytically derive a relationship between perturbations in reservoir properties, such as permeability, porosity or saturation, and changes in dynamic data such as water-cut and tracer response under the stationary streamline assumption. The relationship can be framed entirely in terms of quantities computed by a streamline simulator. Then sensitivities of the production response with respect to reservoir parameters are formulated along streamlines.

As described earlier, streamline method decouples flow and transport by a coordinate transformation from the physical space to one following flow directions - the tracer time of flight along streamlines. The time of flight can be defined as

$$\tau = \int_{\psi} s(\mathbf{x}) dr \quad (4.18)$$

where the integral is along the streamline trajectory,  $\psi$ ,  $r$  is measured along streamlines, and  $s(\mathbf{x})$  is the ‘slowness’, defined as a reciprocal of magnitude of interstitial velocity  $\mathbf{v}$  adjusted for partitioning properties of the tracer, is given by

$$s(\mathbf{x}) = \frac{1}{|\nu(\mathbf{x})|} (S_w + K_o S_o) \quad (4.19)$$

where  $K_o$  is the partitioning coefficient of tracer defined as the ratio of tracer concentration in oil phase to that in water phase. Introducing the Darcy equation, the slowness becomes

$$s(\mathbf{x}) = \frac{\phi(\mathbf{x})}{\lambda_t k(\mathbf{x}) |\nabla P|} (S_w + K_o S_o) \quad (4.20)$$

Because  $s(\mathbf{x})$  is a composite function involving reservoir properties, its first order variation will be given by

$$\delta s(\mathbf{x}) = \frac{\partial s(\mathbf{x})}{\partial k} \delta k(\mathbf{x}) + \frac{\partial s(\mathbf{x})}{\partial \phi} \delta \phi(\mathbf{x}) + \frac{\partial s(\mathbf{x})}{\partial S_w} \delta S_w \quad (4.21)$$

where the partial derivatives are

$$\begin{aligned} \frac{\partial s(\mathbf{x})}{\partial k} &= \frac{-\phi(\mathbf{x})}{\lambda_t k^2(\mathbf{x}) |\nabla P|} (S_w + K_o S_o) = -\frac{s(\mathbf{x})}{k} \\ \frac{\partial s(\mathbf{x})}{\partial \phi} &= \frac{1}{\lambda_t k(\mathbf{x}) |\nabla P|} (S_w + K_o S_o) = \frac{s(\mathbf{x})}{\phi} \\ \frac{\partial s(\mathbf{x})}{\partial S_w} &= \frac{\phi(\mathbf{x})}{\lambda_t k(\mathbf{x}) |\nabla P|} (1 - K_o) = \frac{(1 - K_o)}{(S_w + K_o S_o)} s(\mathbf{x}) \end{aligned} \quad (4.22)$$

Note that for unit partitioning coefficient, the tracer response will be insensitive to saturation changes as one might expect. Also, in the above expressions, we have ignored pressure changes resulting from small variations in permeability and assumed that the end point water relative permeability varies little with saturation change near residual oil saturation (Yoon<sup>12</sup>). Under these assumptions, since streamline trajectory is a function of pressure, it is natural to assume that streamlines do not shift as a result of small perturbation in permeability or saturation. Now it is possible to relate the change in traveltime  $\delta\tau$  to the change in slowness:

$$\delta\tau = \int_{\psi} \delta s(\mathbf{x}) dr = \int_{\psi} \left[ -\frac{s(\mathbf{x})}{k(\mathbf{x})} \delta k(\mathbf{x}) + \frac{s(\mathbf{x})}{\phi(\mathbf{x})} \delta \phi(\mathbf{x}) + \frac{(1 - K_o)}{(S_w + K_o S_o)} s(\mathbf{x}) \delta S_w \right] dr \quad (4.23)$$

Under the stationary streamline assumption, streamline tracer traveltime sensitivity along a single streamline  $\psi$  at a producer with respect to permeability, porosity, and saturation at

particular grid block containing  $\mathbf{x}$  is given by integrating Eq. 4.24 from the inlet to the outlet of streamline within the grid block:

$$\begin{aligned}\frac{\partial \tau(\psi)}{\partial k} &= \int_{inlet}^{outlet} \left[ -\frac{s(\mathbf{x})}{k(\mathbf{x})} \right] dr(\psi) \\ \frac{\partial \tau(\psi)}{\partial \phi} &= \int_{inlet}^{outlet} \left[ \frac{s(\mathbf{x})}{\phi(\mathbf{x})} \right] dr(\psi) \\ \frac{\partial \tau(\psi)}{\partial S_w} &= \int_{inlet}^{outlet} \left[ \frac{(1 - K_o)}{(S_w + K_o S_o)} s(\mathbf{x}) \right] dr(\psi)\end{aligned}\tag{4.24}$$

Note that the slowness in the grid block of interest is known from pressure solution and the integration can be carried out while tracing streamlines. The traveltime sensitivity can then be obtained by integrating the streamline sensitivities over all streamlines contributing a producer from a single streamline simulation.

For an injected concentration history  $C_0(t)$ , the corresponding tracer concentration response at the producer along with single streamline can be written as

$$C(t) = C_0 \left( t - \int_{\psi} s(\mathbf{x}) dr \right)\tag{4.25}$$

Consider a small perturbation in reservoir properties about an initial reservoir model,  $\delta \mathbf{m}$ . The resulting changes in slowness and tracer concentrations can be written as

$$\begin{aligned}s(\mathbf{x}) &= s^0(\mathbf{x}) + \delta s(\mathbf{x}) \\ C(\mathbf{x}, t) &= C^0(\mathbf{x}, t) + \delta C(\mathbf{x}, t)\end{aligned}\tag{4.26}$$

where  $s^0$  and  $C^0$  are initial slowness distribution in the reservoir and the associated tracer response, respectively.

If we assume that streamlines do not shift as a result of small perturbations in medium properties, then the change in concentration response at the producing well can be derived based on a Taylor series expansion<sup>35</sup>

$$\delta C(\mathbf{x}, t) = -C_0'(t - \tau) \int_{\psi} \delta s(\mathbf{x}) dr\tag{4.27}$$

Tracer travel time and concentration sensitivities with respect to permeability, porosity, and water saturation can be obtained by integrating Eq. 4.27 over all streamlines contributing to a producer.

Also, we can see that the above expressions for sensitivity of tracer concentration and water cut response only involve quantities that are readily available once we generate the velocity field and define the streamline trajectories in a streamline simulator. Thus, in a single forward run of a streamline simulator we may derive all the sensitivity coefficients required to solve the inverse problem.

The estimated change in  $\delta C$  due to a perturbation in reservoir properties,  $\delta \mathbf{m}$ , is used in construction of sensitivity matrix,  $\mathbf{G}$ , for minimization of the objective function

#### 4.4.4 Accounting for mobile oil saturations

The general form of Eq. 4.12 for an ideal water flood tracer is given by

$$\phi \frac{\partial((S_w + K_o S_o).C)}{\partial t} + \vec{u} \cdot \nabla((F_w + K_o F_o).C) = Q_i M \delta(t) \quad (4.28)$$

The source term represents a spike of tracer of total mass or activity M, injected into the reservoir over a very short time interval. (For a finite tracer slug, “t=0” corresponds to the time at which half the tracer has been injected. The delta function approximation is an excellent one at the field scale. Only the nearest and quickest of field tracer response curves have sufficiently small dispersion to resolve the width of the original spike). The velocity  $u$  is the total of the two phases, and is used to define the time of flight,

$$\vec{u} \cdot \nabla \tau = \phi \quad (4.29)$$

Expanding from conservation form and utilizing the time of flight gives

$$(S_w + K_o S_o) \frac{\partial C}{\partial \tau} + (F_w + K_o F_o) \quad (4.30)$$

In essence, compared to the total two phase flow, the tracer moves with a retardation factor of

$$\frac{S_w + K_o S_o}{F_w + K_o F_o} \quad (4.31)$$

The dependence of the retardation factor on fractional flow indicates that when both water and oil phases are flowing, the interpretation may be fairly complicated.

Taking the retardation factor into consideration, the “slowness” defined in Eq. 4.20 can be generalized as

$$s(\mathbf{x}) = \frac{\phi(\mathbf{x})}{\lambda_t k(\mathbf{x}) |\nabla P|} \left( \frac{S_w + K_o S_o}{F_w + K_o S_o} \right) \quad (4.32)$$

Since  $S(x)$  is a composite function involving reservoir properties, the partial derivatives of its first order variation will be given by

$$\frac{\partial s(x)}{\partial k} = \frac{\partial}{\partial k} \left\{ \left( \frac{S_w + K_o S_o}{F_w + K_o S_o} \right) \cdot \frac{\phi(\mathbf{x})}{\lambda_t k(\mathbf{x}) |\nabla P|} \right\} = \left( \frac{S_w + K_o S_o}{F_w + K_o S_o} \right) \cdot \frac{s(x)}{k(x)} \quad (4.33)$$

$$\frac{\partial s(x)}{\partial \phi} = \frac{\partial}{\partial \phi} \left\{ \left( \frac{S_w + K_o S_o}{F_w + K_o S_o} \right) \cdot \frac{\phi(\mathbf{x})}{\lambda_t k(\mathbf{x}) |\nabla P|} \right\} = \left( \frac{S_w + K_o S_o}{F_w + K_o S_o} \right) \cdot \frac{s(x)}{\phi(x)} \quad (4.34)$$

$$\frac{\partial s(x)}{\partial S_w} = \frac{\partial}{\partial S_w} \left\{ \left( \frac{S_w + K_o S_o}{F_w + K_o S_o} \right) \cdot \frac{\phi(\mathbf{x})}{\lambda_t k(\mathbf{x}) |\nabla P|} \right\} \quad (4.35)$$

Assuming total mobility is constant, the partial derivative in Eq. 4.35 reduces to

$$\frac{\partial s(x)}{\partial S_w} = \left\{ \frac{(1 - K_o) \left\{ (F_w + F_o K_o) - (S_w + S_o k_o) \frac{\partial f_w}{\partial S_w} \right\}}{(F_w + F_o K_o)^2} \right\} \cdot s(x) \quad (4.36)$$

It is these modifications made to the sensitivity calculations that facilitate the inversion process in the presence of mobile oil saturations.

#### 4.5 Inversion algorithm

Our approach of coupling the finite difference and streamline simulation to obtain a robust and efficient inversion algorithm neglects some of the procedures mentioned in the ‘streamline simulation fundamentals’ section. In our research, we employ ECLIPSE<sup>TM</sup> based on finite difference formulation as our forward model from which, fluxes at grid interfaces is obtained. With the fluxes, we trace the streamlines on which sensitivities are evaluated as 1-D integrals. The flowchart in Fig. 4.3 summarizes the algorithm. The algorithm is applied for permeability and saturation sequentially until an acceptable match is obtain on the tracer elution profiles.



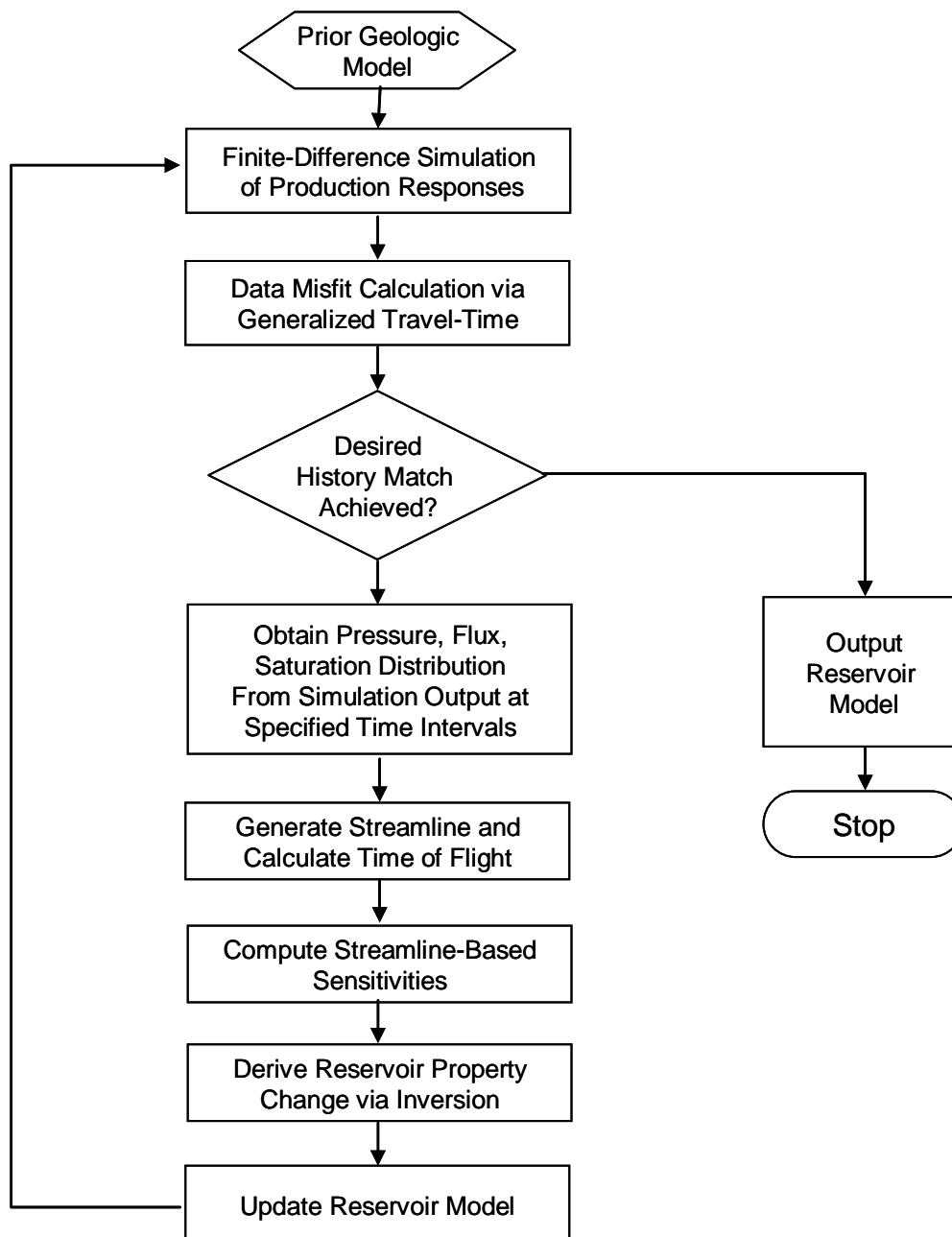


**Fig. 4.3 – Flowchart for history matching finite-difference models using streamline derived sensitivities.**

## CHAPTER V

### SYNTHETIC CASES ON SATURATION AND PERMEABILITY INVERSION

#### 5.1 Description of data set

The first synthetic case we applied the saturation inversion to is a two-dimensional homogenous reservoir with an inverted nine-spot waterflood scheme. The reservoir is divided into 21 grid blocks in both x and y directions with each grid block having a dimension of 52.86 X 52.86 X 37ft. The injected water was tagged with a partitioning tracer having a partitioning coefficient of 10, and the elution observed at the eight producing wells.

The reference saturation distribution is as shown in Fig. 5.1. As indicated in the legend, the top-left corner of the diagram represents a region of high oil saturation while the bottom-right corner is essentially water-filled.

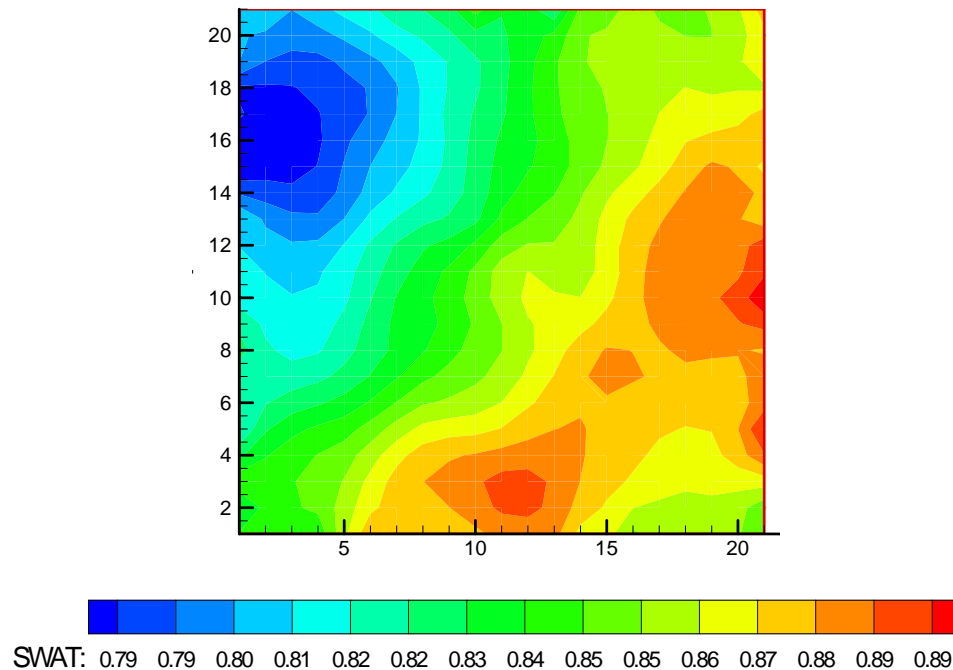


**Fig. 5.1 – Reference saturation distribution.**

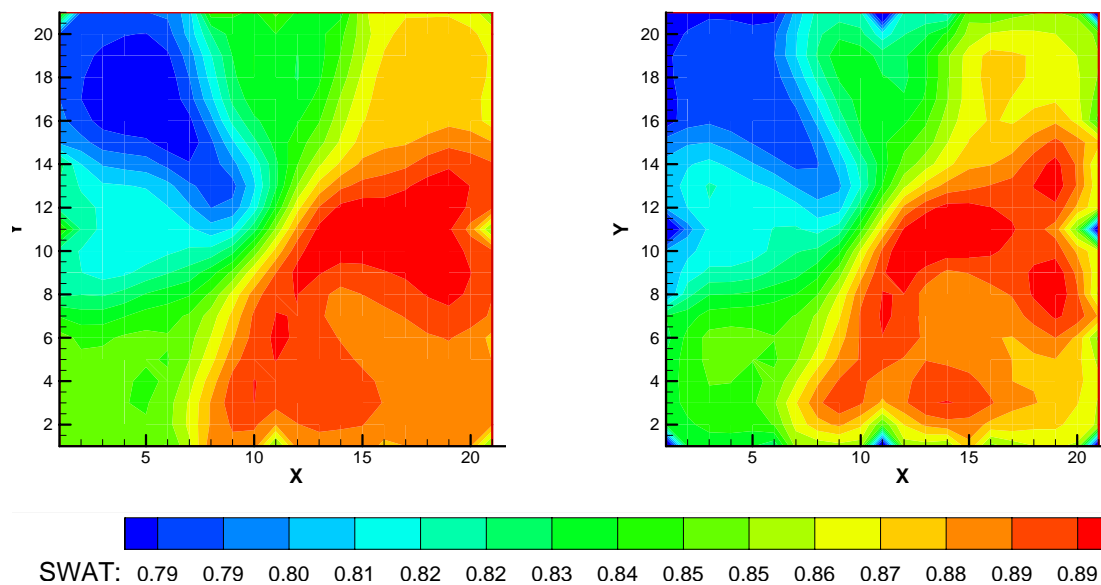
The observed tracer response from the producers was generated by running the forward model (Finite Difference Simulator) with the given data set.

Our objective was to reconstruct the reference saturation (Fig. 5.1) given only the observation data from the eight producers. In general, though not necessary, an inversion procedure has a reasonable prior (guess) model upon which the inversion process is based. When the inverse problem is highly non-unique, a good prior model becomes most essential. However, in reconstructing the saturation distribution, we started with two different prior models, both having uniform saturation distribution. We also demonstrate our extension of the works of Illiasov et al.<sup>2</sup> to situations in which mobile oil saturations exists in the reservoir.

## 5.2 Saturation inversion

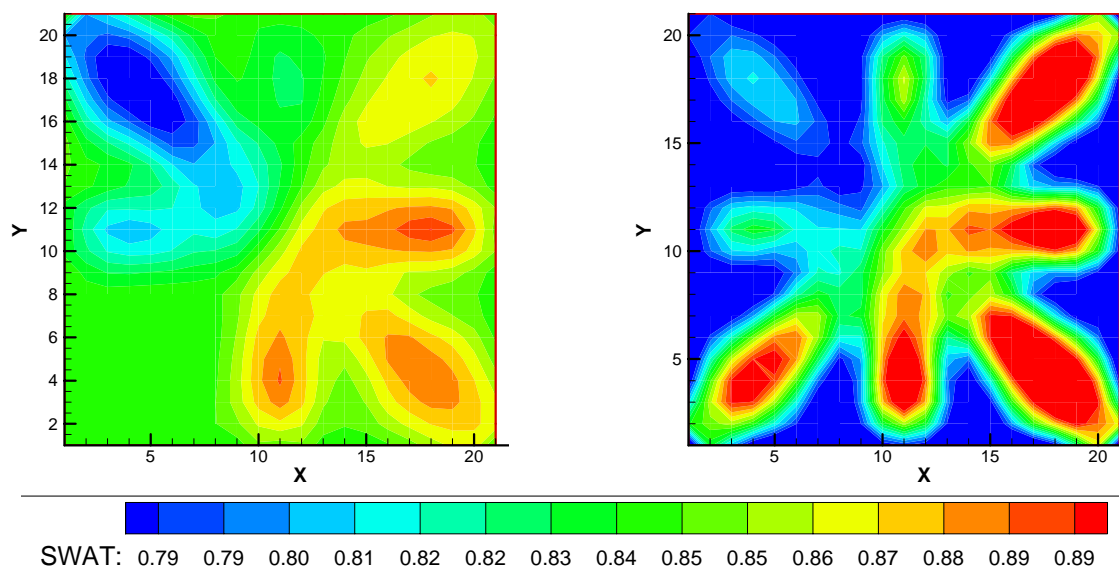
In our approach to the inversion, we applied the generalized travel-time inversion process discussed in chapter four. Our forward model was a commercial finite difference simulator (ECLIPSE<sup>TM</sup>) and we obtained the sensitivities as 1-D integrals along streamlines traced according to flux information obtained from the forward model.

After ten iterations, the reconstructed saturation distribution starting at uniform water saturations of 0.85 and 0.75 are shown in Fig. 5.2 (left and right respectively). A comparison with the reference saturation distribution (Fig. 5.1) indicates that the inversion result clearly resolves the regions of high and low oil saturations.



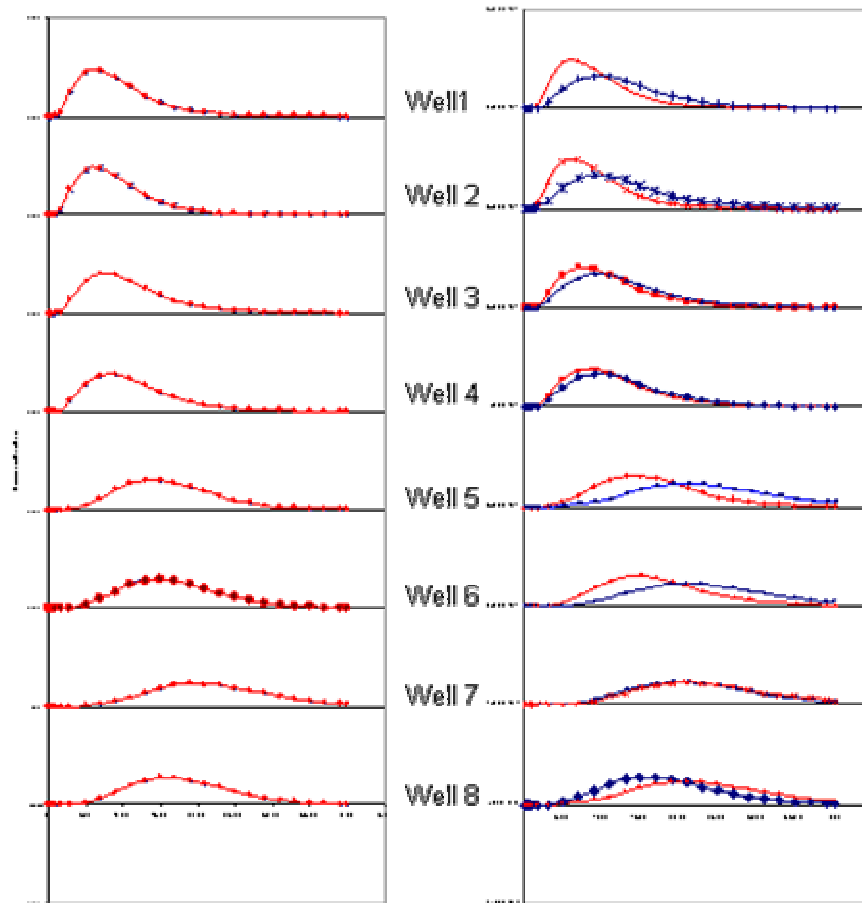
**Fig. 5.2 – Saturation distribution after inversion.**

Fig. 5.3 shows the reconstructed saturation distribution generated using the formulation of Illiasov et al.<sup>2</sup>. It is obvious that the formulation breaks down when the saturation is such as to permit mobility of the oil phase. It is important to note that this limitation actually extends beyond the permissible saturation values for the reference model. It also limits our prior model to immobile oil saturation distributions.



**Fig. 5.3 – Saturation distribution after inversion based on the formulation of Illiasov et al.**

The tracer elution profiles before and after the saturation inversion for all the producing wells are shown in Fig. 5.4. As the inversion is based on the minimization of the data misfit, it is seen that Well 7 has little contribution in reconstructing the saturation distribution as the prior model already gives a match on the observed elution profile at the well. Essentially, we were able to reconstruct the saturation distribution with seven of the eight producers.



**Fig. 5.4 – Initial (right) partitioning tracer elution observed and calculated from the eight producers versus final match (left) on saturation inversion.**

### 5.3 Permeability inversion

The same 2-D reservoir used for the saturation inversion discussed above was used as the synthetic model in testing our permeability inversion. The reference permeability field (Illiasov et al.) is shown in the Fig. 5.5. The saturation distribution is the reference saturation distribution

in Fig. 5.1. In the permeability inversion, the injected water is tagged with a conservative tracer as against the partitioning tracer used in the saturation inversion. Our approach is based on the two-step approach to the inversion of PITT<sup>2</sup> in which case the permeability field is regenerated through the inversion of the observed response of a conservative tracer and the saturation distribution is obtained by inverting the response of the partitioning tracer. However, the formulation is general and we could have reconstructed the permeability field through the inversion of the partitioning tracer as it is equally sensitive to permeability distribution.

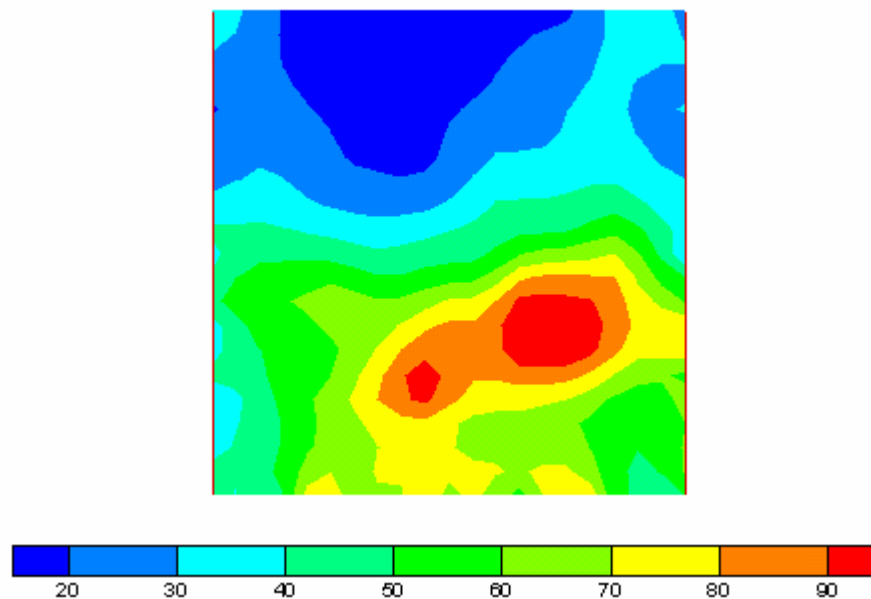


**Fig. 5.5 – Reference permeability distribution.**

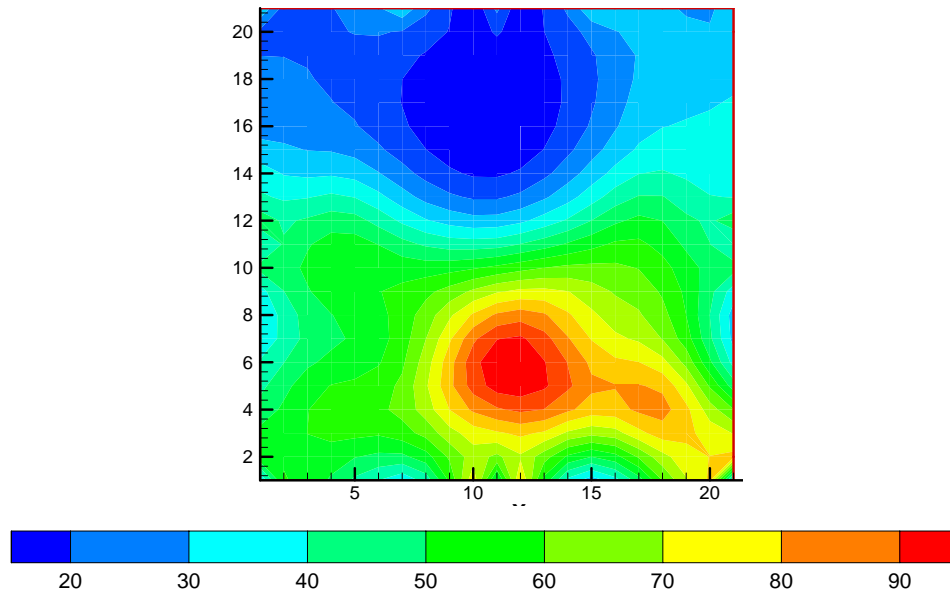


**Fig. 5.6 – Permeability distribution obtained on generalized travel-time inversion.**

Like we did in the saturation inversion we started with a uniform permeability close to the average of the true permeability field. The resulting permeability distribution after a few iterations of the generalized travel-time inversion is shown in Fig. 5.6. We see that the inversion process is able to identify the high as well as the low permeability regions. The data mismatch before and after the permeability inversion are shown in Fig. 5.7.

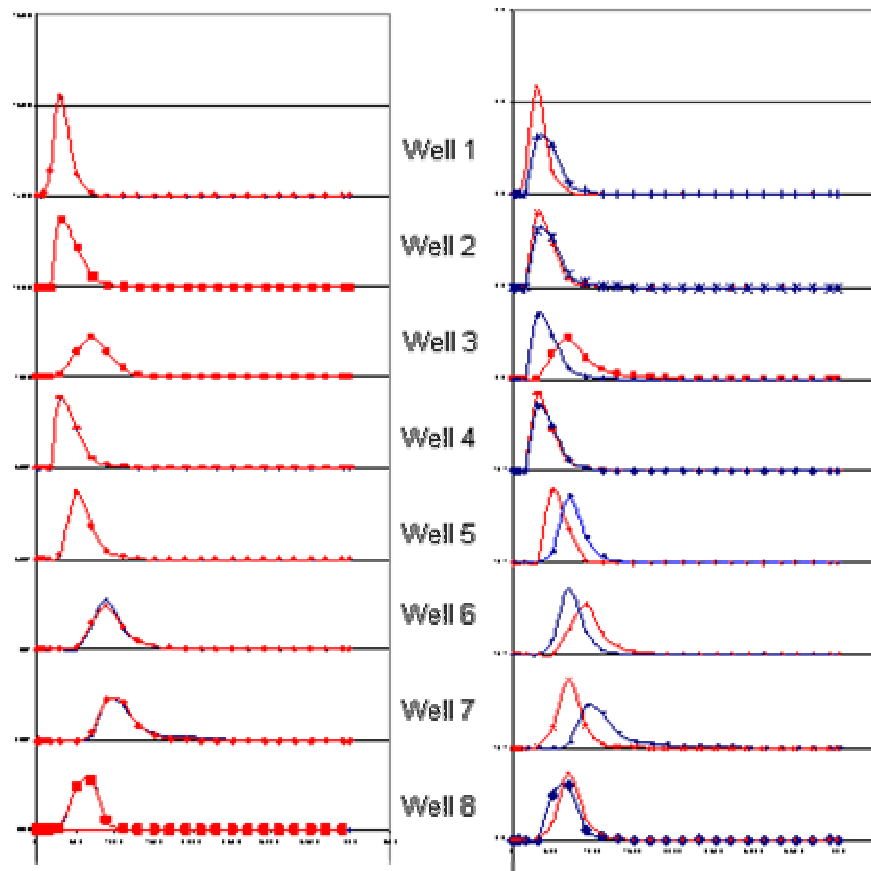


**Fig. 5.7 – Initial (right) conservative tracer elution observed and calculated from the eight producers versus final match (left) on permeability inversion.**

#### 5.4 Sequential inversion

Using the same reservoir model, the injected water was tagged with both a partitioning and a conservative tracer. The elution profile of both tracers was then observed at the eight producers. Our approach to reconstruction of the permeability and saturation distribution here is through a sequential inversion on permeability and saturation. Hence, starting with a uniform permeability and saturation distributions, a permeability inversion is done. With the resulting permeability distribution, a saturation inversion is performed. This represents a sequential iteration on both permeability and saturation. This sequential process is then performed for a preset number of iterations during which resulting permeability and saturation distributions are updated, resulting in a successive refining of both permeability and saturation distribution.



Three sequential iterations were performed on the synthetic case described above. The resulting permeability and saturation distribution after each iteration are shown in Fig. 5.8.

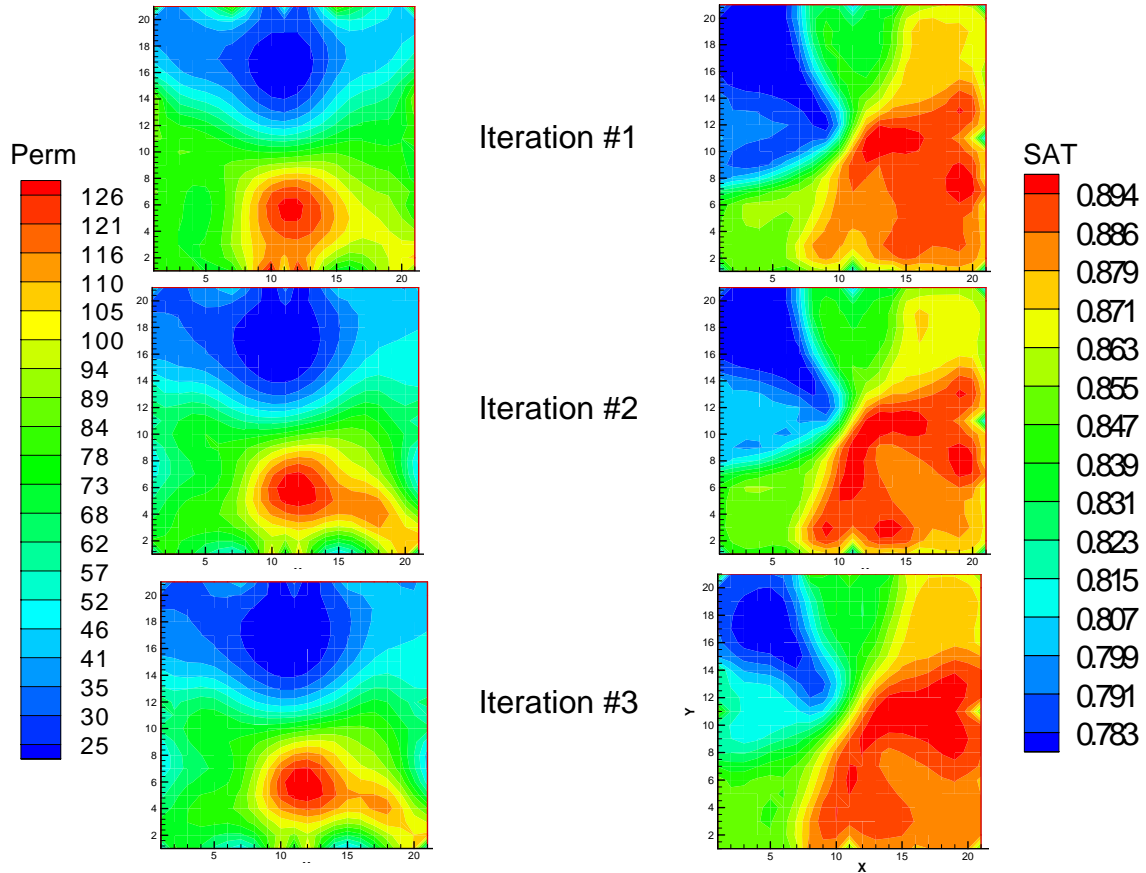


**Fig.5.8 – Refining of permeability and saturation distributions during sequential inversion.**

It is evident that with successive iterations, we obtain a refinement in our distribution estimates.

While refinements are obtained in the distribution estimates with successive sequential iterations, at the first sequential iteration, we see that regions of highs and lows are clearly identified. This is highlighted in the reduction in RMS error over the iterations as shown in Fig. 5.9. The drop in the RMS error is largest in the first sequential iteration for both saturation and permeability distributions. Subsequent sequential iterations result in comparatively insignificant RMS error in both travel time and amplitude.

Fig. 5.9 also shows the highly non-unique nature of saturation inversion. This is deduced from the almost perfect match obtained on saturation inversion at each estimate of permeability distribution. In contrast, the RMS error obtained on permeability inversion only reduces with refinement in saturation distribution estimate.

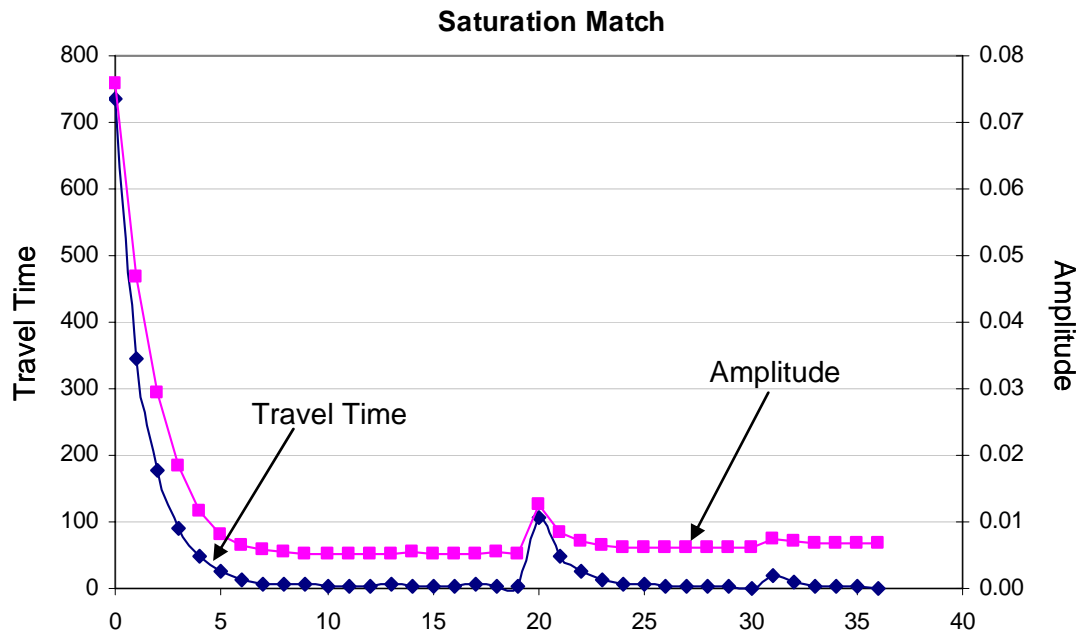


**Fig. 5.9 – RMS error on travel time and amplitude during sequential inversion (saturation).**

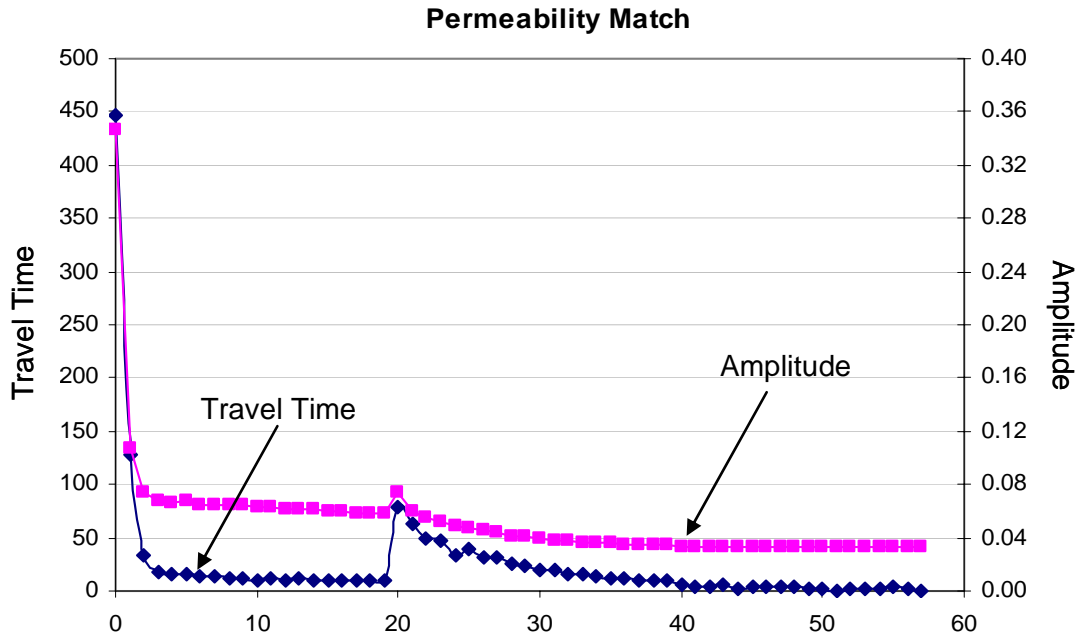


**Fig. 5.10 – RMS error on travel time and amplitude during sequential inversion (permeability).**

## 5.5 Conclusion

We have shown in this section that our approach of coupling the finite difference and the streamline simulator for a robust and computationally efficient inversion procedure is capable of reconstructing both permeability and saturation distribution through a minimization of the data misfit based on the generalized travel-time inversion.

We have also shown that our reformulation of the sensitivities for saturation inversion is necessary in order to obtain a representative saturation distribution without constraints on the prior model. That our approach works, gives us the confidence to apply the two-step inversion<sup>2</sup> to a field case. We apply our approach to the Ranger field case as discussed in Chapter VI.

## CHAPTER VI

### RANGER FIELD: INVERSION APPROACH TO RESERVOIR CHARACTERIZATION

#### 6.1 Description of data set

The Ranger field case is a multi-well, multi-tracer injection study carried out in the McClesky sandstone of the Ranger Field, Texas. This field has been the focus of a tracer study over the years due to the scale of the project as well as the availability of data set. Lichtenberger.<sup>11</sup> offered the first description of the data. Further description of the data set was provided by Allison<sup>9</sup> and Illiasov<sup>2</sup> in their M.S theses. In this research, we have used these references as the primary sources of our data set.

The 320 area of interest spans over 320 acres and includes 13 producers and 4 injectors injecting water tagged with 7 different tracers. The seven tracers injected includes 5 conservative tracers consisting of four decaying (tritium, Cobalt-57, Cobalt-58, Cobalt-60) and one chemical tracer (sodium thiocyanate, NaSCN) and two partitioning tracers (Tertiary butyl alcohol, TBA, and Isopropyl alcohol IPA).

All tracers were injected in small slugs on the same day except for TBA, which was injected in a small slug twenty days later than the others. Tracer sampling continued for 826 days after injection of the first set of tracers. Tracer injection pattern is shown in Fig. 6.1. Injection locations and the amounts of each tracer injected are given in Table 6.1. The partitioning coefficients defined as the ratio of tracer concentration in oil phase to that in water phase, of TBA and IPA are 0.2 and 0.04 respectively.

**Table 6.1 – Amount and injection location of tracer.**

<b>Tracer</b>	<b>Well</b>	<b>Amount</b>	<b>Half-life</b>
tritium	38	10 Ci	4475 days
NaSCN	38	5655 lbs	-
IPA	38	880 gals	-
TBA	38	880 gals	-
Co-57	41	30 mCi	270 days
Co-58	45	100 mCi	71 days
Co-60	42	30 mCi	1920 days

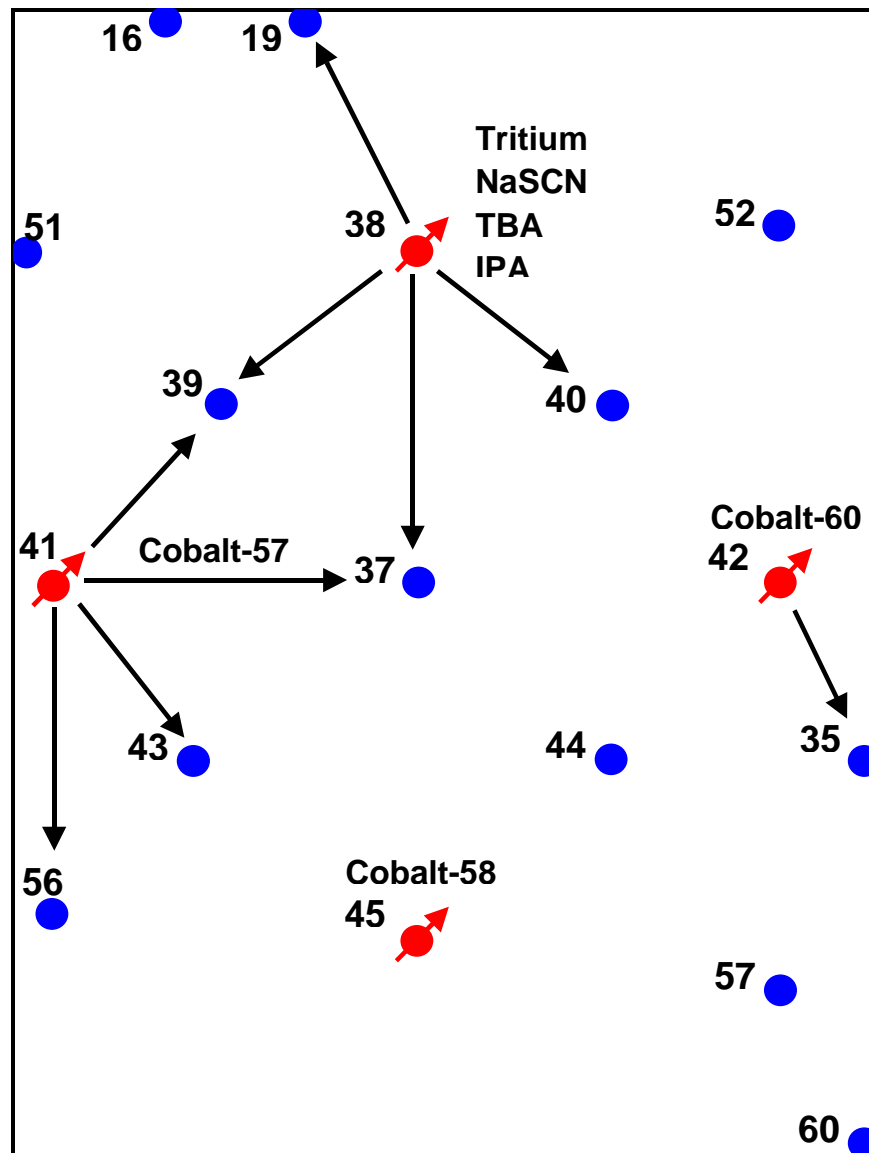


Fig. 6.1 – Tracer injection pattern (Illiasov<sup>2</sup>).

### 6.1.1 Reservoir model

Static reservoir model parameters are summarized in Table 6.2. For the purpose of comparing results, we used a 31x45x6 grid for this model, which corresponds to 100x100 ft grid blocks in both  $X$  and  $Y$  directions. A total of 141 core samples were available for analysis.

Analysis of the core data by Illiasov et al.<sup>2</sup> indicated little variation in porosity but significant heterogeneity as regards permeability, and an effective layering system. This led to the division

of the reservoir into six primary layers, and assigning uniform porosity to all the layers, with significant variation within and across the layers. The net thickness map from Lichtenberger<sup>11</sup> was incorporated in the form of Net-Gross ratio as shown in Figs. 6.2 and 6.3. Other parameters, such as depth, reservoir pressure and viscosity, were adopted from Allison.<sup>10</sup>

**Table 6.2 – Initial reservoir model (Illiasov et al.).**

<b>Parameter</b>	<b>Type</b>	<b>Value</b>
Depth	constant	3400 (ft)
Reservoir pressure	constant	150 (psia)
Porosity	uniform	0.1347 (fract)
Total gross thickness	constant	24 (ft)
Net thickness	NGR distribution	<b>Fig. 6.2</b>
Permeability	heterogeneous	Dykstra-Parson coefficient = 0.74 log-mean = 2.5 log-standard deviation = 0.57
Initial oil saturation	uniform	0.45 and 0.60 (fract)
Inversion oil saturation range		min – 0.3 (fract) max – 0.7 (fract)
Fluid viscosity	oil water	2.7 (cp) 0.5 (cp)

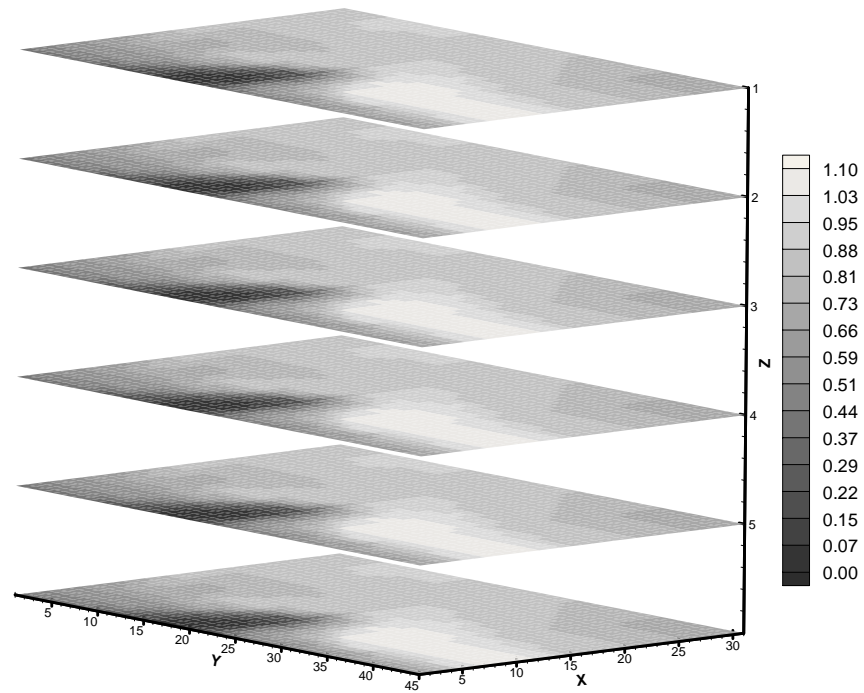


**Fig. 6.2 – Net-gross ratio distribution – layered view (Illiasov<sup>2</sup>).**

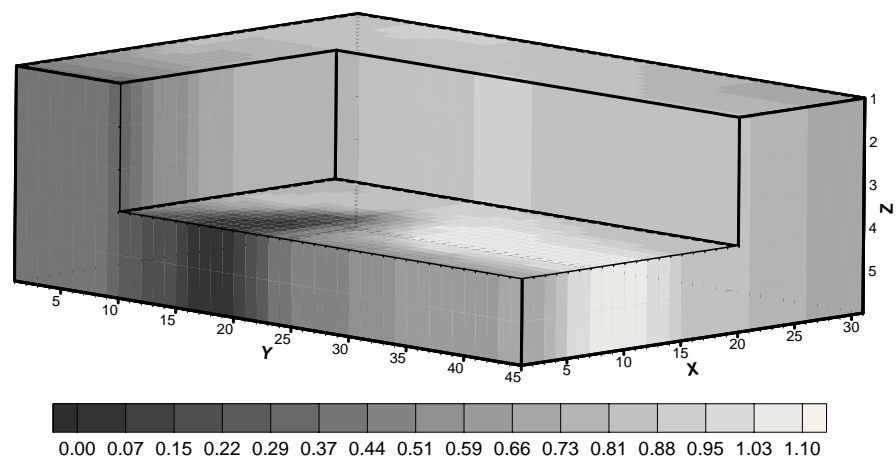


**Fig. 6.3 – Net-gross ratio distribution – 3D cut-away view (Illiasov<sup>2</sup>).**



### Permeability distribution

From the core data, Illiasov et al.<sup>2</sup> generated a cumulative distribution function of the log of permeability from which the Dykstra Parson's coefficient of variation was estimated. Using the  $V_{DP}$ , a log-mean permeability and log-standard deviation was obtained.

Using Sequential Gaussian Simulation, an unconditioned permeability distribution was generated with the calculated mean permeability and variance with a spherical variogram of 500 and 5 ft horizontal and vertical range respectively.

The initial permeability field generated is shown in layered view in Fig. 6.4 and in a 3D cut-view in Fig. 6.5. The vertical permeability is set to one-tenth the value of the horizontal permeability data.

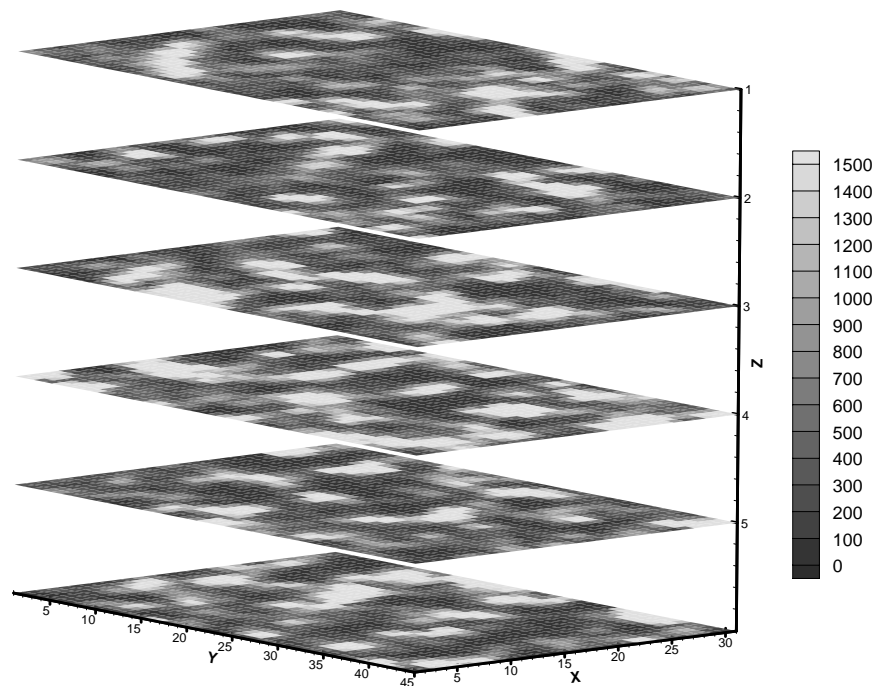


**Fig. 6.4 – Initial permeability distribution – layered view (Illiasov<sup>2</sup>).**

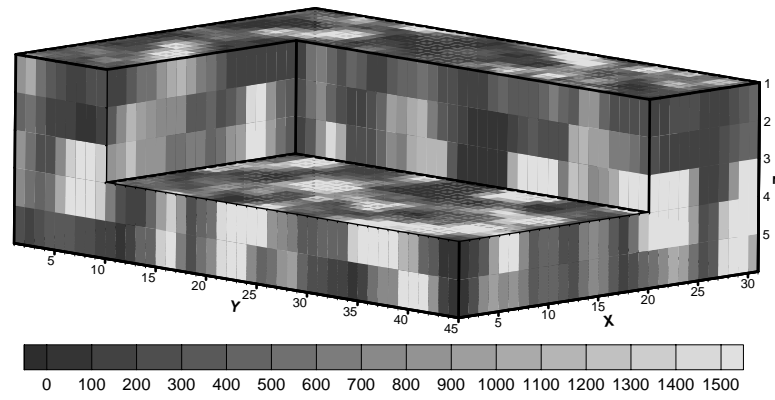


**Fig. 6.5 – Initial permeability distribution - 3D cut-away view (Illiasov<sup>2</sup>).**

### Relative permeability

Relative permeability data were fitted with the exponential relative permeability formulas with the parameters summarized in Table 6.3, similarly to Allison.<sup>10</sup>

**Table 6.3 – Relative permeability parameters.**

Parameter	Value
Irreducible water saturation, $S_{wirr}$	0.10
Residual to water oil saturation, $S_{owr}$	0.45
End-point water relative permeability at residual oil saturation, $K_{rw\ Sor}$	0.46
End-point oil relative permeability at irreducible water saturation, $K_{rw\ Swirr}$	0.66
Water relative permeability exponent	3.0
Oil relative permeability exponent	3.5

### Oil saturation

The reservoir is assumed to be at uniform oil saturation equal to 0.45. For saturation inversion cases, we set the maximum and minimum oil saturation to equal 0.55 and 0.2, respectively.

#### 6.1.1 Well production and injection rates

The production and injection rates used are obtained from Allison et al.<sup>9</sup>. For the purpose of precision, and reconstruction of representative permeability and saturation fields, we have used the actual rates for the inversion as opposed to the averaged rates used by Illiasov et al.<sup>2</sup> in their streamline-based inversion. The production history for all the wells is given in Table 6.4.

#### 6.1.2 Observed tracer data

As a precursor to oil saturation distribution determination, we deemed it necessary to determine the permeability distribution through an inversion on the conservative tracer. To facilitate inversion, the observed production data were smoothed using a moving average algorithm. The data were then normalized with the injection concentration, taking into account the 20 day delay in the injection of TBA as discussed in Chapter II. Out of the seven injected tracers, only NaSCN, tritium, TBA, and IPA were recovered in such quantities as would permit their use for inversion. The normalized plots of these tracers in the area of interest are shown in Figs. 6.6 to 6.8.

**Table 6.4 – Actual well production and injection rates.**

Wells	Time, days							
	0-100	101-200	201-300	301-400	401-500	501-600	601-700	701-826
<b>Production wells</b>	<b>Production rate, bbl/day</b>							
16	7	7	20	20	20	20	20	20
19	4	4	14	14	16	56	24	0
35	0	0	0	35	28	40	35	0
37	156	210	236	310	410	448	560	792
39	305	300	350	318	343	423	540	735
40	4	8	60	56	80	0	0	0
43	195	226	211	215	340	426	844	1002
44	59	89	139	139	139	178	175	178
51	14	14	43	43	43	43	43	43
52	10	10	10	10	10	10	10	10
56	37	36	19	66	75	79	95	164
57	42	42	42	42	42	42	42	42
60	20	20	20	20	20	20	20	20
<b>Injection wells</b>	<b>Injection rate, bbl/day</b>							
38	439	483	597	662	783	893	1176	1503
41	307	338	418	463	548	625	823	1052
42	88	97	119	132	157	179	235	301
45	44	48	60	66	78	89	118	150

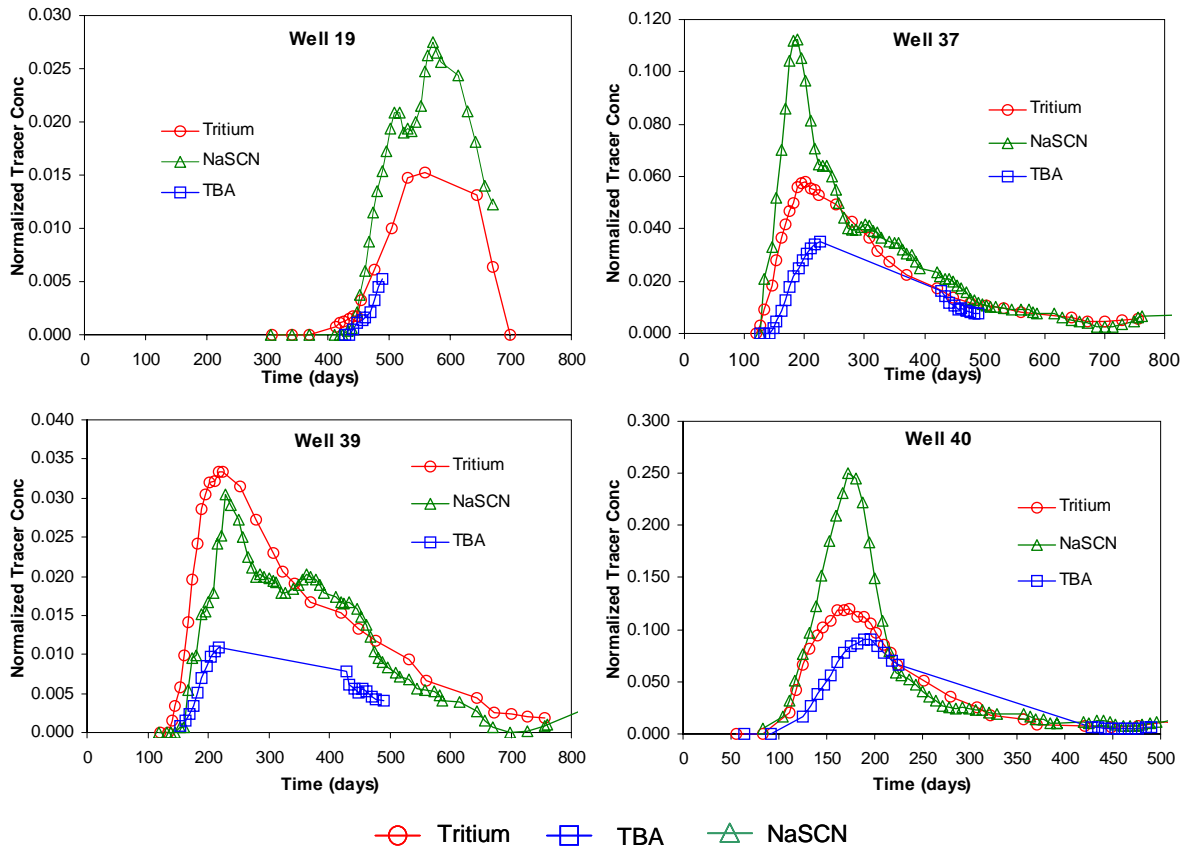
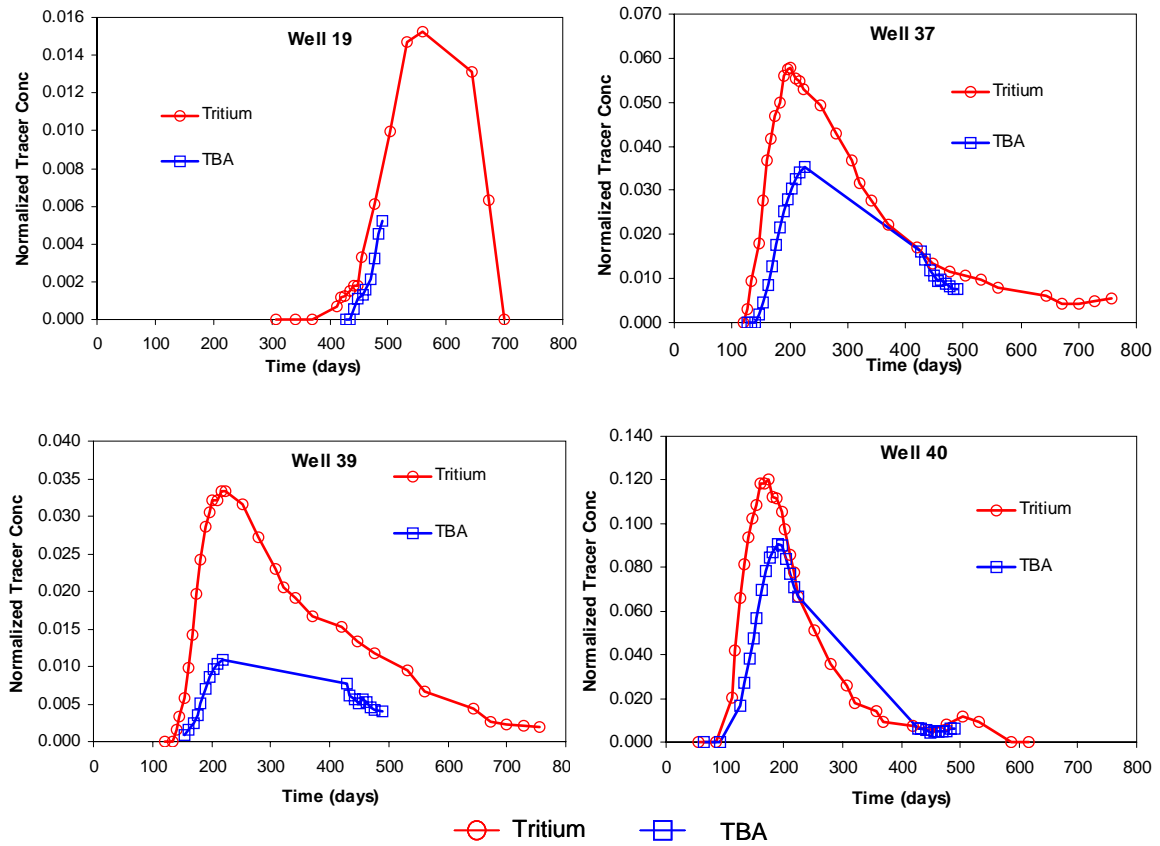
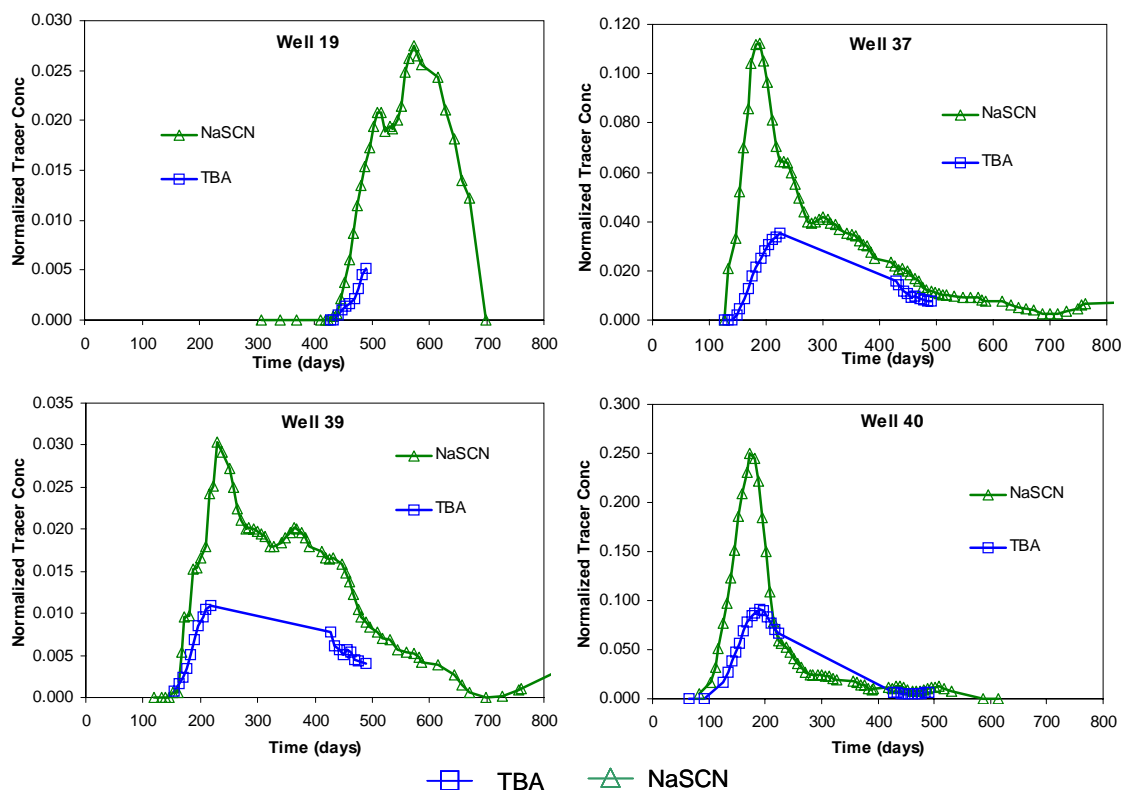


Fig. 6.6 – Observed normalized tracer concentrations at production wells (Illiasov et al.<sup>2</sup>).



**Fig. 6.7 – Observed normalized tritium and TBA tracer concentrations at production wells. (Illiasov et al.<sup>2</sup>).**



**Fig. 6.8 – Observed normalized NaSCN and TBA tracer concentrations at production wells. (Illiasov et al.<sup>2</sup>).**

Lichtenberger<sup>11</sup> pointed out the variation in normalized peaks from well to well as seen in the figures above. Focusing on the difference between the peaks of NaSCN and tritium, he attributed the behavior to a chromatographic delay in the tritium elution due to tritium exchange with immobile hydrogen. For this reason, we considered the tritium data rather unreliable and chose to use NaSCN as the conservative tracer from which to obtain the permeability distribution.

As earlier discussed, a partitioning tracer is required for the saturation inversion. We have chosen to use TBA over IPA because of the higher partitioning coefficient, and hence greater sensitivity of TBA to saturation distribution.

### 6.1.3 Manual history match with finite difference approach

As discussed in the “Literature Review” section, an attempt to match the entire tracer history with a finite-difference chemical simulator through manual parameter adjustments of the Ranger

Field data set was made by Allison et al.<sup>9</sup> and Allison.<sup>10</sup> The authors used a three-layer model with constant layer thicknesses and permeabilities and applied a series of permeability multipliers to each layer to match the conservative tracer responses. Pre-PITT oil saturation was obtained by approximating the multi-year history of the pattern with a simulation of a waterflood at pre-selected constant rates. The PITT was then simulated and the quality of the match on the partitioning tracers was used to judge the adequacy of oil saturation distribution. Simulation required a major effort and yet the overall match was satisfactory at best.

Table 6.5 below summarizes some properties of the reservoir model used by Allison et al.<sup>9</sup>

**Table 6.5– Summary of Allison et al.<sup>9</sup> key model properties.**

Layer	Net Thickness, ft	Permeability in X direction, $K_x$ , md	Permeability in Y direction, $K_y$ , md	Permeability in Z direction, $K_z$ , md
1	11	75	$2 \times K_x$	$0.1 \times K_x$
2	7	500	$2 \times K_x$	$0.1 \times K_x$
3	6	1250	$2 \times K_x$	$0.1 \times K_x$

Fig. 6.9 presents permeability fields of the final finite-difference model with the permeability multipliers marked on the maps. Fig. 6.10 presents the final saturation contours for the three layers of the model. Fig. 6.11, 6.12, and 6.13 present tritium, NaSCN, and TBA matches for the final model by Allison et al.<sup>9</sup>, respectively.

These figures are used for comparison with the results of our inversion work in the later sections.



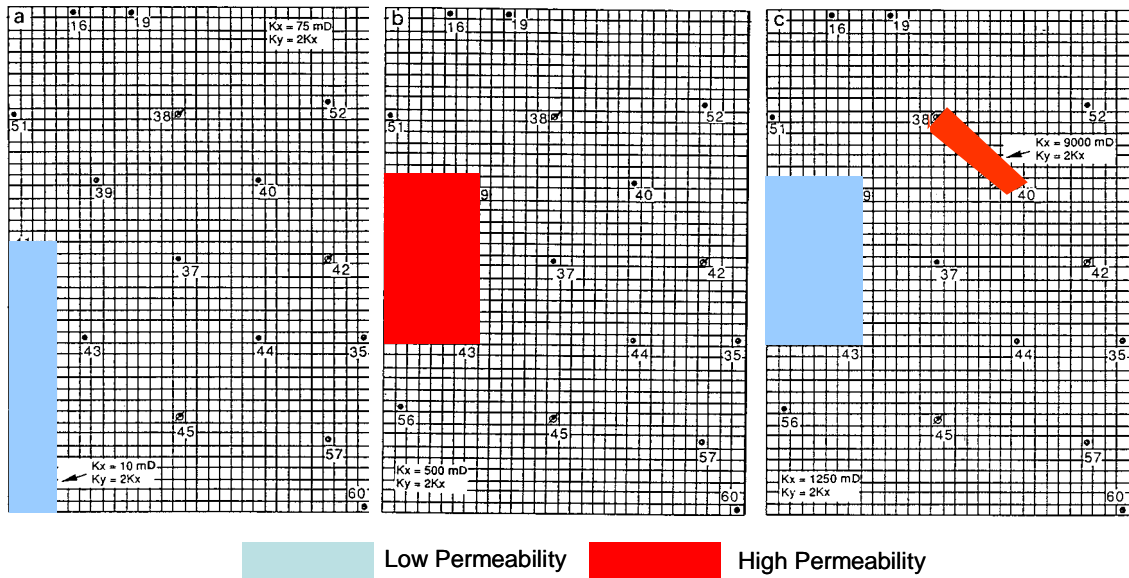


Fig. 6.9 – Permeability fields for layers 1, 2, and 3 of the finite-difference model (Allison et al.<sup>9</sup>)

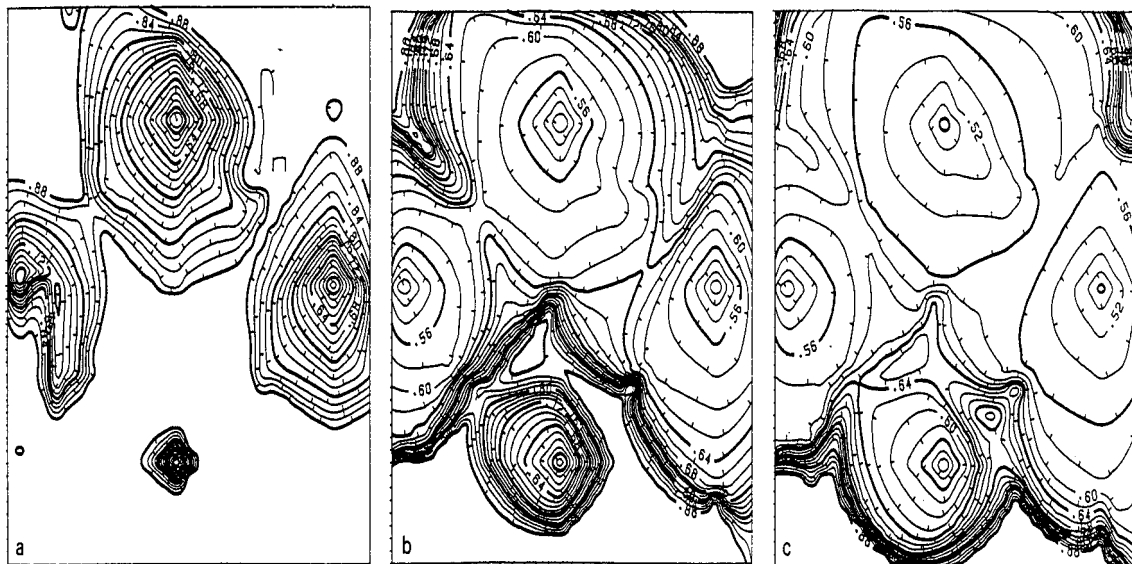


Fig. 6.10 – Saturation distribution for layers 1, 2, and 3 of the finite-difference model (Allison et al.<sup>9</sup>).

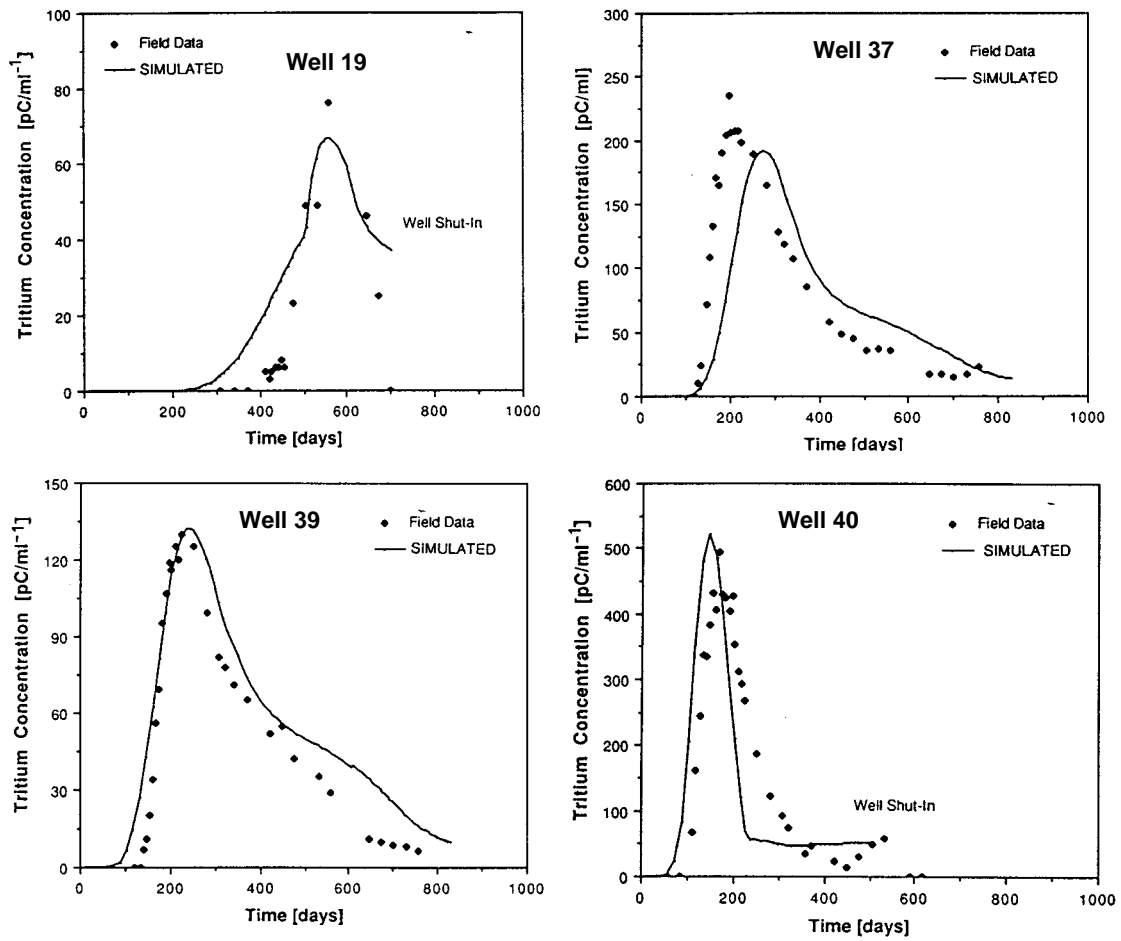


Fig. 6.11 – Tritium match for the finite-difference model (Allison et al.<sup>9</sup>).

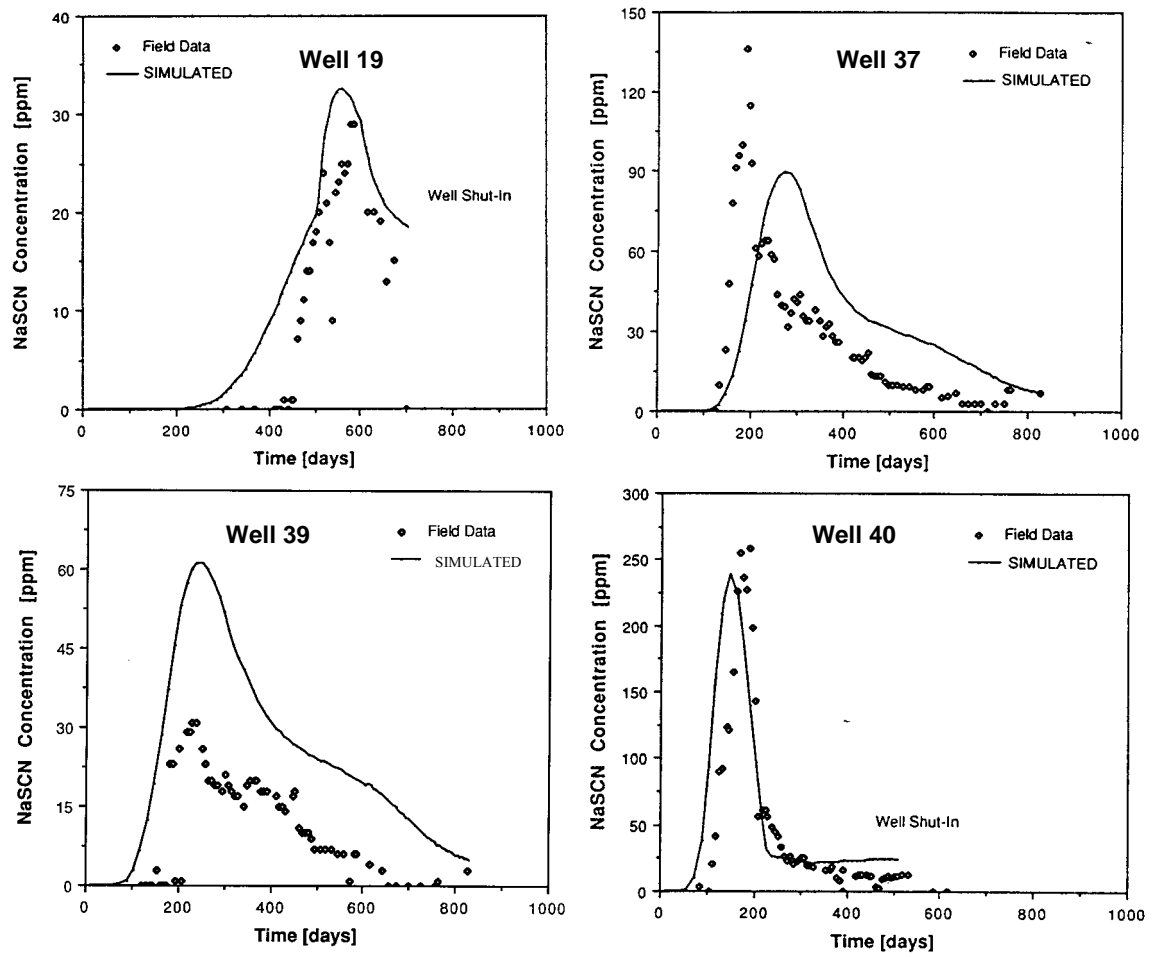


Fig. 6.12 – NaSCN match for the finite-difference model (Allison et al.<sup>9</sup>)

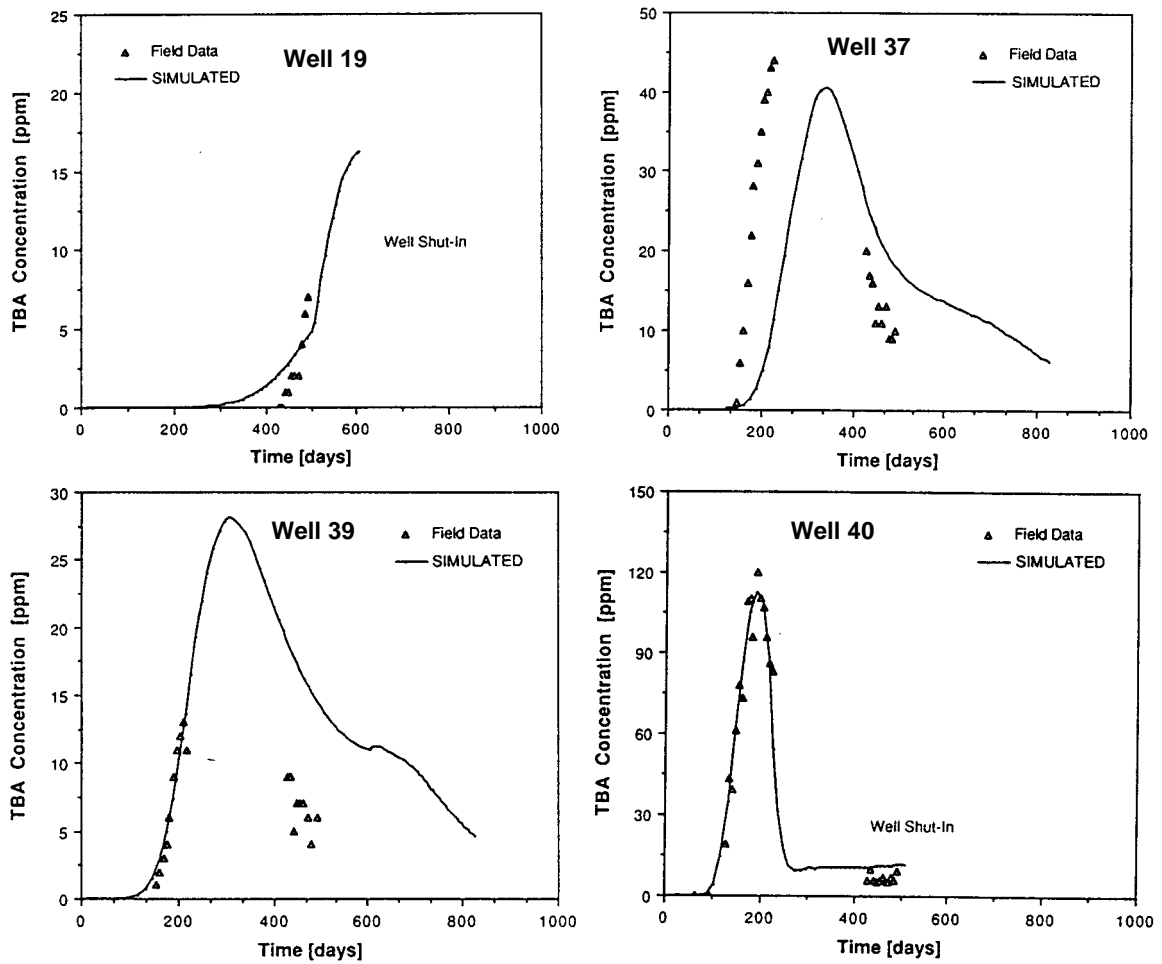
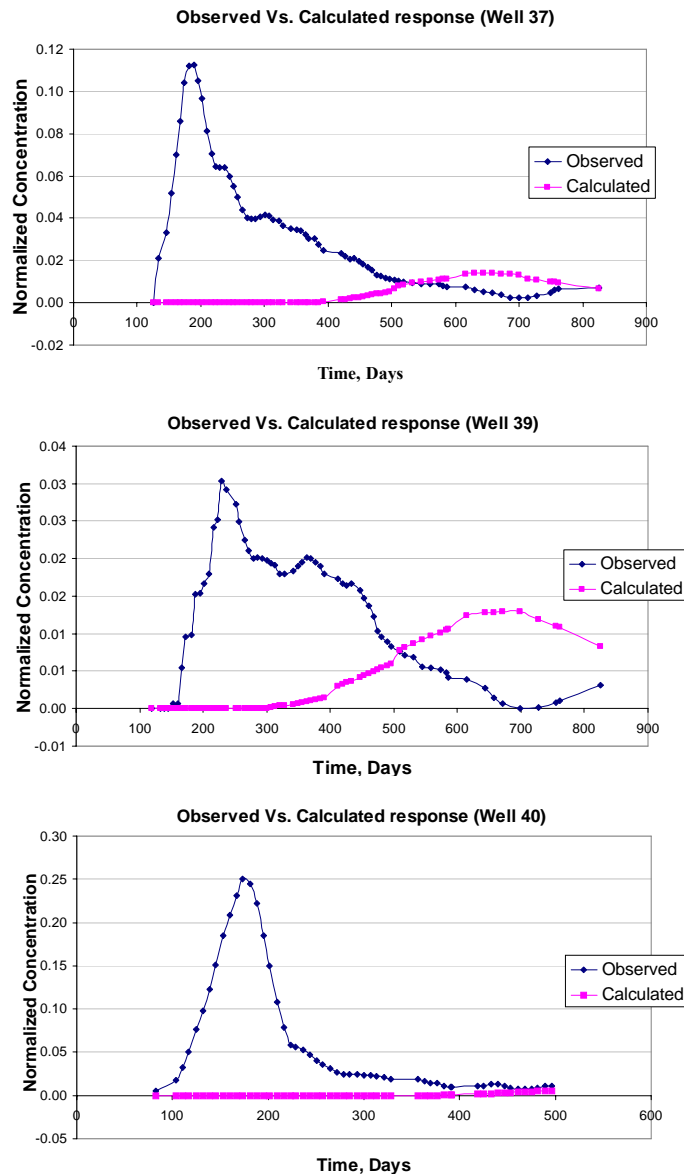


Fig. 6.13 – TBA match for the finite-difference model (Allison et al.<sup>9</sup>).

#### 6.1.4 Result of permeability inversion

In determining the permeability distribution from our permeability inversion phase, we used the NaSCN as the conservative tracer. The area of interest is the northern part of the Ranger field. Three of the wells (Wells 37, 39, and 40) in this region of the field show observation of NaSCN in sufficient quantity to facilitate the inversion. The response generated from the initial model as compared to the observed data is shown in Fig. 6.14.



**Fig. 6.14 – Comparison of calculated and observed normalized concentration using initial permeability distribution.**

After 11 iterations of inversion, the resulting match on the observed data is shown in Fig.6.15.

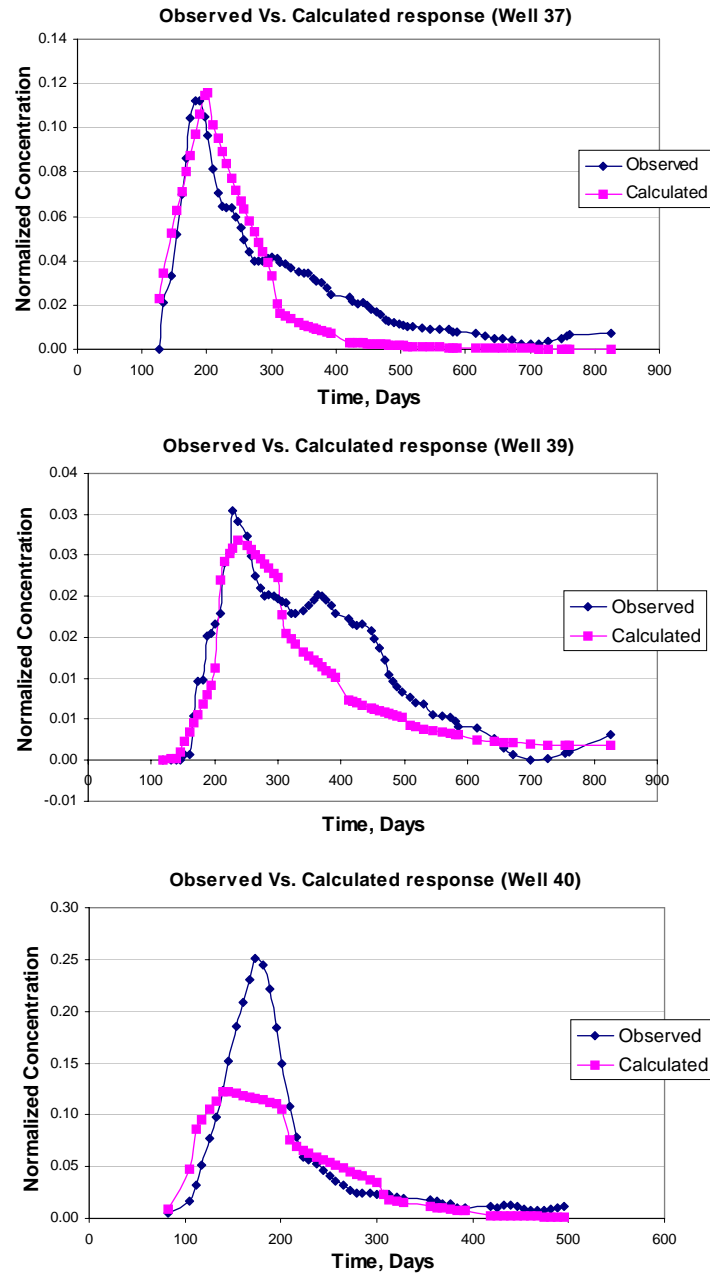
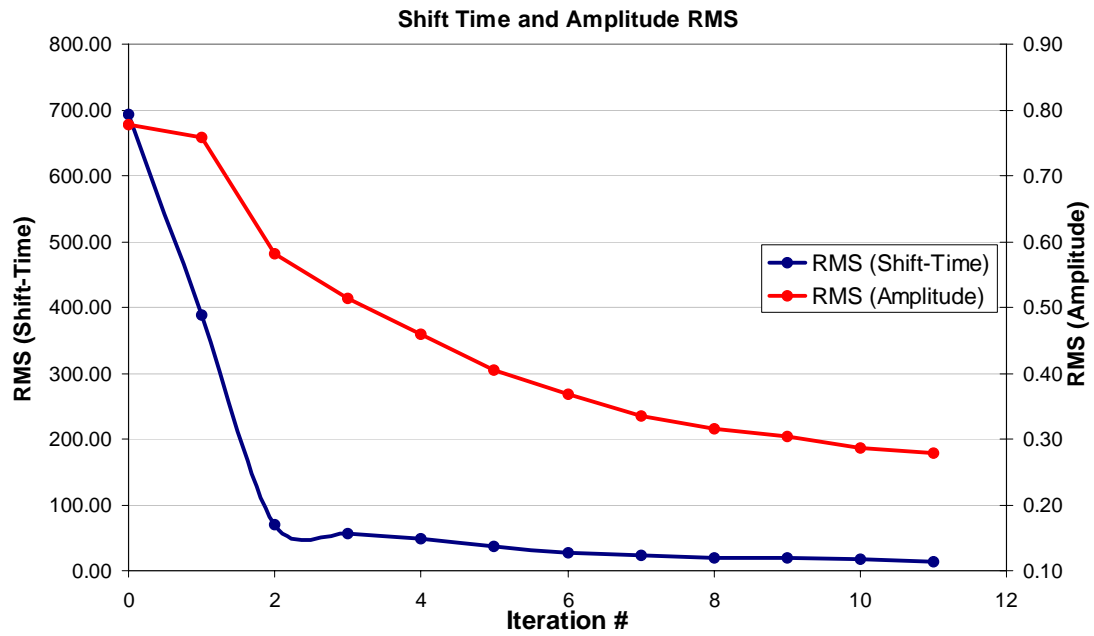
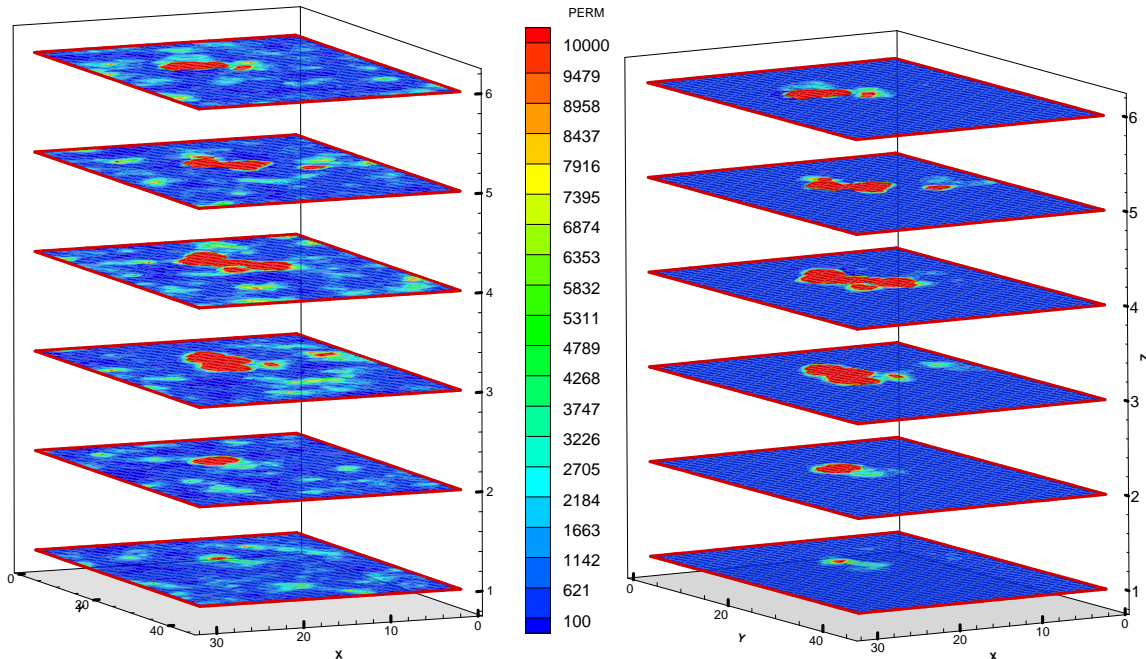


Fig. 6.15 – Comparison of calculated and observed normalized concentration after match.

The misfit in the data in terms of amplitude and shift-time over the eleven iterations is shown in Fig. 6.16.



**Fig. 6.16 – Rapid fall in RMS of amplitude and Travel-Time misfit.**



**Fig. 6.17 – Layer permeability after match (left) and permeability adjustments to initial model (right).**

The permeability distribution after eleven iterations is shown on a layer basis on the left plot in Figure 6.17 and the permeability changes made on the initial model at the end of the eleven iterations are shown on the plot on the right.

#### 6.1.5 Comparison of results with manual history matching approach

Permeability changes in each of the layers necessary to attain the match in Fig. 6.12 are shown in Fig. 6.19. Although only layer one of the manual history match is shown in Fig. 6.18, there is a consistency in the high permeability region required to attain the match both by our method and by manual history matching. The changes are very reasonable as they appear in the regions of location of Wells 37, 39, and 40 which are the observation wells. Other changes seen in Fig. 6.18 on the manual history match outside these regions are a result of matches made on other injected tracers in other wells besides those we considered.



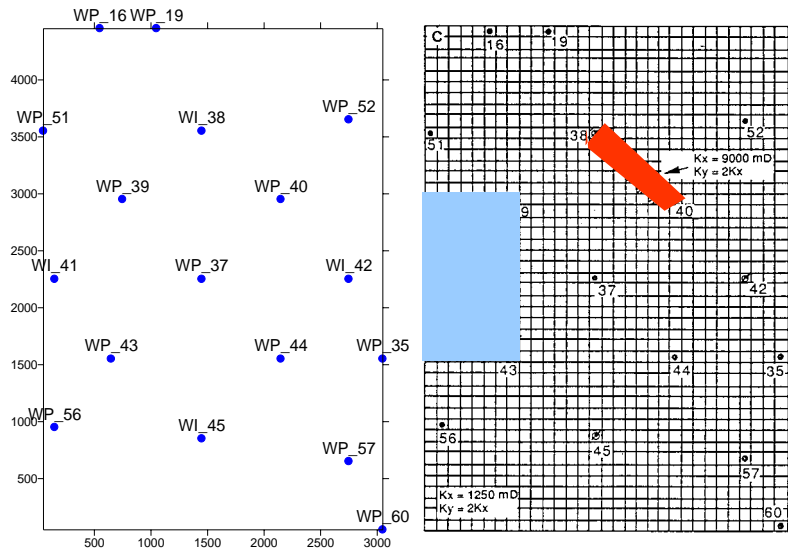


Fig. 6.18 – Major permeability changes in layer one for manual history match

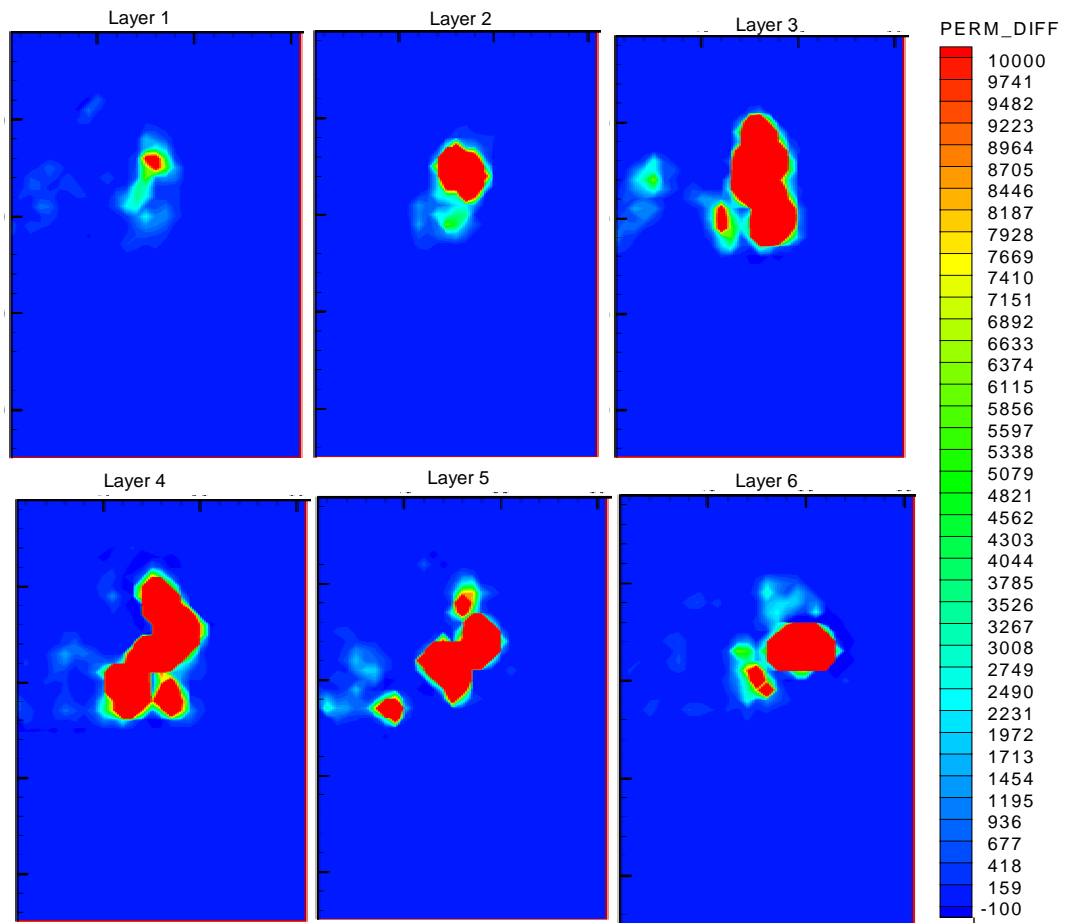
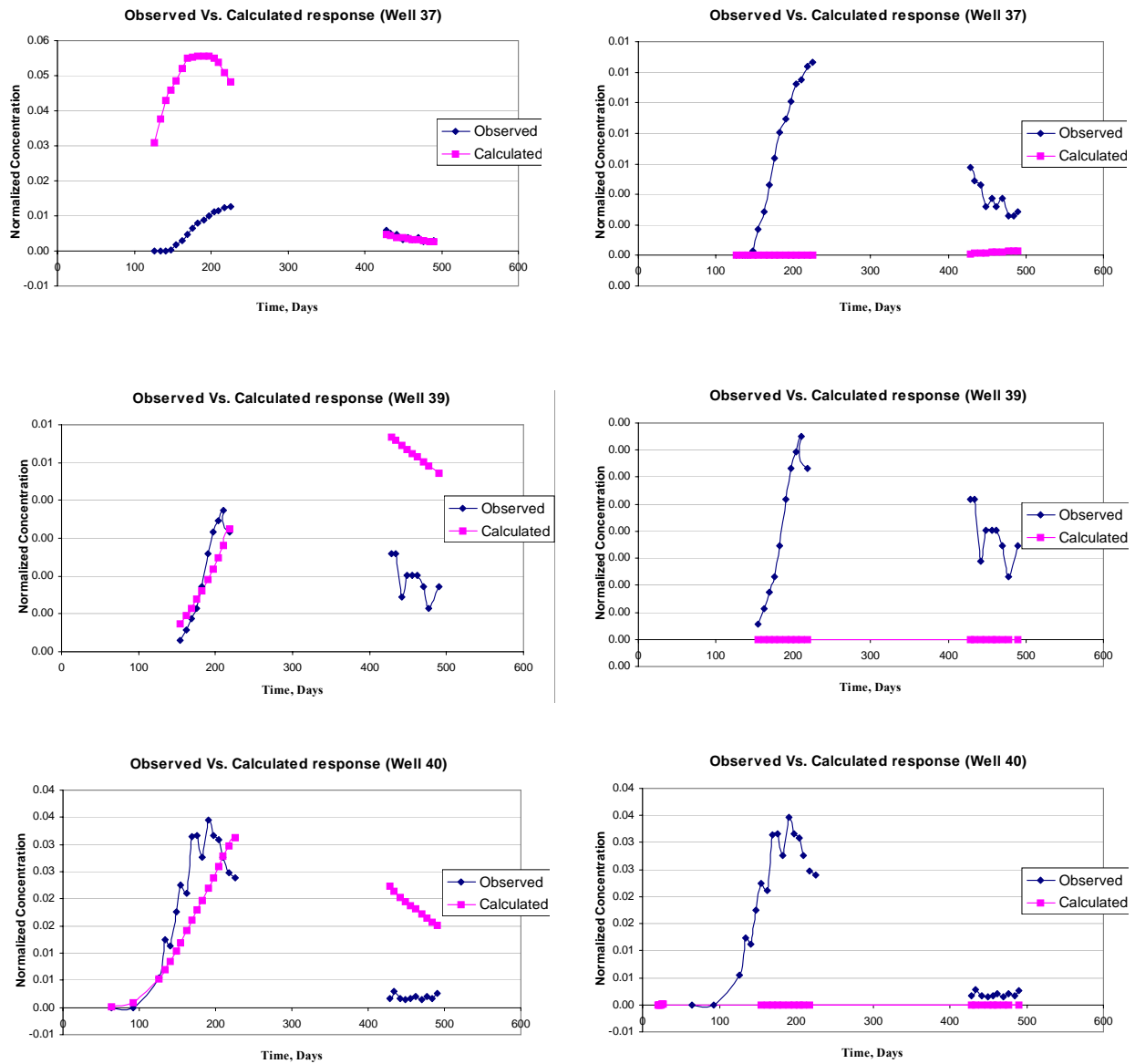


Fig. 6.19 – Permeability changes in each layer necessary to obtain match.

### 6.1.6 Result of saturation inversion

With the obtained permeability distribution, a saturation inversion was done on the partitioning tracer response as described in Chapter V Fig. 6.20 shows observed and calculated tracer concentration at the integrated wells before and after saturation inversion.



**Fig. 6.20 – Observed and calculated partitioning tracer response before (right) and after (left) saturation inversion**

Evident in these plots is the fact that the amplitude matches on the observed data is poor. This is attributed to missing observation data over a time interval. Essentially, this results in ambiguity of the tracer profile in this time interval. This effectively affects the generalized travel time computation and hence, optimal time shift computation.

Fig. 6.21 shows the saturation distribution obtained after inversion.

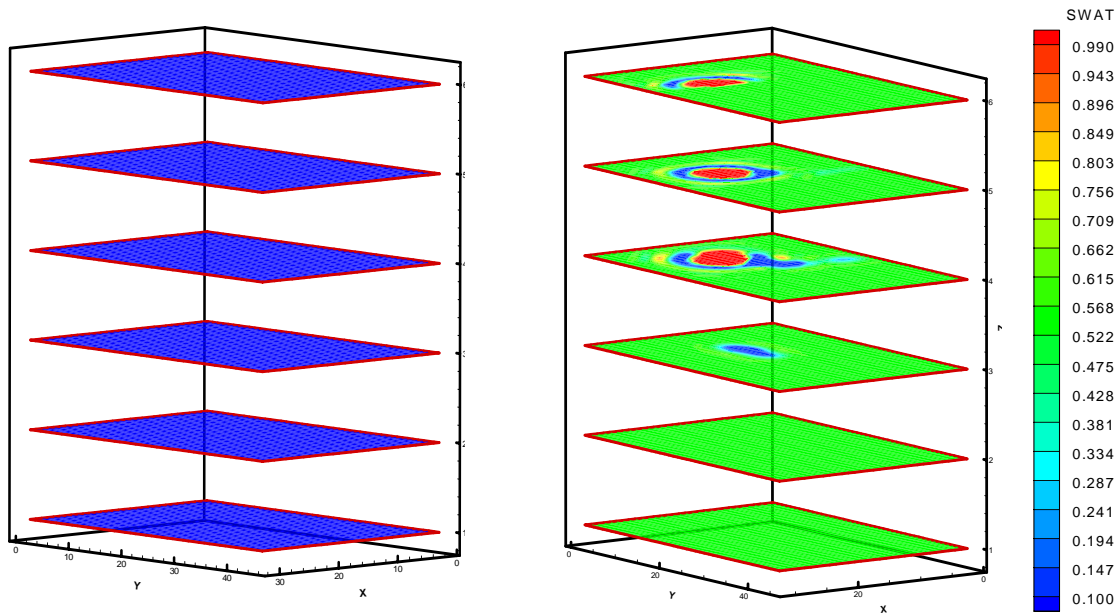


**Fig. 6.21 – Layer saturation distribution before (left) and after (right) inversion.**

## CHAPTER VII

### INTEGRATING ANALYTICAL AND INVERSION RESULTS

#### 7.1 Consistency between analytical and inversion results

From the analyses made using the method of moments in chapter three, the deductions made are listed below for consistency check against the results of inversion.

- Low permeability trend in the North-West direction
- Highest permeability trend and low NTG in the South-East direction
- High permeability and high NTG in the region south of the injector
- “High” oil saturation south of the injector

To assess the consistency of the method of moments with the results obtained from inversion, we pick in turn, each of these deductions and check against the. Matching reservoir model obtained from inversion.

##### 7.1.1 “Low” permeability trend in the north-west direction

Analysis of the results of MOM based on the breakthrough and first temporal moment of elution profile of all injected tracers produced at Well-19 suggested a non-preference of fluid migration in the north-west direction. A cursory glance at the distribution of contours of resulting permeability distribution after inversion (Fig. 7.1) shows the sparse spread of contours in this direction, hence the agreement between inversion and MOM results.

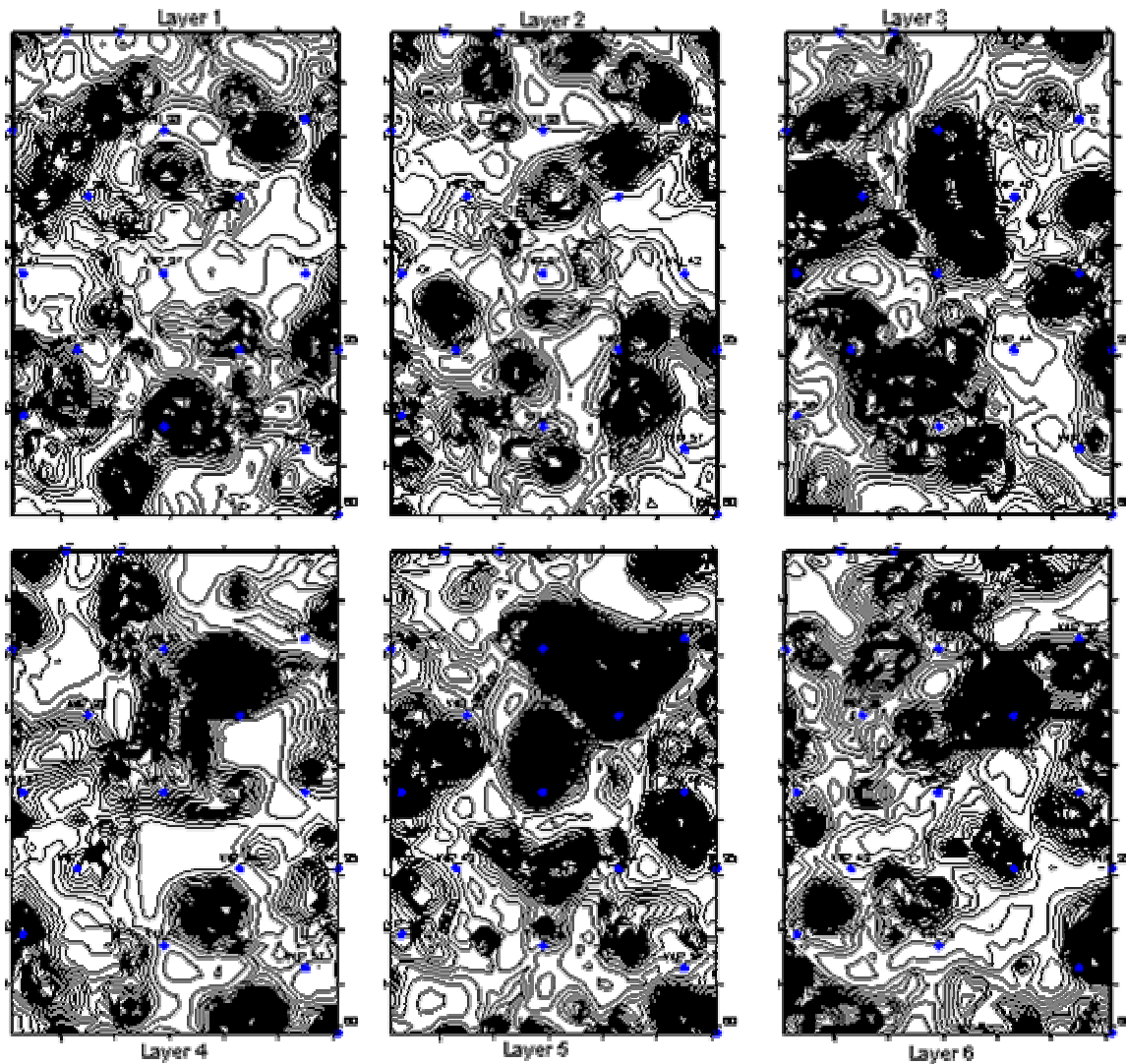


**Fig. 7.1 – Contour map of permeability distribution after inversion.**

#### 7.1.2 Highest permeability and low NTG in the south-east direction

The contour map of permeability distribution after inversion shown in Fig. 7.1 is in agreement with this deduction. We notice a consistency in the high density of contour lines, in all layers in the north-west direction in the area of interest. The orientation of the dense contour is seen to be in alignment with a straight line connecting the injector with Well-40. The early breakthrough of tracer from this well then seems reasonable.

The reservoir model used in generating the match has a net-to-gross ratio (NTG) shown in Fig.6.2. The aerial distribution of the NTG displayed indicates that the NTG in this region is

significantly less than that at the location of Wells 37 and 39. This also agrees with a previous deduction.

#### 7.1.3 High permeability and high NTG in the region south of the injector

Fig. 7.1 shows continually, a high density of the contours in the region south of the injector on all the reservoir layers. This again is consistent with the MOM analysis. The plot of NTG distribution confirms the deduction made on NTG.

#### 7.1.4 High oil saturation south of the injector

The saturation distribution obtained from the results of the inversion shown in Chapter six agrees with this deduction made from MOM estimates. However, the quantitative estimates made from both methods differ significantly.

Tang<sup>37</sup> extended the Brigham<sup>1</sup> model for residual oil saturation determination and applied it to the ranger field case. In making estimates of residual oil saturation, Tang chose the interwell region between the injector well and Well 40. The resulting average oil saturation determined using the extended Bingham model is 0.41. This estimate compares well with other direct comparison methods as well as the MOM estimate made in this research.

The estimates made from the saturation inversion is however not consistent with these results. This again reflects the highly non-unique nature of saturation inversion. If a different prior model is started with, we are likely to get closer results to those obtained from the direct comparison methods. This again emphasizes the need for a composite tracer analysis approach to reservoir characterization in which case estimates from quick analytical methods such as MOM and extended Brigham model are used as the prior model for the inversion process.

## CHAPTER VIII

### CONCLUSIONS AND RECOMMENDATIONS

#### 8.1 Consistency between analytical and inversion results

Many of the key observations and conclusions were presented throughout the body of this thesis. The following are a summary of some key conclusions we reached on the basis of our work.

1. Coupling a finite difference based forward model with the formalism of streamline simulation that enables the evaluation of sensitivities as 1-D integrals along streamlines affords an efficient means of reservoir characterization while preserving complexities of the physical processes.
2. Sound qualitative reservoir description can be obtained from quick data analyses such as MOM. However, such analyses cannot replace the rigor and detail characterization capability of the inversion process.
3. The problem of determining both permeability and saturation through inversion is inherently ill-posed. Sometimes we may not be able to resolve the permeability/saturation uncertainty only by matching the observed data. In such cases, incorporating all available knowledge about the parameter properties into the model prior to inversion is necessary. Having a good initial estimate of the model parameters that are relatively close to the true value is very important to result in reasonable results during inversion.
4. We find that our extension of the formulation of the saturation inversion to situations whereby the oil phase is mobile gives better resolution and has less limitation on the prior model to be used for inversion. However, the formulation is extremely sensitive to the relative permeability curves. Estimates of saturation distribution are only as good as how well the relative permeability curve model fluid flow in the reservoir.
5. Through inversion of the PITT, we were able to locate areas of high and low oil saturation. This information is invaluable when making decisions on EOR or infill drilling.
6. We observe that the finite difference based forward model is incapable of reproducing multiple peaks seen in the observed data. This limits our ability to optimally minimize the

amplitude data mismatch. Since multiple peaks are a measure of layering and or reservoir heterogeneity, this translates to loss of resolution on reservoir heterogeneity during the inversion process as the number of layers is already fixed.

7. We obtained as good or better match of the NaSCN tracers through inversion as was achieved by Allison et al.<sup>9</sup> through manual history matching. The resulting permeability fields share common characteristics with the fields presented by Allison et al.<sup>9</sup> but, due to the nature of automatic inversion, have less personal bias.
8. Results of the permeability inversion are in total agreement with preliminary reservoir description obtained through analytical methods of interpretation.

## **8.2 Recommendations**

Based on the conclusions presented above, and other findings during the course of the research, we recommend the following.

1. A good initial model incorporating all available knowledge about the reservoir should be built before inversion. Qualitative and quantitative analyses from quick analytical methods such as MOM and Brigham-Abbaszadeh technique to layer determination should be done and results intuitively incorporated in the inversion process.
2. The largest feasible partitioning coefficient of a partitioning tracer, as determined by rigorous test design, for a PITT should be used. This offers greater sensitivity to fluid distribution and improves the resolution of the inversion process.
3. Saturation inversion achieved through minimization of data misfit of tracer data alone is highly non-unique. To improve on the effort of reconstructing saturation distribution, we recommend a “joint inversion” in which case, the objective function includes a minimization on both water-cut and tracer concentration data misfit.



## NOMENCLATURE

$C$	= tracer concentration or covariance
$C(t_n)$	= non-partitioning tracer landmark peak-normalized concentration
$C(t_p)$	= non-partitioning tracer landmark peak-normalized concentration
$\mathbf{d}$	= data vector
$\mathbf{D}$	= dispersion coefficient
$\mathbf{g}$	= forward model or computed model response
$\mathbf{G}$	= sensitivity matrix or Frechet derivative of $\mathbf{g}$
$\mathbf{I}$	= identity matrix
$J$	= objective function
$k$	= permeability
$\mathbf{K}$	= permeability tensor
$K_o$	= partitioning coefficient of tracer
$K_{50}$	= 50 <sup>th</sup> -percentile permeability
$K_{84.1}$	= 84.1 <sup>st</sup> -percentile permeability,
$\mathbf{L}$	= spatial difference operator
$M$	= number of parameters
$\mathbf{m}$	= parameter vector
$N$	= number of dynamic data observations
$P$	= pressure
$pr$	= number of pressure solving steps in streamline simulation
$\mathbf{q}$	= gradient of objective function
$\mathbf{r}$	= earth response vector
$\mathbf{R}$	= resolution matrix
$s$	= slowness
$\mathbf{s}$	= stochastic residual component
$S_w$	= water saturation
$S_{wi}$	= initial water saturation
$t$	= time
$t_n$	= landmark time for non-partitioning tracer
$t_p$	= landmark time for partitioning tracer
$S_{orw}$	= residual to water oil saturation.

$\mathbf{v}$	= velocity vector
$V_{DP}$	= Dykstra-Parson coefficient
$\mathbf{W}$	= weighting matrix
$\mathbf{x}$	= spatial coordinate vector
$\boldsymbol{\varepsilon}$	= residual vector
$\phi$	= porosity
$\tau$	= time of flight or phase function
$\psi, \chi$	= bi-streamline functions
$\gamma$	= weighting factor

## REFERENCES

1. Brigham, W.E. and Abbaszadeh-Dehghani, M.: "Tracer Testing for Reservoir Description," *JPT* (May 1987) 519-527.
2. Illiasov, P.: "Inversion of Field-Scale Partitioning Tracer Response for Characterizing Oil Saturation Distribution: A Streamline Approach," MS thesis, Texas A&M University, College Station, TX (2000).
3. Cooke, C.E. Jr.: "Method of Determining Fluid Saturations in Reservoirs," U.S. Patent No. 3590923 (1971).
4. Tang, J.S.: "Partitioning Tracers and In-Situ Fluid-Saturation Measurements," *SPE Formation Evaluation* (1995), **10**, No.1, 33-39.
5. Deans, H.A. and Carlisle, C.T.: "Single-Well Tracer Test in Complex Pore Systems," paper SPE 14886 SPE/DOE paper presented at the 1986 Fifth Symposium on Enhanced Oil Recovery, Tulsa, Apr. 20-23.
6. Vasco, D.W., Yoon, S., and Datta-Gupta, A.: "Integrating Dynamic Data Into High-Resolution Reservoir Models Using Streamline-Based Analytic Sensitivity Coefficients," *SPE Journal* (1999), **4**, No.4, 389-399.
7. Yoon, S., Barman, I., Datta-Gupta, A., and Pope, G.A.: "In-Situ Characterization of Residual NAPL Distribution Using Streamline-Based Inversion of Partitioning Tracer Tests," paper SPE 52729 presented at the 1999 SPE/EPA Exploration and Production Environmental Conference, Austin, TX, March 1-3.
8. Sen, M.K., Datta-Gupta, A., Stoffa, P.L., Lake, L.W., and Pope, G.A.: "Stochastic Reservoir Modeling Using Simulated Annealing and Genetic Algorithms," paper SPE 24754 presented at the 1992 SPE Annual Technical Conference and Exhibition, Washington, DC, October 4-7.
9. Allison, S.B., Pope, G.A., and Sepehrnoori, K., "Analysis of Field Tracers for Reservoir Description," *J. Pet. Sci. Eng.* (1991), **5**, 173-186.
10. Allison, S.B.: "Analysis and Design of Field Tracers for Reservoir Description," MS Thesis, University of Texas at Austin, Austin, TX (1998).
11. Lichtenberger, J.: "Field Application of Interwell Tracers for Reservoir Characterization of Enhanced Oil Recovery Pilot Areas," paper SPE 21652 presented at the 1991 SPE Production Operations Symposium, Oklahoma City, April 7-9.

12. Yoon, S.: "Dynamic Data Integration Into High Resolution Models Using Streamline-Based Inversion," PhD dissertation, Texas A&M University, College Station, TX (2000).
13. Datta-Gupta, A., Lake, L.W., and Pope, G.A.: "Characterizing Heterogeneous Permeable Media with Spatial Statistics and Tracer Data Using Sequential Simulated Annealing," *Mathematical Geology* (1995), **27**, No.6, 763-787.
14. McLaughlin, D., and Townley, L.R.: "A Reassessment of the Groundwater Inverse Problem," *Water Resources Research* (1996), **32**, No.5, 1131-1161.
15. Paige, C. C. and Saunders, M. A.: "LSQR: An Algorithm for Sparse Linear Equations and Sparse Least Squares," *ACM Transactions on Mathematical Software* (1982), **8**, No.1, 43-71.
16. Crane, M. J. and Blunt, M. J.: "Streamline-based Simulation of Solute Transport," *Water Resources Research* (1999), **35**, No 10, 3061-3078.
17. Hutchins, R.D., Dovan, H.T., and Saniford, B.B.: "Aqueous Tracers for Oilfield Applications," paper SPE 21049 presented at the 1991 SPE International Symposium on Oilfield Chemistry, Anaheim, CA, Feb. 20-22.
18. Vilela, M.A., Zepa, L.B., and Mengual, R.: "Water and Gas Tracers at El Furrial Field," paper SPE 53737 presented at the 1991 SPE Latin American and Caribbean Petroleum Engineering Conference, Caracas, Venezuela, Apr. 21-23.
19. Dugstad, P., Aurdal, T., Galdiga, C., and Hundere, I.: "Application of Tracers to Monitor Fluid Flow in the Snorre Field: A Field Study," paper SPE 56427 presented at the 1999 SPE Annual Technical Conference and Exhibition, Houston, Oct. 3-6.
20. Tomich, J.F., Dalton, R.L., Deans, H.A., and Shallenberger, L.K.: "Single-Well Tracer Method to Measure Residual Oil Saturation," *JPT* (February 1973) 211-218.
21. Deans, H.A. and Mut, A.D.: "Chemical Tracer Studies to Determine Water Saturation at Prudhoe Bay," *SPE Reservoir Engineering* (February 1997) 52-57.
22. Tang, J.S. and Harker, B.C.: "Interwell Tracer Test to Determine Residual Oil Saturation in a Gas-Saturated Reservoir, Part II, Field Application," paper SPE/CIM 30-130 presented at SPE/CIM International Technical Meeting, Calgary, June 11-13.
23. Wood, K.N., Tang, J.S., and Luckasavitch, R.J.: "Interwell Residual Oil Saturation at Leduc Miscible Pilot," paper SPE 20543 presented at the 1990 SPE Annual Technical Conference and Exhibition, New Orleans, Sep. 23-26.

24. Agca, C., Pope, G.A., and Sepehrnoori, K.: "Modeling and Analysis of Tracer Flow in Oil Reservoirs," *Journal of Petroleum Science and Engineering* (1990), **4**, 3-19.
25. Jin, M., Delshad, M., Dwarakanath, V., McKinney, D.C., Pope, G.A., Sepehrnoori, K., Tilburg, C.E., and Jackson, R.E.: "Partitioning Tracer Test for Detection, Estimation, and Remediation Performance Assessment of Subsurface Non Aqueous Phase Liquids," *Water Resources Research* (1995), **31**, No 5, 1201-1211.
26. Annable, M.D., Rao, P.S.C., Hatfield, K., Graham, W.D, Wood, A.L., and Enfield, C.G.: "Partitioning Tracers for Measuring Residual NAPL: Field-Scale Test Results," *Journal of Environmental Engineering* (1998), **124**, No.6, 498-503.
27. Dwarakanath, V., Deeds, N., and Pope, G.A.: "Analysis of Partitioning Interwell Tracer Tests," *Environmental Science & Technology* (1999), **33**, No.21, 3829-3836.
28. Deeds, N.E., Pope, G.A., and McKinney, D.C.: "Vadose Zone Characterization at a Contaminated Field Site Using Partitioning Interwell Tracer Technology," *Environmental Science & Technology* (1999), **33**, No.16, 2745-2751.
29. Wilson, R.D. and Mackay, D.M.: "Direct Detection of Residual Nonaqueous Phase Liquid in the Saturated Zone Using SF<sub>6</sub> as a Partitioning Tracer," *Environmental Science & Technology* (1995), **29**, No.5, 1255-1258.
30. Hirasaki, G.J., Miller, C.A., Tanzil, D., Pope, G.A., Lawson, J.B.: "Field Demonstration of the Surfactant/Foam Process for Aquifer Remediation," paper SPE 39292 presented at the 1997 SPE Annual Technical Conference and Exhibition, San Antonio, Oct. 5-8.
31. James, A.I., Graham, W.D., Hatfield, K., Rao, P.S.C., Annable, M.D.: "Optimal Estimation of Residual Non-aqueous Phase Liquid Saturations Using Partitioning Tracer Concentration Data," *Water Resources Research* (1997), **33**, No.12, 2621-2636.
32. James, A.I., Graham, W.D., Hatfield, K., Rao, P.S.C., Annable, M.D.: "Estimation of Spatially Variable Residual Nonaqueous Phase Liquid Saturations in Nonuniform Flow Fields Using Partitioning Tracer Data," *Water Resources Research* (2000), **36**, No.4, 999-1012.
33. King, M.J. and Datta-Gupta, A.: "Streamline Simulation: A Current Perspective," *In Situ* (1998), **22**, No.1, 91-140.
34. Datta-Gupta, A. and King, M. J.: "A Semianalytic Approach to Tracer Flow Modeling in Heterogeneous Permeable Media," *Advances in Water Resources* (1995), **18**, No.1, 9-24.

35. Vasco, D. W. and Datta-Gupta, A.: "Asymptotic Solutions for Solute Transport: A Formalism for Tracer Tomography," *Water Resources Research* (1999), **35**, No.1, 1-16.
36. Datta-Gupta, A., Vasco, D.W., and Long, J.C.S.: "On the Sensitivity and Spatial Resolution of Transient Pressure and Tracer Data for Heterogeneity Characterization," *SPE Formation Evaluation* (1997), **12**, No.2, 137-144.
37. Tang, J.: "Extended Brigham Model for Residual Oil Saturation Measurement by Partitioning Tracer Tests," paper SPE 84874 presented at the 2003 SPE International Improved Oil Recovery Conference, Kuala Lumpur, Malaysia, October 20-21.

**APPENDIX A**

**MOM SWEPT VOLUME CALCULATIONS USING AVERAGE**

**RATES**

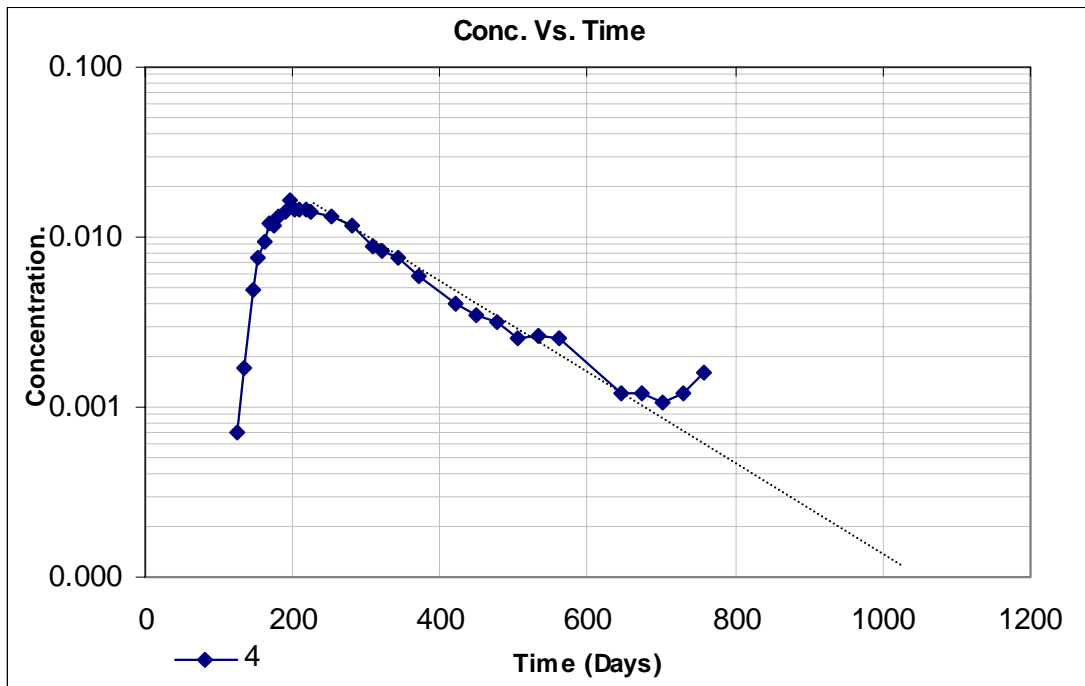


Fig. A.1 – Semi-log plot of observed tritium concentration versus time for Well 37



**Table A.1 – Swept pore volume calculation (Well 37) using tritium.**

<b>Time (days)</b>	<b>Concentration (ppm)</b>	<b>C*Time (ppm-day)</b>	<b>Delt, <math>\Delta t</math> (days)</b>	<b>C*Time* <math>\Delta t</math> (ppm-day<sup>2</sup>)</b>	<b>C*Delt(<math>\Delta t</math>) (ppm-day)</b>
120	0	0	120	0	0
126	0.000699	0.0881118	126	11.10209	0.088112
133	0.001678	0.223174	7	1.562218	0.011746
146	0.004965	0.72489	13	9.42357	0.064545
154	0.007552	1.163008	8	9.304064	0.060416
161	0.009301	1.497461	7	10.48223	0.065107
168	0.01196	2.00928	7	14.06496	0.08372
174	0.01154	2.00796	6	12.04776	0.06924
182	0.01329	2.41878	8	19.35024	0.10632
189	0.01427	2.69703	7	18.87921	0.09989
196	0.01643	3.22028	7	22.54196	0.11501
202	0.01441	2.91082	6	17.46492	0.08646
210	0.01455	3.0555	8	24.444	0.1164
217	0.01455	3.15735	7	22.10145	0.10185
224	0.01392	3.11808	7	21.82656	0.09744
252	0.01322	3.33144	28	93.28032	0.37016
280	0.01154	3.2312	28	90.4736	0.32312
308	0.008951	2.756908	28	77.19342	0.250628
322	0.008322	2.679683871	14	37.5155742	0.116507994
342= $t$	0.007483= $C$	2.559185966	20	51.18371932	0.149659998
370	0.005944	2.199280037	28	61.57984104	0.166432003
420	0.004056	1.703520084	50	85.1760042	0.20280001
448	0.003427	1.535296	28	42.988288	0.095956
476	0.003147	1.497972	28	41.943216	0.088116
504	0.002517	1.26856805	28	35.51990541	0.070476003
532	0.002587	1.376283947	28	38.53595051	0.072435997
560	0.002517	1.409520056	28	39.46656157	0.070476003
644= $t_b$	0.001189= $C_b$	0.765716	84	64.320144	0.099876
				973.771774	3.242899811

**Table A.2 – MOM parameter estimates (Well 37) using tritium.**

<b>Parameter</b>	<b>Estimated value</b>	<b>Units</b>
m (pc)	220285632.1	Pc (pico curies)
Fraction of tracer produced $f=m/M$	0.082474941	-
Total Swept Volume (bbls)	276456.077	Barrels (bbls)
Net Swept Volume (bbls)	22800.69855	Barrels (bbls)

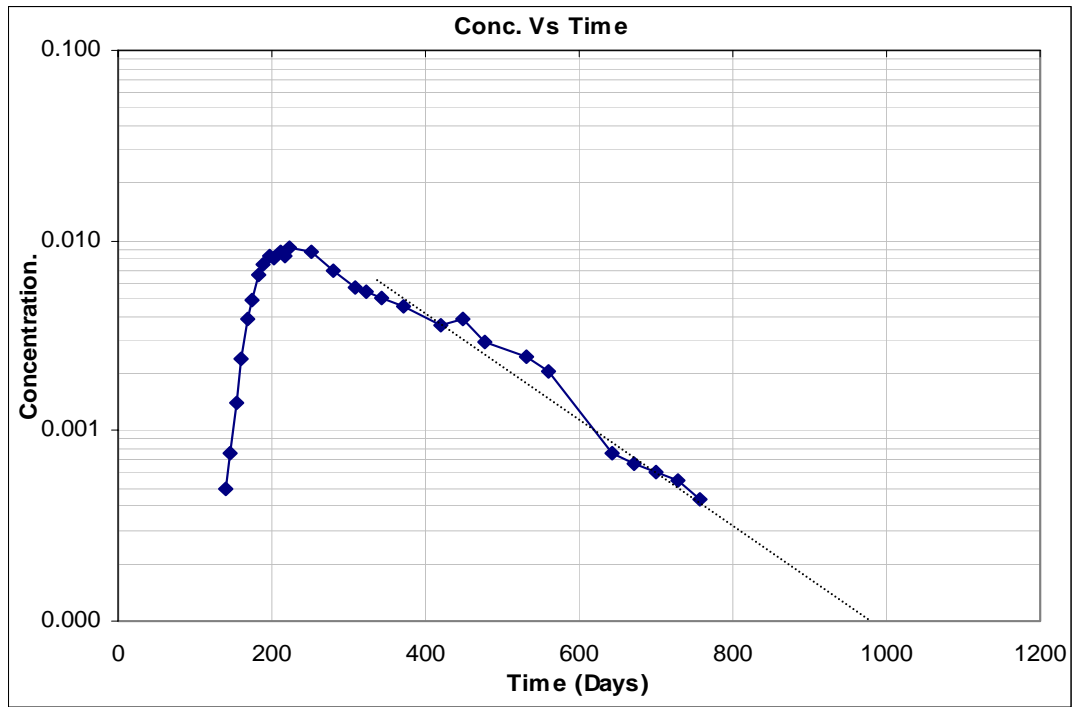


**Fig. A.2 – Semi-log plot of observed tritium concentration versus time for Well 39**

**Table A.3 – Swept pore volume calculation (Well 39) using tritium.**

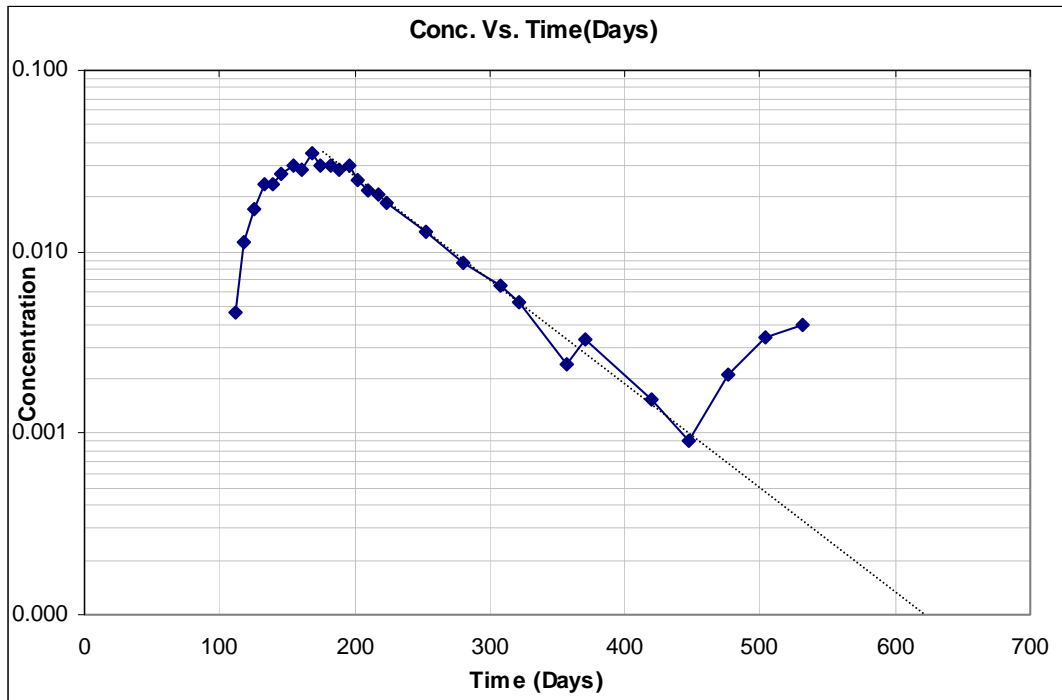
<b>Time (days)</b>	<b>Concentration (ppm)</b>	<b>C*Time (ppm-day)</b>	<b>Delt, <math>\Delta t</math> (days)</b>	<b>C*Time* <math>\Delta t</math> (ppm-day<sup>2</sup>)</b>	<b>C*Delt(<math>\Delta t</math>) (ppm-day)</b>
120	0	0	120	0	0
133	0	0	13	0	0
140	0.0004895	0.06853	140	9.5942	0.06853
146	0.0007692	0.112303197	6	0.673819182	0.0046152
154	0.001399	0.215445985	8	1.723567877	0.011191999
161	0.002378	0.382857984	7	2.680005887	0.016645999
168	0.003916	0.657888	7	4.605216	0.027412
174	0.004825	0.839550035	6	5.037300209	0.028950001
182	0.006643	1.209026018	8	9.672208146	0.053144001
189	0.007483	1.414286981	7	9.900008868	0.052380999
196	0.008322	1.631111922	7	11.41778345	0.058253997
202	0.008112	1.638624061	6	9.831744364	0.048672002
210	0.008741	1.835609937	8	14.6848795	0.069927998
217	0.008392	1.821063913	7	12.74744739	0.058743997
224	0.009091	2.036384022	7	14.25468816	0.063637001
252	0.008741	2.202731924	28	61.67649388	0.244747992
280	0.006923	1.938439972	28	54.27631922	0.193843997
308	0.005734	1.766071969	28	49.45001514	0.160551997
322	0.005455	1.756509968	14	24.59113955	0.076369999
342=t	0.004965=C	1.698029966	20	33.96059932	0.099299998
370	0.004545	1.681649963	28	47.08619896	0.127259997
420	0.003636	1.52712	50	76.356	0.1818
448	0.003846	1.723007955	28	48.24422275	0.107687997
476	0.002937	1.398012	28	39.144336	0.082236
532	0.002448	1.302336	56	72.930816	0.137088
560	0.002028	1.135680056	28	31.79904157	0.056784003
644	0.0007692	0.495364787	84	41.61064212	0.064612798
672	0.0006783	0.455817587	28	12.76289242	0.018992399

Table A.3 continued

Time (days)	Concentration (ppm)	C*Time (ppm-day)	Delt, $\Delta t$ (days)	C*Time* $\Delta t$ (ppm-day <sup>2</sup> )	C*Delt( $\Delta t$ ) (ppm-day)
700	0.0006084	0.425879986	28	700.711586	2.113380372
728	0.0005455	0.397124015	28	1401.423172	4.226760743
756=tc	0.0004406= $C_b$	0.333093608	28	2802.846344	8.453521487
				5605.692688	16.90704297

Table A.4 – MOM parameter estimates (Well 39) using tritium.

Parameter	Estimated value	Units
m (pc)	1144790935	Pc (pico curies)
Fraction of tracer produced $f=m/M$	0.428609726	-
Total Swept Volume (bbls)	280727.9394	Barrels (bbls)
Net Swept Volume (bbls)	120322.7252	Barrels (bbls)



**Fig. A.3 – Semi-log plot of observed tritium concentration versus time for Well 40**

**Table A.5 – Swept pore volume calculation (Well 40) using tritium.**

Time (days)	Concentration (ppm)	C*Time (ppm-day)	Delt, $\Delta t$ (days)	C*Time* $\Delta t$ (ppm-day <sup>2</sup> )	C*Delt( $\Delta t$ ) (ppm-day)
56	0	0			
84	0	0	28	0	0
112	0.004615	0.51688	112	57.89056	0.51688
118	0.01126	1.32868	6	7.97208	0.06756
126	0.017130001	2.158380126	8	17.26704101	0.137040008
133	0.023499999	3.125499867	7	21.87849907	0.164499993
140	0.023429999	3.28019986	7	22.96139902	0.164009993
146	0.02685	3.9201	6	23.5206	0.1611
154	0.030139999	4.641559846	8	37.13247877	0.241119992
161	0.02839	4.57079	7	31.99553	0.19873
168	0.034619998	5.816159664	7	40.71311765	0.242339986
174	0.030069999	5.232179826	6	31.39307896	0.180419994
182	0.029650001	5.396300182	8	43.17040146	0.237200008
189	0.02825	5.33925	7	37.37475	0.19775
196	0.029859999	5.852559804	7	40.96791863	0.209019993
202	0.02476	5.00152	6	30.00912	0.14856
210	0.021819999	4.58219979	8	36.65759832	0.174559992
217	0.02056	4.46152	7	31.23064	0.14392
224	0.01867	4.18208	7	29.27456	0.13069
252	0.01301	3.27852	28	91.79856	0.36428
280=t	0.008601=C	2.408279888	28	67.43183686	0.240827989
308	0.006434	1.981672031	28	55.48681686	0.180152003
322	0.005245	1.688890032	14	23.64446045	0.073430001
357	0.002378	0.848945964	35	29.71310875	0.083229997
370	0.003287	1.216190037	13	15.81047048	0.042731001
420	0.001538	0.64596	50	32.298	0.0769
448=t <sub>b</sub>	0.0009091=C <sub>b</sub>	0.4072768	28	11.4037504	0.0254548
				868.9963767	4.40240575

**Table A.6 – MOM parameter estimates (Well 40) using tritium.**

<b>Parameter</b>	<b>Estimated value</b>	<b>Units</b>
m (pc)	17768302.04	Pc (pico curies)
Fraction of tracer produced $f=m/M$	0.006652452	-
Total Swept Volume (bbls)	169963.8847	Barrels (bbls)
Net Swept Volume (bbls)	1130.676633	Barrels (bbls)



**APPENDIX B**

**MOM SWEPT VOLUME CALCULATIONS WITH VARIABLE**

**RATES**

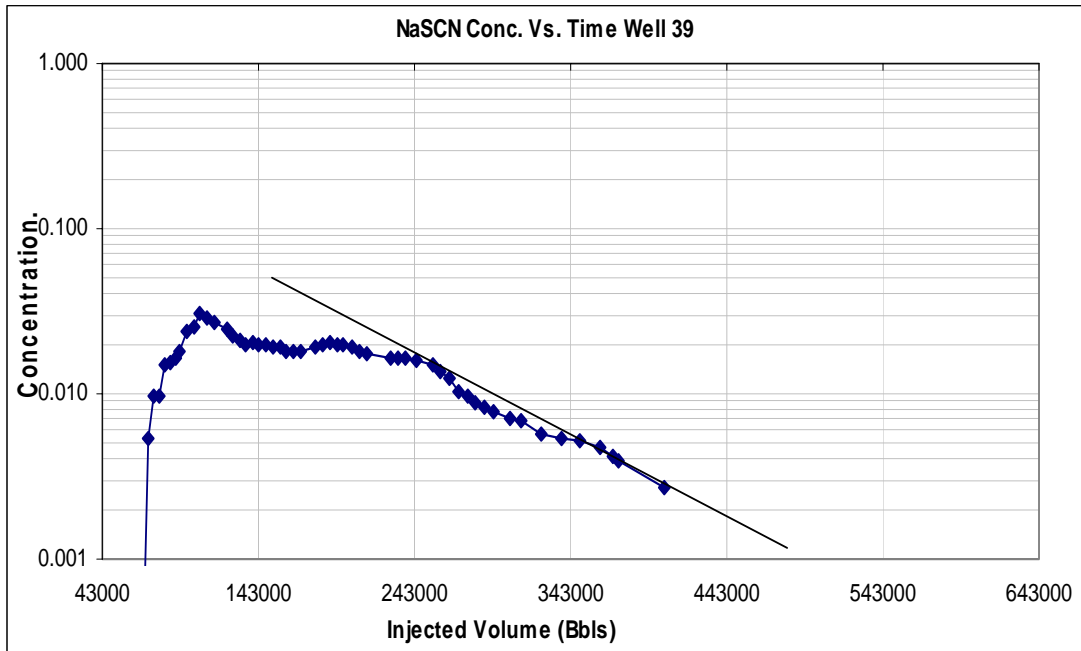


**Fig. B.1 – Semi-log plot of NaSCN concentration versus injected volume for Well 39**

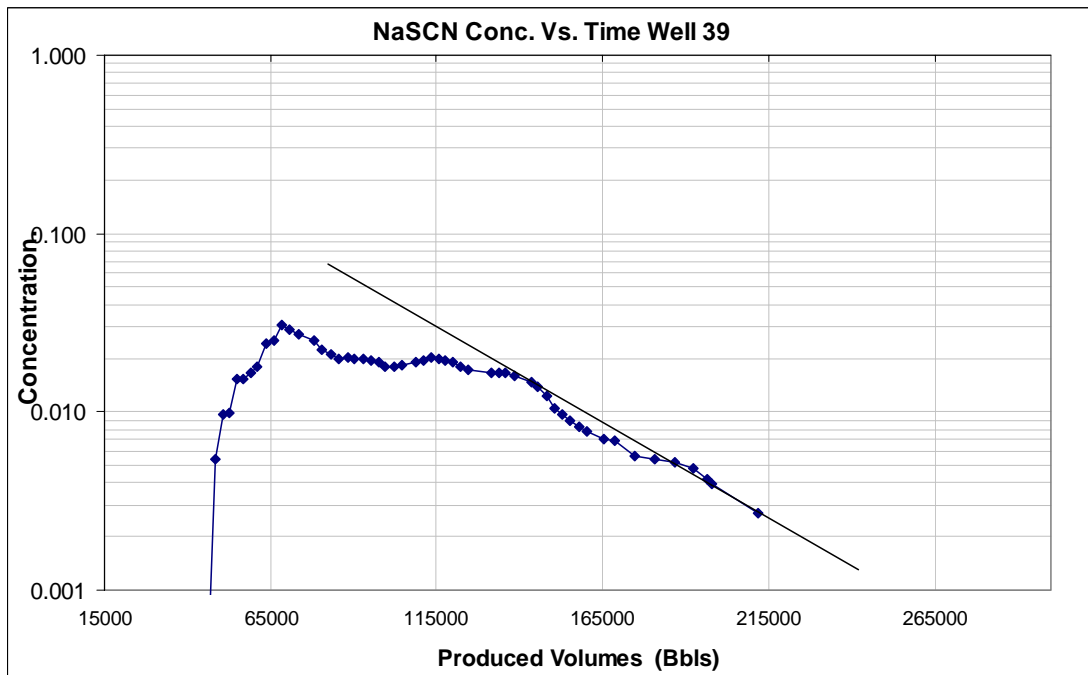


**Fig. B.2 – Semi-log plot of NaSCN concentration versus produced volume for Well 39**

**Table B.1 – Cumulative injected volume versus concentration (Well 39) using NaSCN.**

Time	Conc	Inj_volume	DelV	C*DelV	Cum.C*DV	C*V*DV
119	0	53077	0	0	0	0
132	0	59356	6279	0	0	0
139	0	62737	3381	0	0	0
145	0	65635	2898	0	0	0
153	0.000625	69499	3864	2.415	2.415	167840.085
160	0.000625	72880	3381	2.113125	4.528125	154004.55
167	0.005415	76261	3381	18.308115	22.83624	1396195.158
173	0.009581	79159	2898	27.765738	50.601978	2197908.054
181	0.009789	83023	3864	37.824696	88.426674	3140319.736
188	0.015205	86404	3381	51.408105	139.834779	4441865.904
195	0.015413	89785	3381	52.111353	191.946132	4678817.829
201	0.016662	92797	3012	50.185944	242.132076	4657105.045
209	0.017912	97573	4776	85.547712	327.679788	8347146.903
216	0.024161	101752	4179	100.968819	428.648607	10273779.27
223	0.025202	105931	4179	105.319158	533.967765	11156563.73
229	0.030409	109513	3582	108.925038	642.892803	11928707.69
237	0.029159	114289	4776	139.263384	782.156187	15916272.89
251	0.027285	122647	8358	228.04803	1010.204217	27969406.74
257	0.024994	126229	3582	89.528508	1099.732725	11301094.04
265	0.022494	131005	4776	107.431344	1207.164069	14074043.22
272	0.021036	135184	4179	87.909444	1295.073513	11883950.28
279	0.019995	139363	4179	83.559105	1378.632618	11645047.55
285	0.020203	142945	3582	72.367146	1450.999764	10344521.68
293	0.019995	147721	4776	95.49612	1546.495884	14106782.34
300	0.019787	151900	4179	82.689873	1629.185757	12560591.71
307	0.01937	156534	4634	89.76058	1718.946337	14050582.63
313	0.019162	160506	3972	76.111464	1795.057801	12216346.64
321	0.017912	165802	5296	94.861952	1889.919753	15728301.37
328	0.017912	170436	4634	83.004208	1972.923961	14146905.19

Table B.1 continued

Time	Conc	Inj_volume	DeIV	C*DeIV	Cum.C*DV	C*V*DV
341	0.018329	179042	8606	157.739374	2130.663335	28241973
349	0.018954	184338	5296	100.380384	2231.043719	18503919.23
356	0.019578	188972	4634	90.724452	2321.768171	17144381.14
363	0.020203	193606	4634	93.620702	2415.388873	18125529.63
369	0.019995	197578	3972	79.42014	2494.809013	15691672.42
377	0.019578	202874	5296	103.685088	2598.494101	21035008.54
384	0.018954	207508	4634	87.832836	2686.326937	18226016.13
391	0.017912	212142	4634	83.004208	2769.331145	17608678.69
412	0.017287	227496	15354	265.424598	3034.755743	60383034.35
419	0.016662	232977	5481	91.324422	3126.080165	21276489.86
425	0.016454	237675	4698	77.300892	3203.381057	18372489.51
433	0.016662	243939	6264	104.370768	3307.751825	25460100.78
447	0.015829	254901	10962	173.517498	3481.269323	44229783.76
453	0.014788	259599	4698	69.474024	3550.743347	18035387.16
461	0.013747	265863	6264	86.111208	3636.854555	22893784.09
468	0.012289	271344	5481	67.356009	3704.210564	18276648.91
475	0.010414	276825	5481	57.079134	3761.289698	15800931.27
481	0.009581	281523	4698	45.011538	3806.301236	12671783.21
489	0.008956	287787	6264	56.100384	3862.40162	16144961.21
496	0.008331	293268	5481	45.662211	3908.063831	13391265.3
509	0.007706	304437	11169	86.068314	3994.132145	26202379.31
517	0.007082	311581	7144	50.593808	4044.725953	15764069.29
531	0.006873	324083	12502	85.926246	4130.652199	27847235.58
545	0.005624	336585	12502	70.311248	4200.963447	23665711.41
559	0.005415	349087	12502	67.69833	4268.661777	23632606.92
573	0.005207	361589	12502	65.097914	4333.759691	23538689.63
582	0.00479	369626	8037	38.49723	4372.256921	14229577.14
586	0.004166	373198	3572	14.880952	4387.137873	5553541.524
615	0.003957	403340	30142	119.271894	4506.409767	48107125.73

Table B.1 continued

<b>Time</b>	<b>Conc</b>	<b>Inj_volume</b>	<b>DeIV</b>	<b>C*DeIV</b>	<b>Cum.C*DV</b>	<b>C*V*DV</b>
643	0.002708	436268	32928	89.169024	4595.578791	38901591.76
					126317.6094	937440466.7

**Table B.2 – Cumulative produced volume versus concentration (Well 39) using NaSCN.**

Time	Conc	Inj_volume	DelV	C*DelV	Cum.C*DV	C*V*DV
119	0	53077	0	0	0	0
132	0	59356	6279	0	0	0
139	0	62737	3381	0	0	0
145	0	65635	2898	0	0	0
153	0.000625	69499	3864	2.415	2.415	167840.085
160	0.000625	72880	3381	2.113125	4.528125	154004.55
167	0.005415	76261	3381	18.308115	22.83624	1396195.158
173	0.009581	79159	2898	27.765738	50.601978	2197908.054
181	0.009789	83023	3864	37.824696	88.426674	3140319.736
188	0.015205	86404	3381	51.408105	139.834779	4441865.904
195	0.015413	89785	3381	52.111353	191.946132	4678817.829
201	0.016662	92797	3012	50.185944	242.132076	4657105.045
209	0.017912	97573	4776	85.547712	327.679788	8347146.903
216	0.024161	101752	4179	100.968819	428.648607	10273779.27
223	0.025202	105931	4179	105.319158	533.967765	11156563.73
229	0.030409	109513	3582	108.925038	642.892803	11928707.69
237	0.029159	114289	4776	139.263384	782.156187	15916272.89
251	0.027285	122647	8358	228.04803	1010.204217	27969406.74
257	0.024994	126229	3582	89.528508	1099.732725	11301094.04
265	0.022494	131005	4776	107.431344	1207.164069	14074043.22
272	0.021036	135184	4179	87.909444	1295.073513	11883950.28
279	0.019995	139363	4179	83.559105	1378.632618	11645047.55
285	0.020203	142945	3582	72.367146	1450.999764	10344521.68
293	0.019995	147721	4776	95.49612	1546.495884	14106782.34
300	0.019787	151900	4179	82.689873	1629.185757	12560591.71
307	0.01937	156534	4634	89.76058	1718.946337	14050582.63
313	0.019162	160506	3972	76.111464	1795.057801	12216346.64
321	0.017912	165802	5296	94.861952	1889.919753	15728301.37
328	0.017912	170436	4634	83.004208	1972.923961	14146905.19

Table B.2 continued

Time	Conc	Inj_volume	DeIV	C*DeIV	Cum.C*DV	C*V*DV
341	0.018329	179042	8606	157.739374	2130.663335	28241973
349	0.018954	184338	5296	100.380384	2231.043719	18503919.23
356	0.019578	188972	4634	90.724452	2321.768171	17144381.14
363	0.020203	193606	4634	93.620702	2415.388873	18125529.63
369	0.019995	197578	3972	79.42014	2494.809013	15691672.42
377	0.019578	202874	5296	103.685088	2598.494101	21035008.54
384	0.018954	207508	4634	87.832836	2686.326937	18226016.13
391	0.017912	212142	4634	83.004208	2769.331145	17608678.69
412	0.017287	227496	15354	265.424598	3034.755743	60383034.35
419	0.016662	232977	5481	91.324422	3126.080165	21276489.86
425	0.016454	237675	4698	77.300892	3203.381057	18372489.51
433	0.016662	243939	6264	104.370768	3307.751825	25460100.78
447	0.015829	254901	10962	173.517498	3481.269323	44229783.76
453	0.014788	259599	4698	69.474024	3550.743347	18035387.16
461	0.013747	265863	6264	86.111208	3636.854555	22893784.09
468	0.012289	271344	5481	67.356009	3704.210564	18276648.91
475	0.010414	276825	5481	57.079134	3761.289698	15800931.27
481	0.009581	281523	4698	45.011538	3806.301236	12671783.21
489	0.008956	287787	6264	56.100384	3862.40162	16144961.21
496	0.008331	293268	5481	45.662211	3908.063831	13391265.3
509	0.007706	304437	11169	86.068314	3994.132145	26202379.31
517	0.007082	311581	7144	50.593808	4044.725953	15764069.29
531	0.006873	324083	12502	85.926246	4130.652199	27847235.58
545	0.005624	336585	12502	70.311248	4200.963447	23665711.41
559	0.005415	349087	12502	67.69833	4268.661777	23632606.92
573	0.005207	361589	12502	65.097914	4333.759691	23538689.63
582	0.00479	369626	8037	38.49723	4372.256921	14229577.14
586	0.004166	373198	3572	14.880952	4387.137873	5553541.524
615	0.003957	403340	30142	119.271894	4506.409767	48107125.73

**Table B.2 continued**

<b>Time</b>	<b>Conc</b>	<b>Inj_volume</b>	<b>DeIV</b>	<b>C*DeIV</b>	<b>Cum.C*DV</b>	<b>C*V*DV</b>
643	0.002708	436268	32928	89.169024	4595.578791	38901591.76
					126317.6094	937440466.7

**Table B.3 – MOM parameter estimates (Well 39) using NaSCN.**

<b>Parameter</b>	<b>Estimated value</b>	<b>Units</b>
m	2466.831245	Barrels (bbls)
Fraction of tracer produced $f=m/M$	0.146835193	-
Total Swept Volume	223422.0554	Barrels (bbls)
Net Swept Volume	32806.22066	Barrels (bbls)



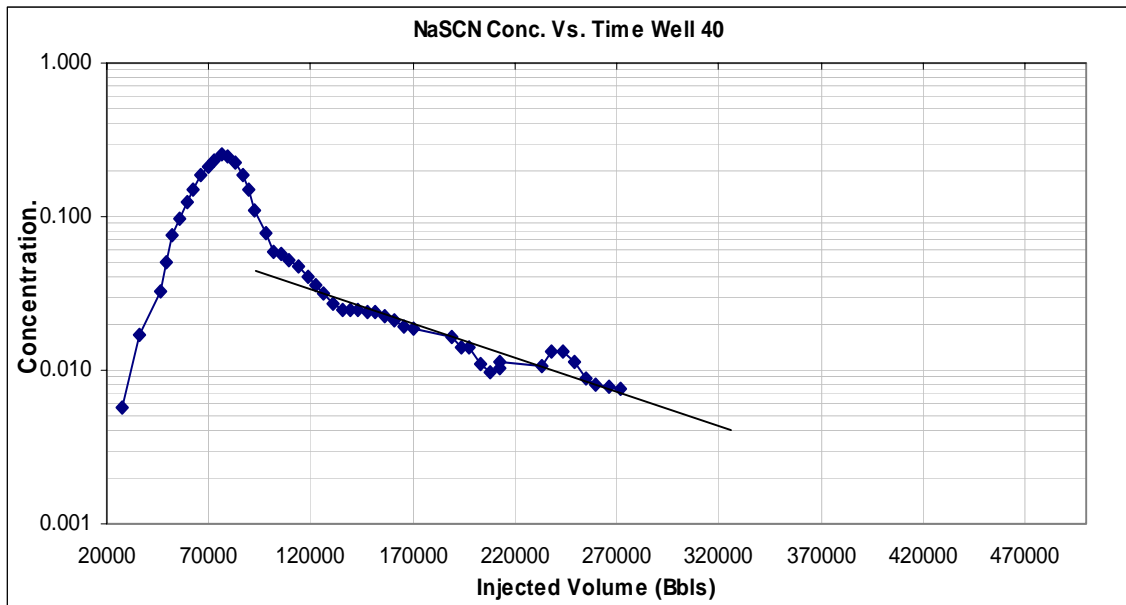


**Fig. B.3 – Semi-log plot of NaSCN concentration versus injected volume for Well 40**

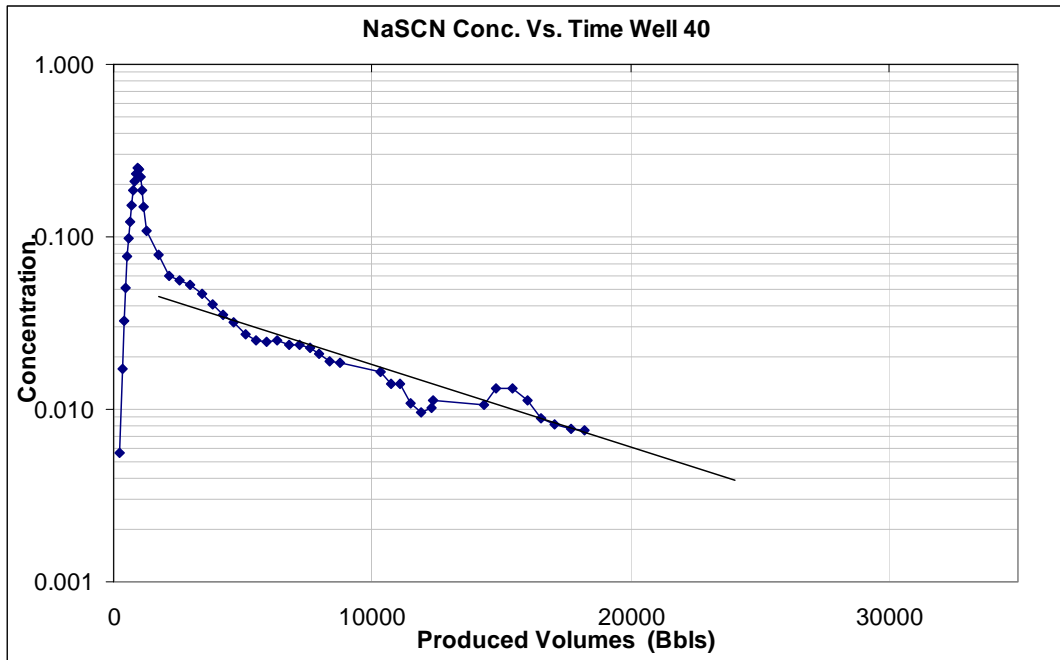


**Fig. B.4 – Semi-log plot of NaSCN concentration versus produced volume for Well 40**

**Table B.4 – Cumulative injected volume versus concentration (Well 40) using NaSCN.**

Time	Conc	Inj_volume	DelV	C*DelV	Cum.C*DV	C*V*DV
62	0	27218	0	0	0	0
83	0.005624	36437	9219	51.847656	51.847656	1889173.042
104	0.017183	45832	9395	161.434285	213.281941	7398856.15
111	0.032492	49213	3381	109.855452	323.137393	5406316.359
117	0.051029	52111	2898	147.882042	471.019435	7706281.091
125	0.076647	55975	3864	296.164008	767.183443	16577780.35
132	0.097476	59356	3381	329.566356	1096.749799	19561740.63
139	0.123094	62737	3381	416.180814	1512.930613	26109935.73
145	0.15142	65635	2898	438.81516	1951.745773	28801633.03
153	0.18537	69499	3864	716.26968	2668.015453	49780026.49
160	0.208906	72880	3381	706.311186	3374.326639	51475959.24
167	0.230984	76261	3381	780.956904	4155.283543	59556554.46
173	0.250562	79159	2898	726.128676	4881.412219	57479619.86
181	0.244939	83023	3864	946.444296	5827.856515	78576644.79
188	0.221611	86404	3381	749.266791	6577.123306	64739647.81
195	0.184329	89785	3381	623.216349	7200.339655	55955479.89
201	0.149754	92797	3012	451.059048	7651.398703	41856926.48
209	0.108514	97573	4776	518.262864	8169.661567	50568462.43
216	0.07873	101752	4179	329.01267	8498.674237	33477697.2
223	0.058944	105931	4179	246.326976	8745.001213	26093662.89
229	0.056444	109513	3582	202.182408	8947.183621	22141602.05
237	0.052487	114289	4776	250.677912	9197.861533	28649727.88
244	0.046863	118468	4179	195.840477	9393.70201	23200829.63
251	0.040823	122647	4179	170.599317	9564.301327	20923494.43
257	0.035616	126229	3582	127.576512	9691.877839	16103855.53
265	0.031659	131005	4776	151.203384	9843.081223	19808399.32
272	0.027285	135184	4179	114.024015	9957.105238	15414222.44
279	0.024994	139363	4179	104.449926	10061.55516	14556455.04
285	0.024577	142945	3582	88.034814	10149.58998	12584136.49

Table B.4 Continued

Time	Conc	Inj_volume	DelV	C*DelV	Cum.C*DV	C*V*DV
293	0.024994	147721	4776	119.371344	10268.96132	17633654.31
300	0.023744	151900	4179	99.226176	10368.1875	15072456.13
307	0.023536	156534	4634	109.065824	10477.25332	17072509.69
313	0.022703	160506	3972	90.176316	10567.42964	14473839.78
321	0.020828	165802	5296	110.305088	10677.73473	18288804.2
328	0.018954	170436	4634	87.832836	10765.56756	14969877.24
356	0.018537	188972	18536	343.601832	11109.16939	64931125.4
363	0.016454	193606	4634	76.247836	11185.41723	14762038.54
369	0.014163	197578	3972	56.255436	11241.67267	11114836.53
377	0.014163	202874	5296	75.007248	11316.67991	15217020.43
384	0.010831	207508	4634	50.190854	11366.87077	10415003.73
391	0.009581	212142	4634	44.398354	11411.26912	9418755.614
392	0.010206	212804	662	6.756372	11418.02549	1437782.987
419	0.011247	232977	20173	226.885731	11644.91123	52859156.95
425	0.010622	237675	4698	49.902156	11694.81338	11860494.93
433	0.013122	243939	6264	82.196208	11777.00959	20050860.78
440	0.013122	249420	5481	71.921682	11848.93127	17938705.92
447	0.011247	254901	5481	61.644807	11910.57608	15713322.95
453	0.008956	259599	4698	42.075288	11952.65137	10922702.69
461	0.008123	265863	6264	50.882472	12003.53384	13527766.65
468	0.007706	271344	5481	42.236586	12045.77042	11460644.19
475	0.007498	276825	5481	41.096538	12086.86696	11376549.13
				12086.86696		1246913030

**Table B.5 – Cumulative produced volume versus concentration (Well 40) using NaSCN.**

Time	Conc	Produced_volume	DeIV	C*DeIV	Cum.C*DV
62	0	248			
83	0.005624	332	0	0	0
104	0.017183	432	100	1.7183	742.3056
111	0.032492	488	56	1.819552	887.941376
117	0.051029	536	48	2.449392	1312.874112
125	0.076647	600	64	4.905408	2943.2448
132	0.097476	656	56	5.458656	3580.878336
139	0.123094	712	56	6.893264	4908.003968
145	0.15142	760	48	7.26816	5523.8016
153	0.18537	824	64	11.86368	9775.67232
160	0.208906	880	56	11.698736	10294.88768
167	0.230984	936	56	12.935104	12107.25734
173	0.250562	984	48	12.026976	11834.54438
181	0.244939	1048	64	15.676096	16428.54861
188	0.221611	1104	56	12.410216	13700.87846
195	0.184329	1160	56	10.322424	11974.01184
201	0.149754	1260	100	14.9754	18869.004
209	0.108514	1740	480	52.08672	90630.8928
216	0.07873	2160	420	33.0666	71423.856
223	0.058944	2580	420	24.75648	63871.7184
229	0.056444	2940	360	20.31984	59740.3296
237	0.052487	3420	480	25.19376	86162.6592
244	0.046863	3840	420	19.68246	75580.6464
251	0.040823	4260	420	17.14566	73040.5116
257	0.035616	4620	360	12.82176	59236.5312
265	0.031659	5100	480	15.19632	77501.232
272	0.027285	5520	420	11.4597	63257.544
279	0.024994	5940	420	10.49748	62355.0312
285	0.024577	6300	360	8.84772	55740.636

**Table B.5 Continued**

<b>Time</b>	<b>Conc</b>	<b>Produced_volume</b>	<b>DeIV</b>	<b>C*DeIV</b>	<b>Cum.C*DV</b>
293	0.024994	6780	480	11.99712	81340.4736
300	0.023744	7200	420	9.97248	71801.856
307	0.023536	7592	392	9.226112	70044.6423
313	0.022703	7928	336	7.628208	60476.43302
321	0.020828	8376	448	9.330944	78155.98694
328	0.018954	8768	392	7.429968	65145.95942
356	0.018537	10336	1568	29.066016	300426.3414
363	0.016454	10728	392	6.449968	69195.2567
369	0.014163	11064	336	4.758768	52651.00915
377	0.014163	11512	448	6.345024	73043.91629
384	0.010831	11904	392	4.245752	50541.43181
391	0.009581	12296	392	3.755752	46180.72659
392	0.010206	12352	56	0.571536	7059.612672
419	0.011247	14320	1968	22.134096	316960.2547
425	0.010622	14800	480	5.09856	75458.688
433	0.013122	15440	640	8.39808	129666.3552
440	0.013122	16000	560	7.34832	117573.12
447	0.011247	16560	560	6.29832	104300.1792
453	0.008956	17040	480	4.29888	73252.9152
461	0.008123	17680	640	5.19872	91913.3696
468	0.007706	18240	560	4.31536	78712.1664
475	0.007498	18800	560	4.19888	78938.944
				561.562728	

**Table B.6 – MOM parameter estimates (Well 39) using NaSCN.**

<b>Parameter</b>	<b>Estimated value</b>	<b>Units</b>
m	638.0647006	Barrels (bbls)
Fraction of tracer produced $f=m/M$	0.03798	-
Total Swept Volume	120993.1745	Barrels (bbls)
Net Swept Volume	4595.325812	Barrels (bbls)

**APPENDIX C****COMPUTING SENSITIVITIES WITH RESPECT TO SHIFT -TIME**



Given the objective function below

$$J_p = \sum_{i=1}^{N_{aj}} [y_j^{obs}(t_i + \Delta t_j) - y_j^{cal}(t_i)]^2 = f(\Delta t_j) \quad (C.1)$$

Let  $\tau$  represent  $\Delta \tau$

$$\frac{\partial \Delta \tau}{\partial m} = \frac{\frac{\partial}{\partial m} \left[ \frac{\partial J}{\partial \tau} \right]}{\frac{\partial}{\partial \tau} \left[ \frac{\partial J}{\partial \tau} \right]} = \frac{\frac{\partial^2 J}{\partial m \partial \tau}}{\frac{\partial^2 J}{\partial \tau^2}} \quad (C.2)$$

Solving the numerator,

$$\frac{\partial^2 J}{\partial m \partial \tau} = \frac{\partial}{\partial m} \left( \frac{\partial}{\partial \tau} \sum [y^{obs}(t_i + \tau) - y^{cal}(t_i)]^2 \right) \quad (C.3)$$

$$\frac{\partial^2 J}{\partial m \partial \tau} = 2 \sum \frac{\partial}{\partial m} (y^{obs}(t_i + \tau) - y^{cal}(t_i)) \frac{\partial y^{obs}(t_i + \tau)}{\partial \tau} \quad (C.4)$$

$$\frac{\partial^2 J}{\partial m \partial \tau} = 2 \sum \left( -\frac{\partial y^{cal}(t_i)}{\partial m} \right) \frac{\partial y^{obs}(t_i + \tau)}{\partial \tau} \quad (C.5)$$

Solving the denominator,

$$\frac{\partial^2 J}{\partial \tau^2} = \frac{\partial}{\partial \tau} \left[ \frac{\partial J}{\partial \tau} \right] = \frac{\partial}{\partial \tau} \left\{ \sum \left( 2[y^{obs}(t_i + \tau) - y^{cal}(t_i)] \frac{\partial y^{obs}(t_i + \tau)}{\partial \tau} \right) \right\} \quad (C.6)$$

$$\frac{\partial^2 J}{\partial \tau^2} = \left\{ 2 \sum \frac{\partial}{\partial \tau} \left( [y^{obs}(t_i + \tau) - y^{cal}(t_i)] \frac{\partial y^{obs}(t_i + \tau)}{\partial \tau} \right) \right\} \quad (C.7)$$

$$\frac{\partial^2 J}{\partial \tau^2} = 2 \sum \left( [y^{obs}(t_i + \tau) - y^{cal}(t_i)] \frac{\partial^2 y^{obs}(t_i + \tau)}{\partial \tau^2} + \frac{\partial y^{obs}(t_i + \tau)}{\partial \tau} \cdot \frac{\partial}{\partial \tau} [y^{obs}(t_i + \tau) - y^{cal}(t_i)] \right) \quad (C.8)$$

$$\frac{\partial^2 J}{\partial \tau^2} = 2 \sum \left( [y^{obs}(t_i + \tau) - y^{cal}(t_i)] \frac{\partial^2 y^{obs}(t_i + \tau)}{\partial \tau^2} + \left[ \frac{\partial y^{obs}(t_i + \tau)}{\partial \tau} \right]^2 \right) \quad (C.9)$$

Combining Eqs. C.2, C.5, C.9,

$$\frac{\partial \Delta \tau}{\partial m} = \frac{2 \sum \left( -\frac{\partial y^{cal}(t_i)}{\partial m} \right) \frac{\partial y^{obs}(t_i + \tau)}{\partial \tau}}{2 \sum \left( [y^{obs}(t_i + \tau) - y^{cal}(t_i)] \frac{\partial^2 y^{obs}(t_i + \tau)}{\partial \tau^2} + \left[ \frac{\partial y^{obs}(t_i + \tau)}{\partial \tau} \right]^2 \right)} \quad (\text{C.10})$$

$$\frac{\partial \Delta \tau}{\partial m} = \frac{\sum \left( -\frac{\partial y^{cal}(t_i)}{\partial m} \right) \frac{\partial y^{obs}(t_i + \tau)}{\partial \tau}}{\sum \left( [y^{obs}(t_i + \tau) - y^{cal}(t_i)] \frac{\partial^2 y^{obs}(t_i + \tau)}{\partial \tau^2} + \left[ \frac{\partial y^{obs}(t_i + \tau)}{\partial \tau} \right]^2 \right)} \quad (\text{C.11})$$

## VITA

Adedayo Stephen Oyerinde completed his Bachelor of Science at University of Ibadan, Department of Petroleum Engineering, Nigeria in May 2000. His permanent address is 83, Hospital road, Badagry, Lagos, Nigeria.